2017-07-01

Full-Scale Testing of Blast-Induced Liquefaction Downdrag on Driven Piles in Sand

Luke Ian Kevan
Brigham Young University

Full-Scale Testing of Blast-Induced Liquefaction Downdrag on Driven Piles in Sand

Luke Ian Kevan

A thesis submitted to the faculty of
Brigham Young University
in partial fulfillment of the requirements for the degree of

Master of Science

Kyle M. Rollins, Chair
Kevin W. Franke
Paul W. Richards

Department of Civil and Environmental Engineering

Brigham Young University

ABSTRACT

Full-Scale Testing of Blast-Induced Liquefaction Downdrag on Driven Piles in Sand

Luke Ian Kevan
Department of Civil and Environmental Engineering, BYU
Master of Science

Deep foundations such as driven piles are often used to bypass liquefiable layers of soil and bear on more competent strata. When liquefaction occurs, the skin friction around the deep foundation goes to zero in the liquefiable layer. As the pore pressures dissipate, the soil settles. As the soil settles, negative skin friction develops owing to the downward movement of the soil surrounding the pile. To investigate the magnitude of the skin friction along the shaft three driven piles, an H-pile, a closed end pipe pile, and a concrete square pile, were instrumented and used to measure soil induced load at a site near Turrell, Arkansas following blast-induced liquefaction. Measurements were made of the load in the pile, the settlement of the ground and the settlement of piles in each case. Estimates of side friction and end-bearing resistance were obtained from Pile Driving Analyzer (PDA) measurements during driving and embedded O-cell type testing.

The H-pile was driven to a depth of 94 feet, the pipe pile 74 feet, and the concrete square pile 72 feet below the ground surface to investigate the influence of pile depth in response to liquefaction. All three piles penetrated the liquefied layer and tipped out in denser sand. The soil surrounding the piles settled 2.5 inches for the H-pile, 2.8 inches for the pipe pile and 3.3 inches for the concrete square pile. The piles themselves settled 0.28 inches for the H-pile, 0.32 inches for the pipe pile, and 0.28 inches for the concrete square pile. During reconsolidation, the skin friction of the liquefied layer was 43% for the H-pile, 41% for the pipe pile, and 49% for the concrete square pile. Due to the magnitude of load felt in the piles from these tests the assumption of 50% skin friction developing in the liquefied zone is reasonable. Reduced side friction in the liquefied zone led to full mobilization of skin friction in the non-liquefied soil, and partial mobilization of end bearing capacity. The neutral plane, defined as the depth where the settlement of the soil equals the settlement of the pile, was outside of the liquefied zone in each scenario. The neutral plane method that uses mobilized end bearing measured during blasting to calculate settlement of the pile post liquefaction proved to be accurate for these three piles.

Keywords: Downdrag, Liquefaction, Neutral Plane, Driven Pile, Settlement, Static Load Test, CAPWAP analysis, AFT-Cell test

ACKNOWLEDGEMENTS

I would like to take the time to thank those who contributed to this project. Particularly, the Arkansas Highway and Transportation Department and the National Science Foundation (Grant CMMI-1650576) who were the primary sources of funding for this project. I also am grateful for all those who donated labor or materials including Chris Hill Construction, McKinney Drilling Company, The International Association of Foundation Drilling, GRL Engineers Incorporated, GEI Consultants, Fugro/Loadtest, The Missouri Department of Transportation, Kolb Grading, Pile Driving Contractors Association, Applied Foundation Testing, Skyline Steel, Nucor-Yamato Steel, W&W AFCO Steel, International Construction Equipment, Texas Concrete Partners. I would also like to acknowledge our partners at the University of Arkansas, Dr. Richard Coffman and Elvis Ishimwe.

I want to especially thank Dr. Kyle Rollins for his guidance and patience with me as I tried to finish my thesis and understand the difficult concepts we are working with. I am most grateful, however, to my wife who supported me and was patient with me as I worked long hours to finish my work.

TABLE OF CONTENTS

LIST OF TABLES

LIST OF FIGURES

1 INTRODUCTION

1.1 Problem Statement

Liquefaction has caused significant damage to infrastructure in most major earthquakes. Deep foundations are typically used to support bridge and high-rise structures when weak or liquefiable soils are encountered. Deep foundations can bypass liquefiable layers and bear in more competent strata at depth. Dead and live loads imposed on the pile foundation are typically resisted by positive skin friction acting on the side of the pile and by end-bearing resistance at the toe of the pile. However, when liquefaction occurs in a layer along the pile, settlement of that layer, and the associated movement of the soil above it, could exceed the settlement of the pile. If this is the case, the liquefied layer and the layers above it slide down relative to the pile leading to negative skin friction along that length of the pile, as shown in Figure 1.1-1. Negative skin friction acting along the pile creates a "dragload".

The neutral plane is defined as the depth where the settlement in the pile and the settlement in the soil are the same and the depth in the pile where the load is the greatest. Below the neutral plane, the positive skin friction and end bearing provide upward resistance which decreases the load in the pile. The location of the neutral plane is found iteratively, such that the applied loads plus the negative skin friction above the neutral plane are equal to the positive skin friction plus the mobilized end bearing below the neutral plane. Also, the end-bearing resistance mobilized must be consistent with the settlement of the pile toe. Thus, the location of the neutral plane creates a force equilibrium based on the soil settlement and the pile settlement.

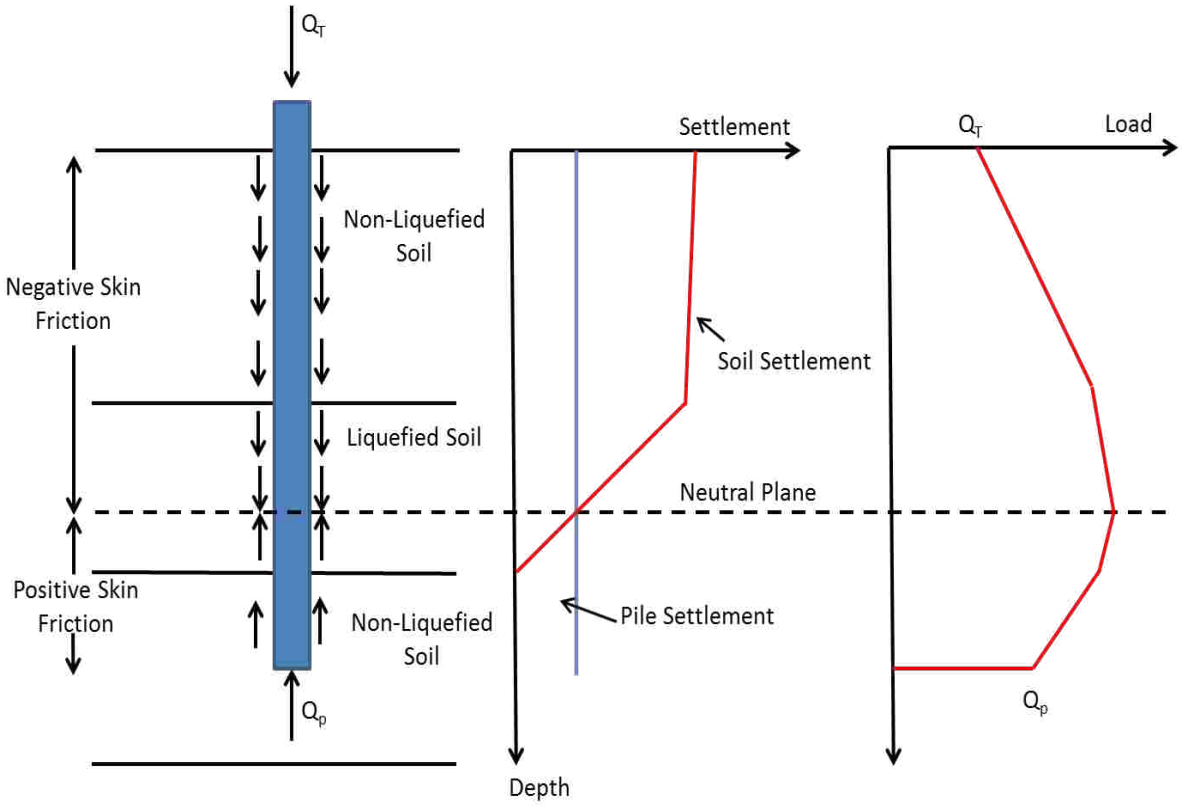

Figure 1.1-1 Relationship between liquefaction induced settlement, positive and negative skin friction and the neutral plane.

In contrast to non-liquefiable layers, where the negative skin friction might simply be equivalent to the positive skin friction, the negative skin friction in liquefiable layers immediately following liquefaction is likely to be a very small fraction of the pre-liquefaction value or perhaps zero. However, as the earthquake induced pore pressures dissipate in the liquefiable layer, the skin friction at the pile-soil interface is likely to increase. Therefore, the negative skin friction which ultimately develops in liquefied layers might be related to the rate of pore pressure dissipation and the increase in effective stress.

In the absence of test results, some investigators have used theoretical concepts to predict the behavior of piles when subjected to liquefaction induced dragloads. Boulanger et al. (2004) defined negative skin friction in the liquefied zone in terms of the effective stress during

reconsolidation, but concluded that the negative skin friction could be assumed to be zero with little error in the computed pile force or settlement. Fellenius and Siegel (2008) applied their "unified pile design" approach which was developed for downdrag in clays, to the problem of downdrag in liquefied sand, once again assuming that negative skin friction in the liquefied zone would be zero. They conclude that the liquefaction above the neutral plane would not increase the load in the pile owing to the development of dragload under long-term static conditions prior to liquefaction.

In a full-scale blast induced liquefaction test Rollins and Strand (2004) discovered that the skin friction on a driven pipe pile in the liquefied zone could be as much as 50% of the positive pre-liquefaction skin friction due to the rapidly dissipating pore pressures. Hollenbaugh (2014) confirmed these results for auger-cast piles and found the side friction to be about 50% of the pre-liquefied side friction. These results strongly indicate that side friction in the liquefied zone is not zero as has been assumed. However, additional test data is necessary to develop a reliable design procedure to predict negative skin friction and resulting pile performance.

To further develop the understanding of negative skin friction on piles in liquefied sand, and the resulting pile response, a field testing program was undertaken using an H pile, a pipe pile and a pre-cast concrete pile. Controlled blasting was used to induce liquefaction and observe subsequent pile behavior. This thesis describes the test program, the test results, and implications for design practice based on analysis of the test results.

1.2 Research Objectives and Scope

The objectives of this research are to determine:

1. The negative skin friction that develops on piles in liquefied sand layers and the non-liquefied layers above them following liquefaction and pore pressure dissipation.

2. The distribution of load that develops in the piles and the resulting pile settlement relative to the soil settlement.

3. The ability of the neutral plane approach to predict the load in the pile and pile settlement relative to measured results.

To accomplish these research objectives, tests were performed on three piles after blast induced liquefaction at a site near Turrell, Arkansas west of Memphis Tennessee. The test piles consisted of one 92 feet long HP 14x117 steel H-pile, one 78 feet long 18 in diameter closed-ended steel pipe pile, and one 74 feet long 18 in by 18 in precast concrete pile. Controlled blasting was employed to liquefy a 10 to 20 ft-thick layer of sand along the pile after a 118.5-kip static load was applied to each pile. The axial load distribution along the length of the pile due to negative skin friction was measured after liquefaction along with pile settlement and soil settlement so that the neutral plane approach could be evaluated. Load distribution in the piles prior to liquefaction was obtained from Bi-directional (Osterberg-cell) type load tests on companion test piles adjacent to the piles that were tested with blast liquefaction. In addition, load distribution was obtained from CAPWAP analyses of velocity and force measurements obtained during pile driving and from static load tests.

1.3 Outline of Report

The remainder of this thesis consists of five additional chapters. Chapter 2 contains a review of the current literature and design approaches for dealing with downdrag on piles in liquefied sand. The third chapter explains the geotechnical setting, and site characterization. This chapter also contains preliminary calculations and predictions pertaining to the subsequent blast test. Chapter 4 explains the test layout, pile installation, and instrumentation for the test. This chapter also contains the results of the AFT-Cell test, and the results from the CAPWAP

analyses. Chapter 5 describes the results of the blast liquefaction tests and compares measured behavior with predicted behavior using the neutral plane approach. The sixth and final chapter offers a summary of the test program and conclusions based on the results of the field testing and subsequent analysis.

2 INTRODUCTION

2.1 Overview

There have been several publications evaluating skin friction on piles, under static conditions. Little, however, has been published concerning skin friction during a liquefaction event. There is some controversy regarding the appropriate approach for the design of the piles, failure mechanisms, and other considerations, which will be discussed in this literature review. Most research has been evaluation of case studies. However, some research has been performed using full scale testing in the field, and some has been performed in the lab using shake tables and centrifuges. Others have produced finite element models attempting to match test results found in the laboratory.

2.2 Current Research

Fellenius and Siegel (2008) presented several ideas related to downdrag, many of which are related to liquefaction downdrag. One of the more important ideas is piles that are installed to transfer from soft or loose soil layers to denser soil layers will always develop negative skin friction, regardless of surcharge, a drop in the water table, or liquefaction. He suggests the development of negative skin friction in soft or loose soils due to pore pressure build up around the pile during construction. Over time these pore pressures dissipate causing the soil to settle relative to the pile, this will create negative skin friction which causes the pile to settle as well.

Where the settlement of the surrounding soil equals the settlement of the pile, there will be a neutral plane. This is also where the load in the pile will be a maximum. There will be positive skin friction below the neutral plane, and end-bearing mobilization associated with the static pile settlement. The difficulty with some of these assumptions is that there must be cumulative profile settlement to induce downdrag, but in this case, it is only along the pile shaft.

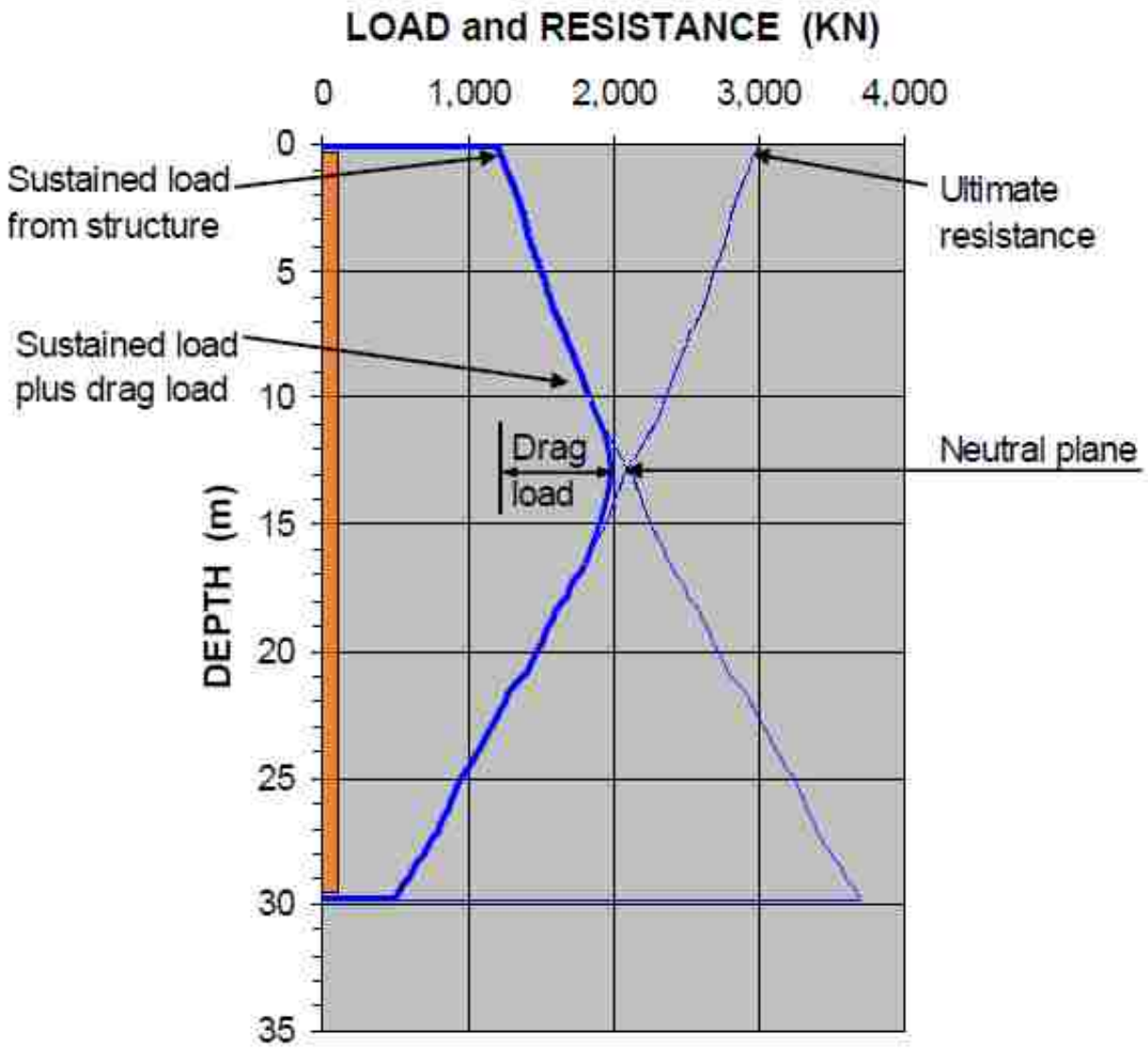

Figure 2.2-1 Load vs. depth in a driven pile showing the neutral plane before liquefaction, (Fellenius and Siegel 2008)

Figure 2.2-1 shows the static load distribution of a pile with dissipating pore pressures leading to a static neutral plane. The case studies associated with this idea were long-term, static conditions (Fellenius 2006). A cumulative settlement profile is developed from compaction of a layer. The drag forces presented here, however, seem to be developed by a small radius of soil surrounding the pile due solely to pile installation. The assumption then is the soil surrounding the pile settles, creating a downward dragload and the pile settles. The end-bearing increases and develops force beyond what it developed under applied loads. The pile settles more than the surrounding soil from the base up to the neutral plane and positive skin friction forms. From the surface, down to the neutral plane the soil settles more than the pile and negative skin friction develops. It is as if the soil directly around the pile is settling such that it creates a drag load which causes the pile to settle and creates a positive upward friction and a static neutral plane.

Fellenius and Siegel (2008) present some other ideas that are important in the discussion of pile design, with the assumption that the static condition is the same as the one in Figure 2.2-1. Figure 2.2-2 shows how the pile could react if liquefaction happens above the static neutral plane. The negative skin friction in the liquefied zone would go to zero, and there would be a small reduction of the drag load and geotechnical axial capacity. Fellenius and Siegel (2008) argue that no change would occur below the neutral plane and no pile movement or settlement would occur. He does argue that the neutral plane would become lower due to the decrease in dragload. The implications for the settlement suggest that this is not true, and Figure 2.2-2 is inaccurate. Because there is no movement by the soil or pile below the neutral plane, the neutral plane should not move down. In truth, a lower neutral plane would mean the pile settles less. The neutral plane would, however, remain at the same depths and the same positive friction would exist below it, because the pile does not settle at all. The reduction in drag load decreases the

end-bearing, and although end bearing depends on movement, no movement is occurring. Thus, end bearing would be less than it had mobilized previously. Rebounding upward movement in the toe is unlikely to cause an upward movement in the pile toe sufficient enough to cause a section of the skin friction to change from positive to negative and thus lower the neutral plane. Either way, the situation is not critical. The layer would eventually re-mobilize skin friction, most likely negative as Fellenius suggests, which would return the neutral plane to its original depth.

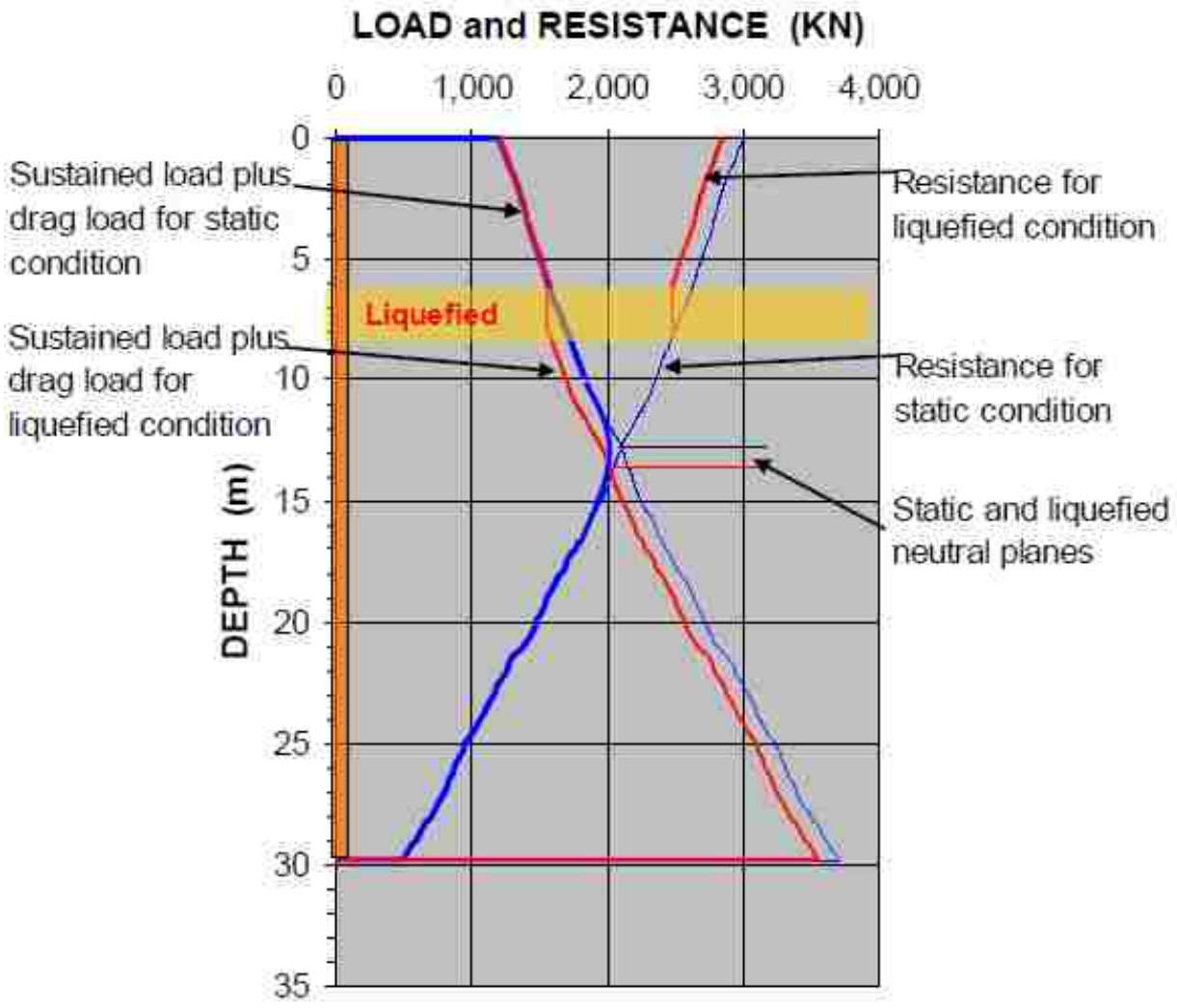

Figure 2.2-2 Load vs. depth in a driven pile showing what happens when liquefaction occurs above the neutral plane, (Fellenius and Siegel 2008)

The next case Fellenius and Siegel consider is when the liquefied layer is below the neutral plane. Unlike the first case, in this situation, the liquefied layer produces dragload. As explained by Fellenius, when liquefaction occurs below the static neutral plane, the neutral plane immediately moves to the bottom of the liquefied layer. At this point, what happens depends on what kind of soil the pile end is bearing in. If the pile toe is bearing in a dense stratum, then the settlement at the toe would be small, and the major concern would become analyzing the pile for buckling. This is not necessarily the case, because when the pile could settle a small amount which would move the neutral plane up into the liquefied layer.

However, if it is bearing in a weak stratum, then the neutral plane moves to the top of the liquefied layer and the settlement in the pile is equal to the settlement of the liquefied layer. The layer above the liquefied zone settles as well, but Fellenius does not expound on this. Figure 2.2-3 shows what would happen as reported by Fellenius. Either way the governing scenario for design would be the one where liquefaction occurs below the neutral plane, and the forces above are then greater than those below the newly liquefied layer causing dragload to lower the neutral plane, and the associated toe penetration.

There is still some confusion regarding the magnitude of the dragload in the liquefied zone, if any at all. There was no dragload in the liquefied zone, when it occurred above the neutral plane, whereas it appears there was dragload in the liquefied zone when it occurred below the neutral plane, Fellenius does not explain this difference. We can assume that settlement in the layers is equal, but the neutral plane location is only affected when liquefaction happens below the pre-liquefaction neutral plane. It is important to understand how dragload might develop in liquefied layers, because this could increase the load in the pile, increase end bearing load and

potentially settlement. It is clear in the previous examples that understanding how dragload might affect the pile is complex.

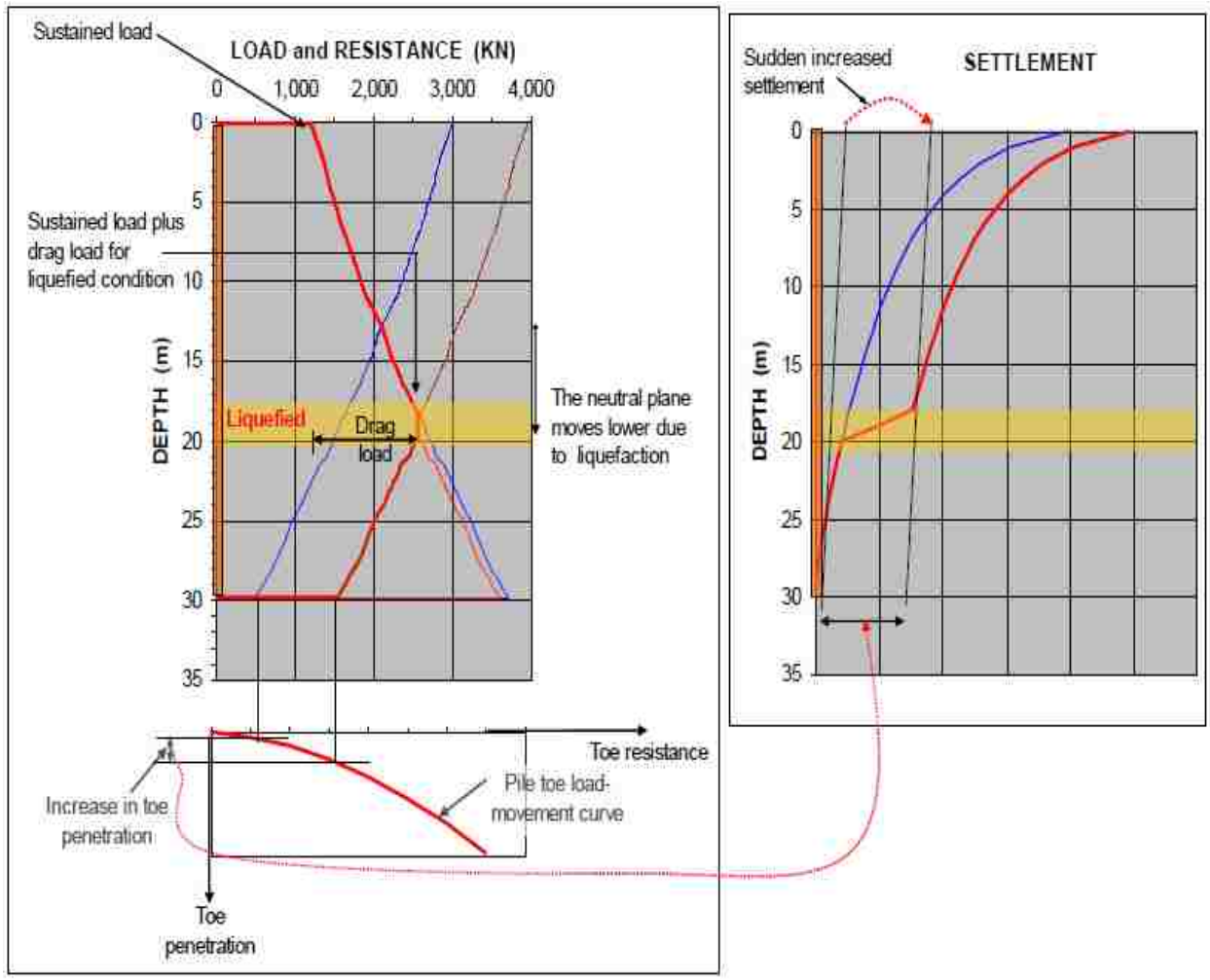

Figure 2.2-3 Load vs. depth in a driven pile showing what happens when liquefaction occurs below the neutral plane, (Fellenius 2008)

The AASHTO LRFD Bridge Design Specifications (AASHTO, 2014) contains very little regarding liquefaction. Basically, the pile is designed with load and resistance factors such that the positive friction along the length of the pile and end-bearing at the base of the pile can resist the applied load and any potential dragload. It isn't clear how this dragload is to occur, whether it

be the static dragload as Fellenius suggests, a consolidation-related development, or a liquefaction-compaction mechanism. Either way the design calls for dragload down to the lowest settling layer. There are two flaws with this simplified method, which Fellenius address, and will be explained here.

First, using factored loads is fundamentally inaccurate. Positive and negative skin friction, the neutral plane, the end-bearing, and settlement, which is integral to all, are closely tied and therefore it is essential to use unfactored loads. Factoring loads creates incorrect neutral planes, incorrect settlements, and an incorrect interpretation of how the pile will react. Rather, safety can be increased by lowering the design neutral plane and therefore decreasing settlements.

The second main flaw is that the AASHTO design does not provide information about anticipated settlements. Settlement is important in determining the location of the neutral plane, and how much end bearing is mobilized. Also, it is possible for settlement to occur below the neutral plane (the pile would be settling more than the layers below the neutral plane). Every segment in the pile is essential and must be considered.

Boulanger and Brandenburg (2004) presented a modified neutral plane solution. This solution focused primarily on the liquefied layer and accounted for variation in excess pore pressures and ground settlement over time as the liquefied layer reconsolidates. They describe an equilibrium that adjusts with time as the pore pressures dissipate rather than an equilibrium based on final at rest conditions. They present the modified neutral plane solution. They argue that the settlement of the pile at the neutral plane may not equal the settlement of the soil at the neutral plane, because the neutral plane moves upward as the soil layer consolidates. Analyzing one small section of the pile the settlement of the pile equals the settlement of the soil at the neutral

plane. Due to the neutral plane changing locations, the soil at its final location was experiencing high settlements the entire duration of consolidation. This is because the neutral plane was experiencing incrementally higher settlements as it changed positions, then at its final location it had the highest compaction.

Wang and Brandenberg (2013) presented another neutral plane solution called the Beam on Nonlinear Winkler Foundation (BNWF) from Wang (2016), and compared their results with a centrifuge by Lam et al. (2009) to see how well their equation correlated to actual data. Their findings were that the settlement of the soil and the settlement of the pile were not equal at the neutral plane, but that the relative velocity of the pile and the soil were equal at the neutral plane. Settlement in the BNWF is dependent on drainage conditions with more settlement occurring in the soil if consolidation starts near the top of the liquefied layer and less consolidation if is commenced on the bottom the liquefied layer. The BNWF tended to under predict settlements when drainage was at the bottom of the liquefied layer and it tended to over predict settlements when drainage was at the top of the liquefied layer. When there was double drainage, the predicted settlement was close to the actual settlement. Another important point of the BMWF is that it shows that as pore pressures dissipate in the liquefied zone and it develops side friction slowly until it returns to a static condition. However, the amount of friction that is developed is small, and they did not give any values as to what the magnitude could be.

Rollins and Strand (2006) conducted full scale blast induced liquefaction tests in Vancouver, BC involving a 12.75 in diameter driven pipe pile. A cross section and plan view of this test is shown in Figure 2.2-5. The single pile was subjected to a static load using hydraulic jacks reacting against a load frame while a layer from 5 m to 15 m was liquefied using a series of explosives charges. At the onset of blasting, the test pile settled slightly, so that the load applied

by the hydraulic jacks dropped almost immediately after the initiation of blasting. This reduced the load the pile was feeling by 156 kN for 18 seconds. Figure 2.2-4 shows the load versus depth curve for the test pile after a pre-blast static load, during blasting then after all the settlement had occurred. The pile fully mobilized positive skin friction after loading the hydraulic jacks. During blasting the skin friction in the liquefied zone was essentially zero, which is expected, however you would expect to see negative skin friction above the liquefied zone. When the load was reapplied, this created positive skin friction above the liquefied zone. Positive skin friction above the liquefied zone stayed the same after the soil settled, and negative skin friction developed in the liquefied zone as pore pressures dissipated. This negative skin friction was equal to approximately 50% of the fully mobilized positive skin friction.

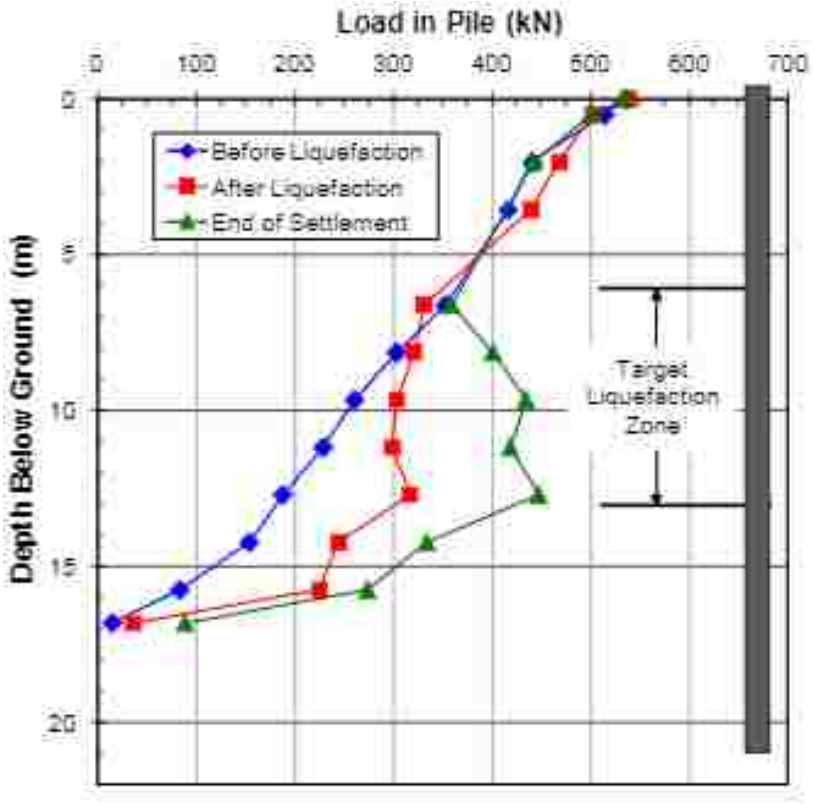

Figure 2.2-4 Pile load vs depth curves before blasting, immediately after blasting and after settlement of the liquefied layer.

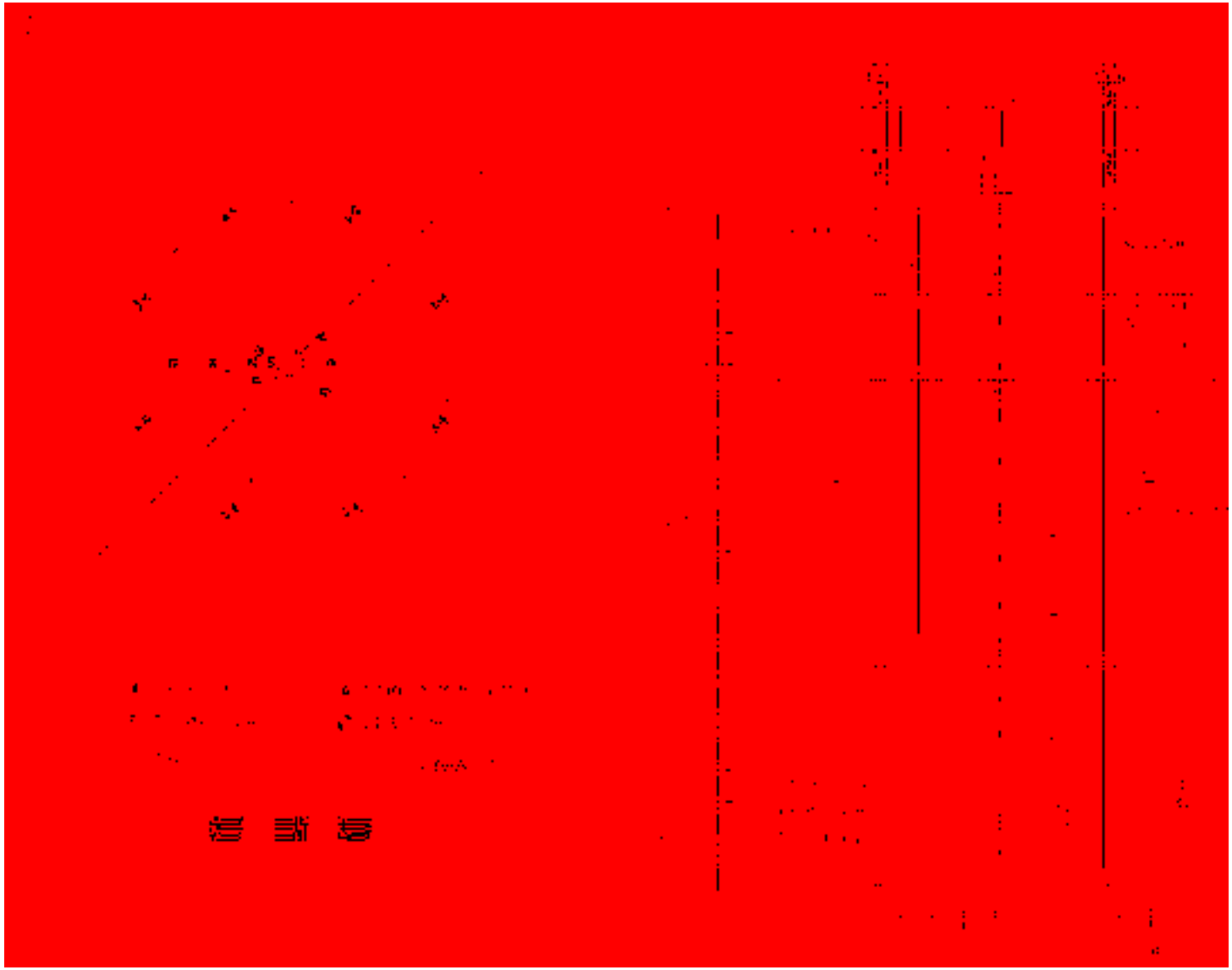

Figure 2.2-5 (a) Plan view and (b) profile view of test pile, blast charges, and instrument layout (Rollins and Strand 2006).

Knappett and Madabhushi (2008) performed scale model centrifuge tests scaled down by the acceleration of the centrifuge, see Figure 2.2-6. The apparatus was a small model with prototype dimensions of 10.4 meters of loose underlain by 12 meters of dense sand. A pile group was driven through the loose sand and into the dense layer, and then connected with a pile cap. The piles were instrumented with strain gauges and base plates to measure skin friction and end bearing. The goal of their experiments was to measure the performance of the pile after liquefaction for cases with and without a pile cap. The piles were place in the apparatus and then backfilled with the layer of loose sand and were embedded in a layer of dense sand (D_r=90%). Even though the pile tips were in denser strata, the sand at the tip still liquefied and the pile group settled relative to the surrounding soil. This is surprising considering the relative density around the piles. Nevertheless, they were unable to develop negative skin friction but they note that the magnitude of the positive skin friction in the liquefied sand is "very similar in magnitude to those measured in a full-scale test." The full-scale test here refers to the test performed by Rollins and Strand (2006).

Rollins and Hollenbaugh (2015) attempted to confirm the value of skin friction in the liquefied zone, by conducting full scale blast induced liquefaction tests on drilled shafts. Their experiments consisted of two separate blasts on three drilled shafts. The first test was conducted with no loads on the shafts, and the second blast was conducted with a static dead load directly applied to the drilled shafts. This prevented the problem that was seen in Rollins and Strand's experiment of not being able to apply a consistent load while the pile settles. The cross section and plan view of their tests are found in Figure 2.2-7 and Figure 2.2-8 respectively.

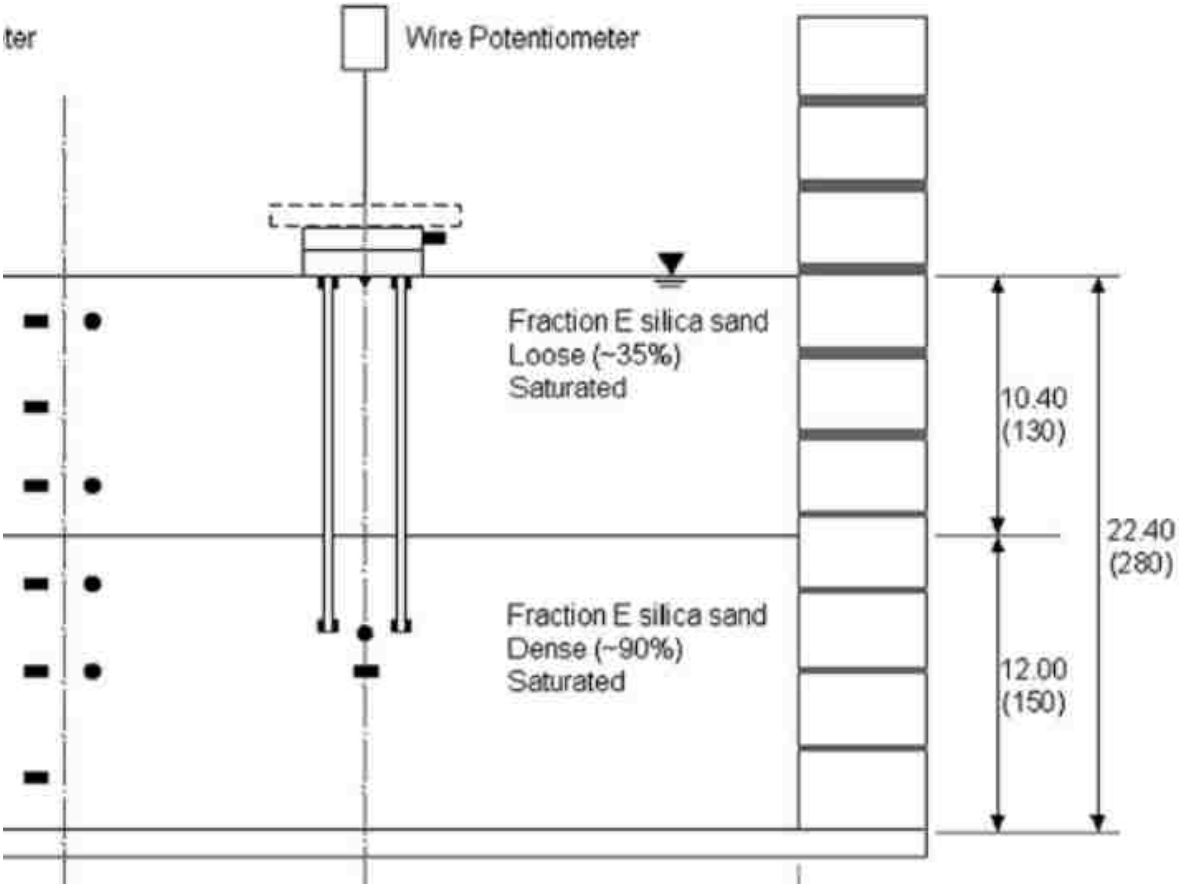

Figure 2.2-6 Cross section of centrifuge test layout (Knappett and Madabhushi 2010).

Their results were consistent with what was found by Rollins and Strand. During the first blast, the soils settled relative to the pile, and downdrag formed with a clear neutral plane. Skin friction outside of the liquefied zone was fully mobilized, and about 50% of the magnitude of fully mobilized skin friction developed in the liquefied layer. Results are shown in Figure 2.2-10. In the figure as the load versus depth curve moves into the liquefied zone there is a clear change in slope in the curve. This indicates the change in magnitude, but also equally important, the slope does not become vertical. Thus, there is skin friction developed, and it is about 50% of the magnitude of fully mobilized skin friction.

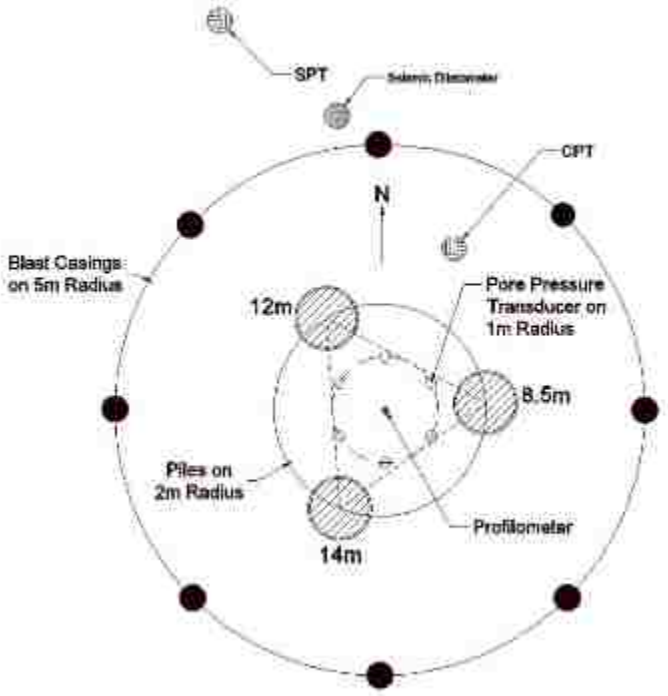

Figure 2.2-7 Plan view of test piles, blast holes and instrumentation (Rollins and Hollenbaugh 2015).

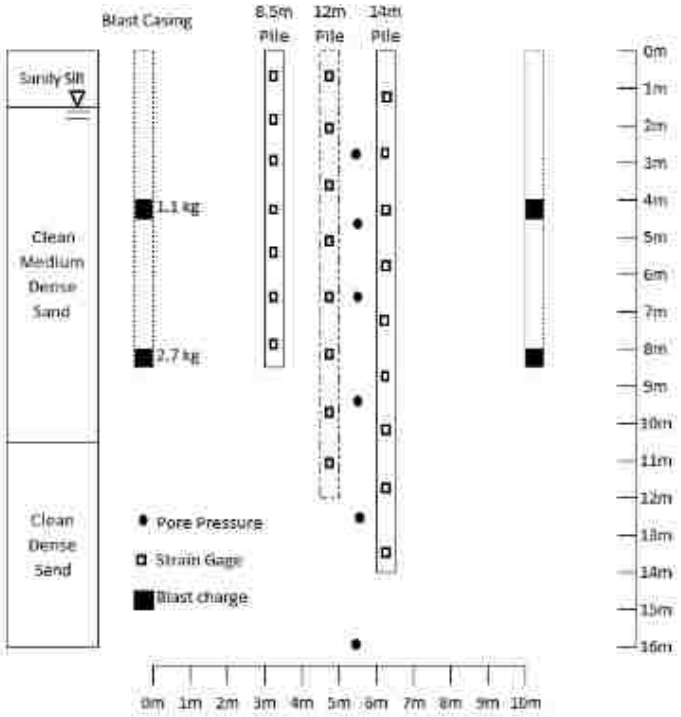

Figure 2.2-8 Elevation view of test piles, blast charges, and instrumentation relative to the soil profile (Rollins and Hollenbaugh 2015).

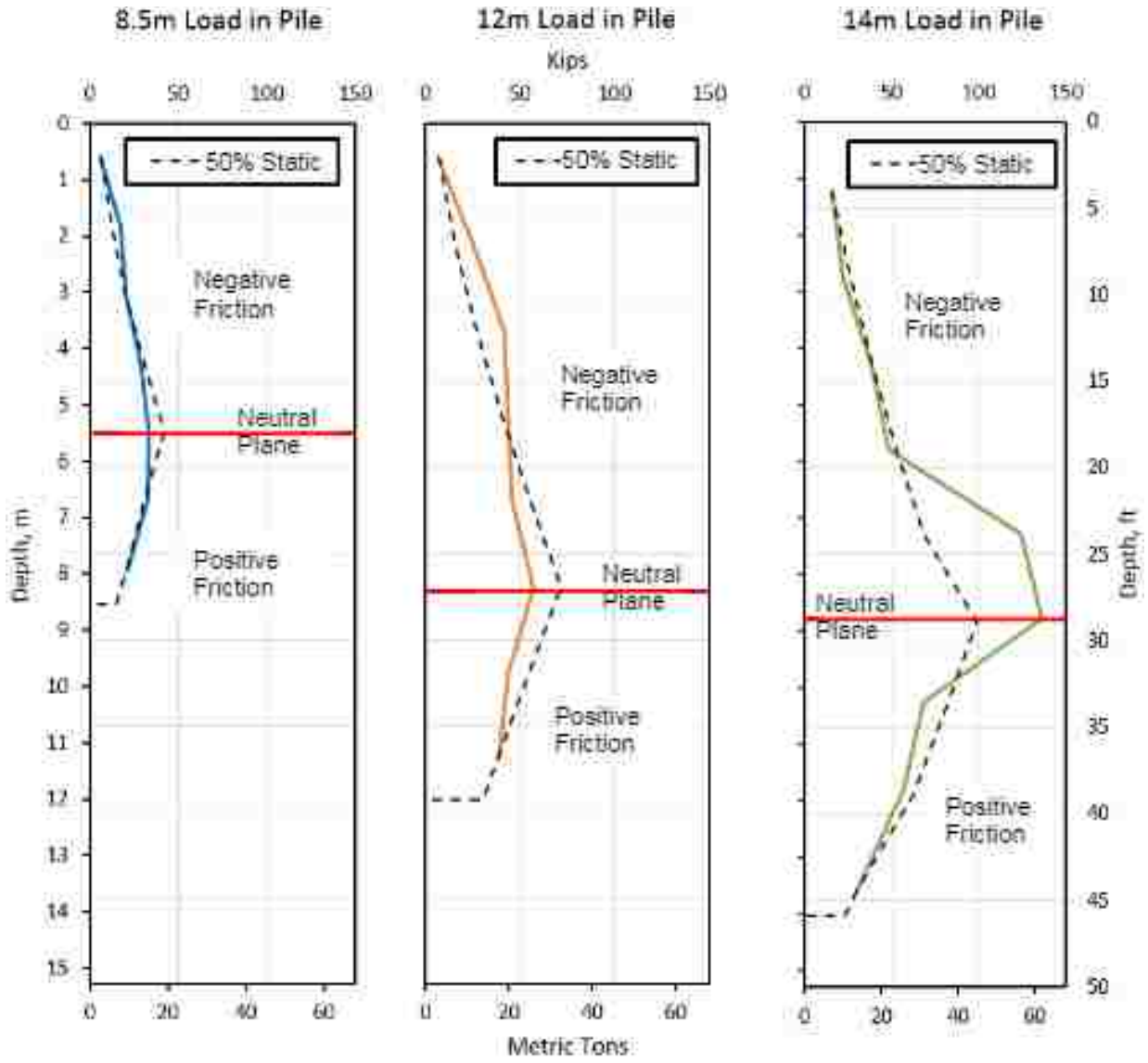

Figure 2.2-9 Interpreted pile load versus depth curves (solid lines) following blast liquefaction along with predicted curves (dashed lines) assuming skin friction equal to 50% of measured average positive skin friction from the static load test (Rollins and Hollenbaugh 2015).

The piles during the second blast were loaded such that the piles settled more than the surrounding soil so only positive skin friction developed along the shaft. Once again, the skin friction outside of the liquefied zone fully mobilized and the magnitude of the skin friction in the liquefied zone during the second blast was about 42%. Figure 2.2-10 Thus, a magnitude of 50% in the liquefied zone is reasonable.

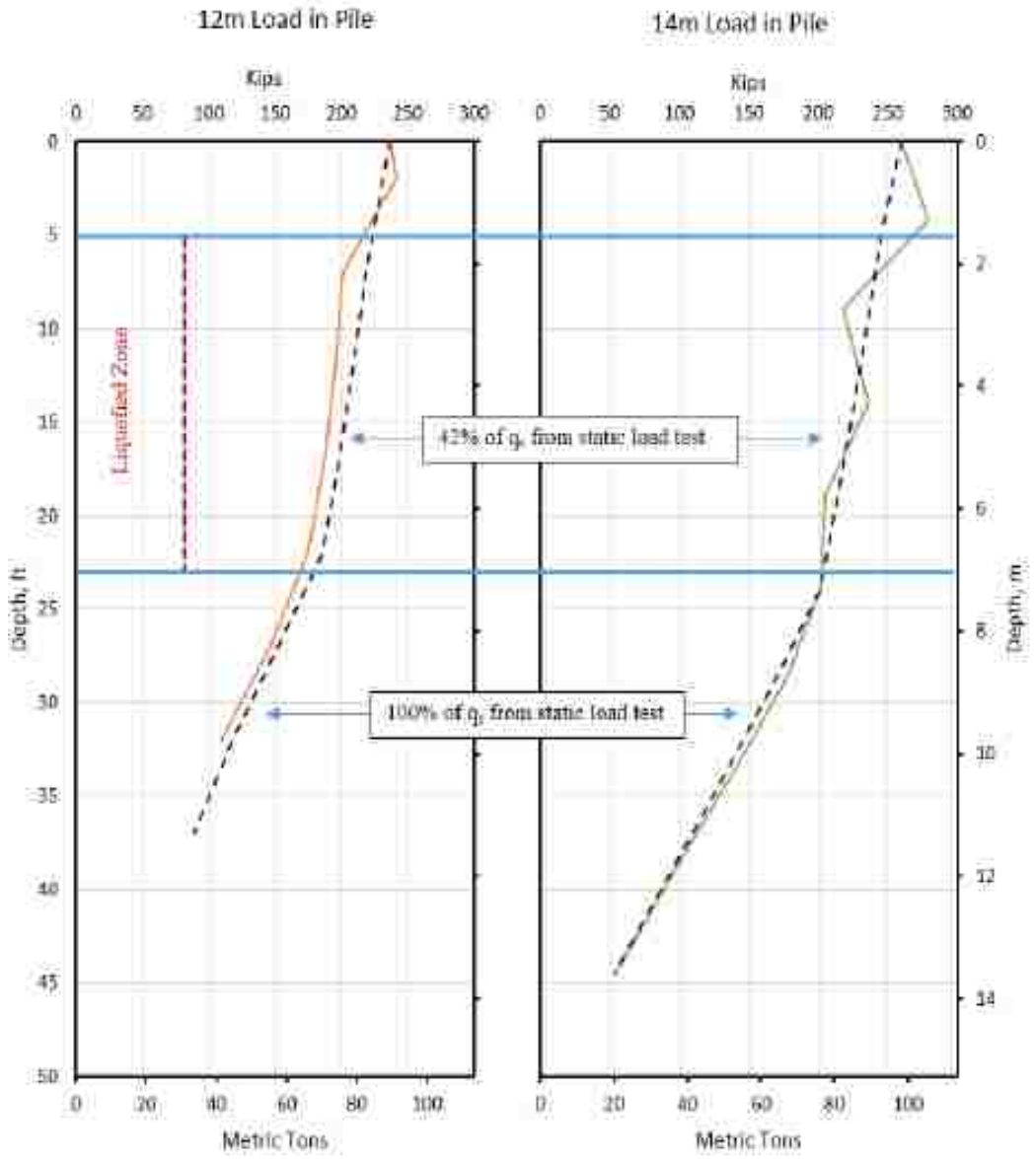

Figure 2.2-10 Load in the piles after the second blast showing resistance in liquefied and non-liquefied section.

Even though it is becoming clearer that the liquefied zone does develop skin friction, there is still a lot of uncertainty how the skin friction should be distributed, what its magnitude should be, and where the neutral plane should fall. There remains some uncertainty as to how the dragload acts after liquefaction induced settlement occurs. Most of these uncertainties are due to lack of good data. Most of the tests and case studies presented here were performed on driven

steel piles, however Hollenbaugh tested drilled shafts and in his report, they appeared to act similar to piles. It would be helpful to have more tests, not only on steel piles, but on pre-cast concrete piles, and drilled shafts.

3 SITE CHARACTERIZATION, AND PRELIMINARY CALCULATIONS

3.1 Geotechnical Site Conditions

The test site for this project is known as the Turrell, Arkansas Test Site (TATS) and is located near, the New Madrid Seismic Zone (NMSZ) in Northeastern Arkansas about 30 minutes northwest of Memphis, Tennessee as shown in Figure 3.1-1. This area was originally investigated by the University of Arkansas in connection with a study static capacity of drilled shafts. The test site is also located within the Mississippi embayment area and as a result has thick layers of clean sand, and silty sand deposits, with a high water table. Due to these factors, the area has a high susceptibility to liquefaction and has experienced liquefaction in the past. The most notable event that caused liquefaction was the New Madrid Earthquake of 1811-1812 in which a series of earthquakes and aftershocks (M_w7.5-7.9) hit the area over a period of 14 months. During this time the area experienced landslides, flow failures and geologic deformations, although structural damage was minimal due to sparse populations at the time.

Prior to this study, soil investigations were performed with personnel from the Missouri Department of Transportation (MoDOT), and the Arkansas State Highway and Transportation Department (AHTD) in conjunction with the University of Arkansas (Race 2015). These investigations included the AHTD conducting standard penetration tests using a standard (30mm diameter) split spoon sampler in all soil deposits (see Figure 3.1-2 and Figure 3.1-3), the MoDOT conducting Cone Penetration Tests (CPT) using a 10 cm^2 cone in all soil deposits (see Figure 3.1-4). In addition, the University of Arkansas conducted unconsolidated-undrained

triaxial compression tests on undisturbed samples of cohesive soil deposits and standard penetration tests using a California split spoon sampler (60mm diameter) in cohesionless soil deposits (see Figure 3.1-5). Seismic data was also obtained by means of a seismic cone penetration test (SPCT) performed by MoDOT. The CPT soundings were performed at the location of the piles (within one to two feet) for this study and are the primary tool for analyzing the soil. Analysis of the SPT results were also performed for comparison purposes. However, it should be noted that the SPT holes were located about 50 feet away from the CPT holes. For reference, the locations of the CPT and SPT holes are shown in Figure 3.1-6. N, C and S are abbreviations for North, Center and South and are used only in the image.

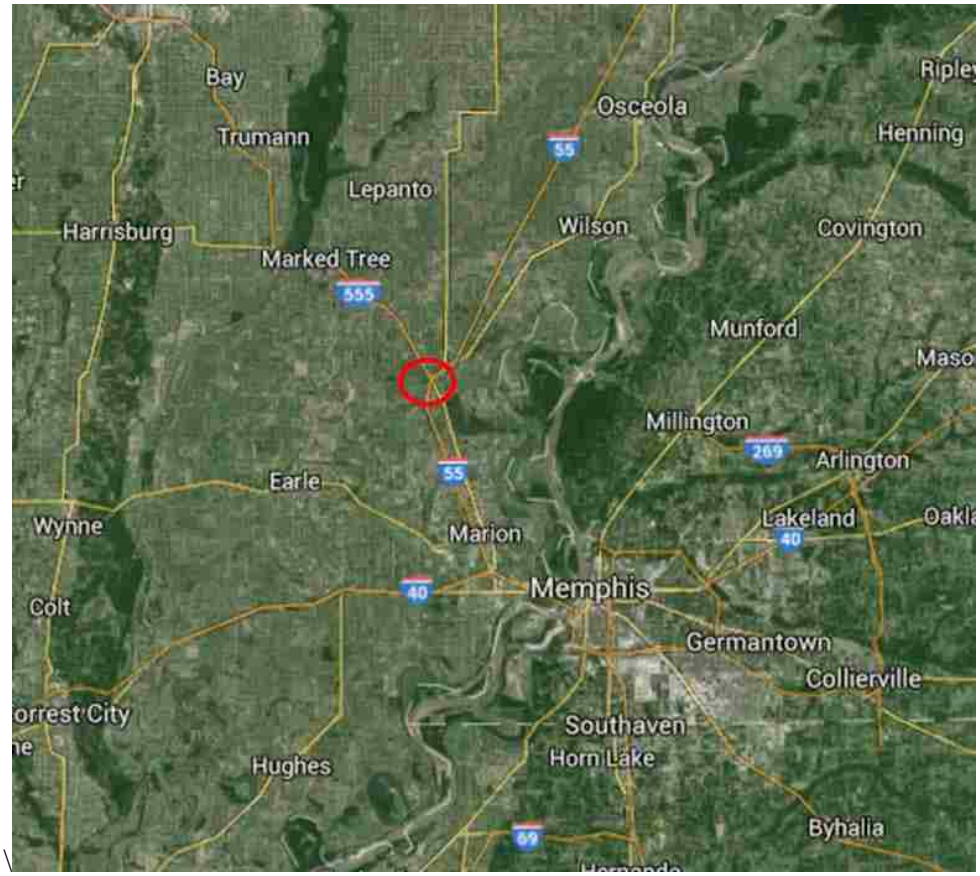

Figure 3.1-1 Location of the Turrell Arkansas Test Site.

Figure 3.1-2 Photo of a student working with a split spoon sampler during SPT testing at TATS field site (Bey 2014).

Figure 3.1-3 Photo of the drill rig for the standard penetration test (SPT) (Bey 2014).

Figure 3.1-4 Photo the Missouri Department of Transportation cone penetration Test (CPT) rig (Bey 2014).

Figure 3.1-5 Photo of the undrained unconsolidated triaxial compression test setup at the University of Arkansas (Race 2015).

Figure 3.1-6 Locations of the SPT and the CPT holes.

Figure 3.1-7 provides plots of the average cone tip resistance, sleeve friction, friction ratio, and pore pressure versus depth profiles obtained from the three CPT tests located near the test piles. One standard deviation boundaries are also plotted in Figure 3.1-7 and the scatter in the data is quite small indicating that the profile is relatively consistent laterally. The CPT averages and standard deviations are based on three CPT's to a depth of 60 feet but only one CPT was available at greater depths. There was no pore pressure data below 60 feet. The non-normalized Soil Behavior Type index, I_c, was calculated by the program CLIQ using equation 3-1 (Robertson 2010) to better identify the soil types in the profile.

$$\mathbf{I_c = [(3.47 - \log Q_t)(\log F_r + 1.22)^2]^{0.5}} \qquad \text{3-1}$$

In this equation Q_t is the normalized cone penetration resistance and is determined from the following equation

$$\mathbf{Q_t = (q_t - \sigma_{vo})/\sigma'_{vo}} \qquad 3\text{-}2$$

where σ_{vo} is the initial vertical total stress and σ'_{vo} is the initial vertical effective stress, and q_t is the total cone tip resistance adjusted for pore water effects using equation

$$\mathbf{q_t = q_c + u_2 * (1 - a)} \qquad 3\text{-}3$$

where q_c is the cone tip resistance, u_2 is the measured pore pressure, and a is the cone area ratio and is equal to 0.8 which is typical. F_r in equation 3-1 is the normalized friction ratio defined as the sleeve resistance f_s divided by the cone tip resistance q_t minus the overburden pressure σ'_{vo}. I_c is plotted as a function of depth in Figure 3.1-8. Generally, the upper 30 feet of the profile is cohesive fine-grained soil while the deeper layers are coarse-grained, cohesionless soils.

Based on the CPT soundings and laboratory tests on samples obtained from conventional borings, an idealized soil profile has been developed as shown in Figure 3.1-7. Generally, the soil profile can be broken down into five layers. The first layer at the surface consists of about 25 feet of high plasticity clay (CH); The clay is underlain by the second layer which consists of about 5 feet of silt to silty clay (ML to CL). The third layer is a poorly graded silty sand (SM) about 10 feet thick. The fourth layer is 20 feet thick and is composed primarily of loose silty sand with an upper dense layer from a depth of 40 to 50 ft and a lower loose sand layer from 50 to 60 feet (SP). At a depth of 60 feet the soil profile transitions into a dense clean sand (SP) which extends to the depth investigated, and this is the fifth layer.

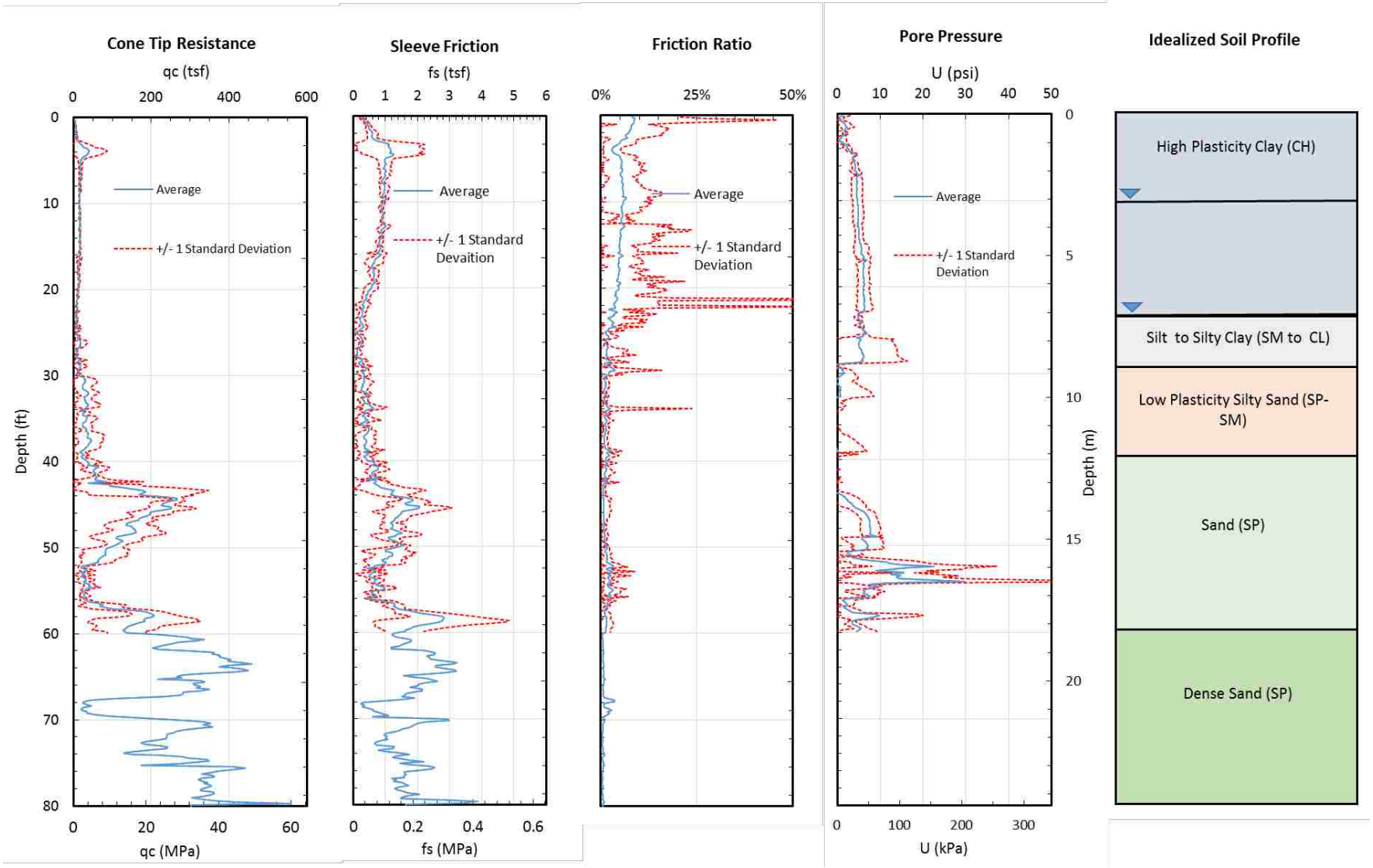

Figure 3.1-7 Plots showing the cone tip resistance, sleeve friction, friction ratio, pore pressure and the idealized soil profile as a function of depth.

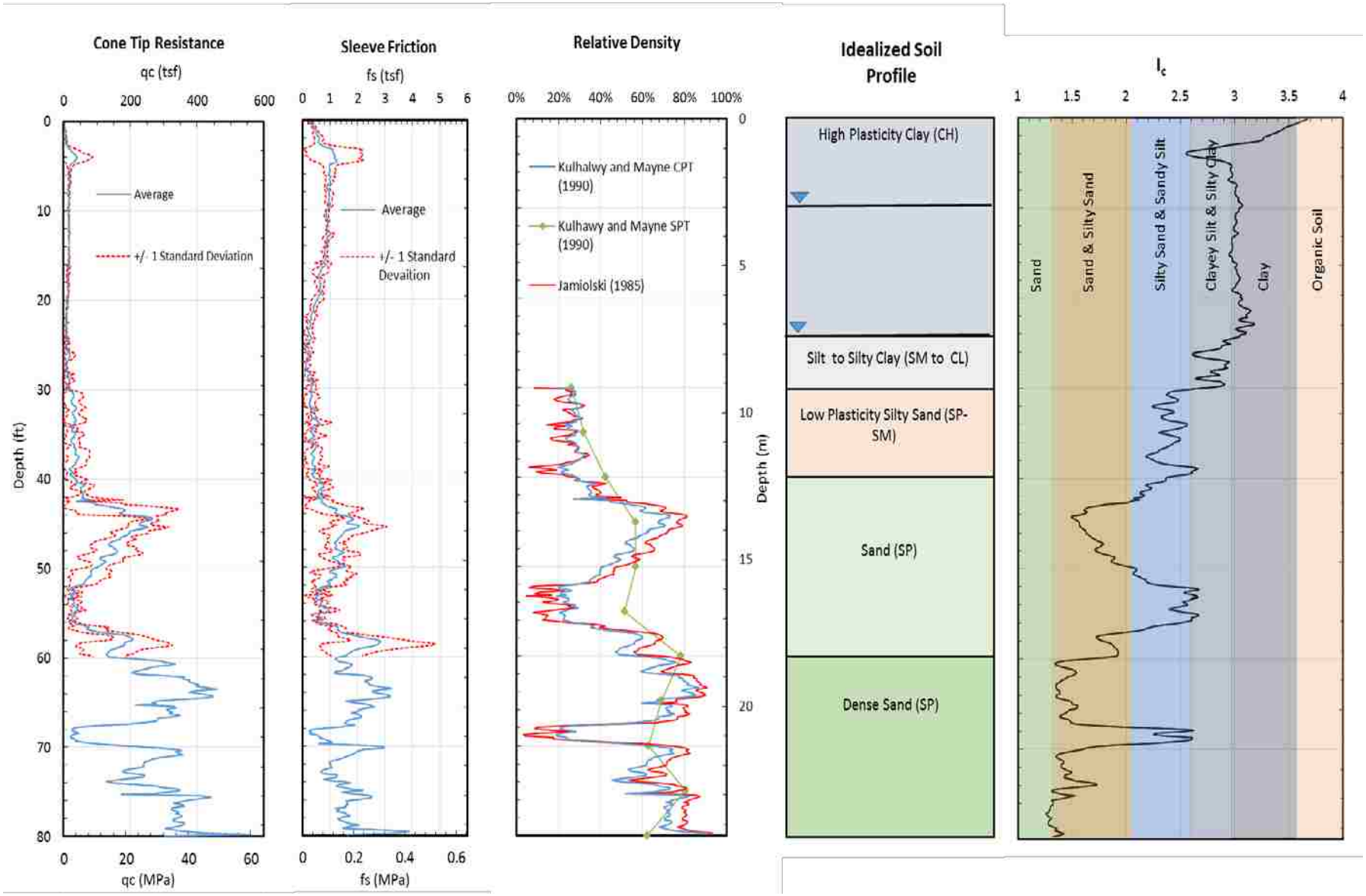

Figure 3.1-8 Plots showing cone tip resistance, sleeve friction, relative density, idealized soil profile, and the soil profile based on the I_{SBT} zones as a function of depth.

The soil profile was originally thought to have a water table of about 10 feet (Race 2015). However, during field investigations it was discovered that the soil profile had two water tables one located at about 10 feet in the clay layer, and one located at a depth of about 25 feet for the sand layer. So, calculations were made such that when dealing with soils in the clay layer a water table of 10 feet was used and when dealing with soils in the sand layers a water table of 25 feet was used. It is important to note that the site is located within the Mississippi River flood plain and the water table fluctuates significantly.

In the sand layers, the relative density (D_r) in percent was calculated using two methods based on the CPT data. The first method developed by Jamiolski et al (1985) computes D_r using the equation

$$\mathbf{D_r}(\%) = -\mathbf{98} + \mathbf{66} * \mathbf{log_{10}}\left(\frac{\mathbf{q_c}}{(\boldsymbol{\sigma_o'})^{\mathbf{0.5}}}\right)$$

3-4

where q_c is the cone tip resistance in t/m^2 and $\boldsymbol{\sigma_o'}$ is the vertical effective stress in t/m^2. In these equations, t is metric tonnes and is equal to 1,000 kg (2205 lb). The second method was developed by Kulhawy and Mayne (1990) and computes D_r using the equation

$$\mathbf{D_r} = \sqrt{\frac{\mathbf{1}}{\mathbf{305}*\mathbf{Q_c}*\mathbf{OCR^{1.8}}}\left[\frac{\frac{\mathbf{q_c}}{\mathbf{p_a}}}{\left(\frac{\boldsymbol{\sigma_o'}}{\mathbf{p_a}}\right)^{\mathbf{0.5}}}\right]} \qquad 3\text{-}5$$

where Qc is the compressibility factor which is assumed to be 1, OCR is the overconsolidation ratio, which is assumed to be 1, q_c is the cone tip resistance in kN/m^2 and σ_o' is the vertical effective stress in kN/m^2 and p_a is the atmospheric pressure in kN/m^2. The atmospheric pressure is assumed to be 100 kN/m^2. In addition, the SPT blow counts from test holes located 55 ft from the test piles were used to compute D_r using the equation

$$\mathbf{D_r} = \left[\frac{(\mathbf{N_1})_{60}}{\mathbf{60}}\right]^{\mathbf{0.5}} \qquad 3\text{-}6$$

developed by Kulhawy and Mayne (1990) where $(N_1)_{60}$ is the SPT blow count corrected for overburden pressure and hammer energy. The relative density profiles from the various holes are provided in Figure 3.1-8. The calculations of the relative densities from the two different CPT methods agree very well with each other, although the Kulhalwy and Mayne (1990) equation provides relative density values that are slightly smaller. The relative density from the SPT is also generally consistent with the calculations based on the CPT data. However, discrepancies are observed at depths of 45 feet, 55 feet and 68 feet. At these depths the CPT provides a relative density that is much smaller than that provided by the SPT data. The difference could be due to differing locations where the tests were taken, or where the fines contents increase suggesting that the CPT is more sensitive to fines than the SPT.

Figure 3.1-9 provides comparison profiles of the CPT cone tip resistance and the SPT blow count along with profiles of the shear wave velocity and unit weight versus depth. Although the SPT blowcount and CPT cone resistance are qualitatively similar in showing low values in the upper cohesive layers and higher values in the deeper granular layers, there is no consistent ratio of $q_c/(N_1)_{60}$ The discrepancies are probably due to differing test locations and the lack of data points from the SPT.

The shear wave velocity (V_s) profile was obtained from the Seismc CPT sounding conducted by MODOT. A V_s below 210 m/s indicates that the sand is loose enough to liquefy if a large enough earthquake were to strike. Almost all of the sand layers have velocities less than 210 m/s except in the dense sand layer at a depth of 45 ft indicating that they are potentially liquefiable.

Unit weights were obtained from three sources. In the cohesive surface layers the unit weight was determined from undisturbed samples obtained with thin-walled shelby tubes. In the sands, the unit weights were derived from correlations with SPT values by Race (2015) and correlations with CPT relative density developed by the US Navy (1982). In addition, total unit weights, γ, were calculated versus depth with the program CLIQ using equation 3-6 developed by Robertson and Cabal (2015)

$$\boldsymbol{\gamma = [0.27 * \log(R_f)] + 0.36 * \left[\log\left(\frac{q_t}{p_a}\right)\right]} \qquad 3\text{-}7$$

where R_f is the friction ratio and q_t is the total cone tip resistance adjusted for pore water effects using Equation 3-3 and p_a is atmospheric pressure.

The three unit weight profiles are similar until a depth of about 30 feet. Once in the sand layer, the CPT based approach predicted consistently higher values than the SPT approach. Once again, this may be due to differing test locations and fewer points from the SPT tests.

Figure 3.2-2 provides plots of I_c, fines content, undrained shear strength and Atterberg limits versus depth. Generally, an I_c greater than 2.6 indicates that a soil is non-liquefiable because of the fines content and plasticity of the soil. Above 30 feet the I_c is considerably above 2.6 as expected. However, below 30 feet the I_c values are generally below 2.6, which means that the soil is susceptible to liquefaction. However from 52 to 56 feet the value is close to 2.6, which means it may not be liquefiable at all. However, 2.6 is not an absolute boundary and sometimes soils around this number are not susceptible and it becomes necessary to look at the fines content and the plasticity index of the soil profile.

The fines content in the upper 30 ft is generally greater than 90%. However, in the sands below 30 ft the average fines content varies from 5 to 10% in cleaner sand layers to 15 to 40% in silty sand layers. Typical fines contents for each of the layers are summarized in

Table 3.1-1. The plasticity index of the surface clay layer is typically between 40 and 50%, while the PI for the underlying silt layer is considerably lower at about 13%. The high plasticity index values at depths above 30 ft indicate that the soil will not liquefy, consistent with the I_c parameter. Unfortunately, Atterberg limits were not performed below 30 feet below ground surface. However, the I_c values indicate that soil types should have a PI of less than 10 below about 30 feet. The potential for liquefaction will be discussed more in subsequent sections of this thesis.

Table 3.1-1 Layer, Symbol, Unit Weight, Fines Content, Plasticity Index, Undrained Shear Strength, Friction Angle and Relative Density

Layer	Symbol	γ (lb/ft^3)	Fines Content	PI	S_u (t/ft^2)	ϕ	D_r (%)
High Plasticity Clay	CH	110	100	45	1.5	-	-
Silt to Silty Clay	(SM to CL)	105	90	10	0.5	-	-
Low Plasticity Silty Sand	(SP-SM)	110	40	-	-	29	25
Loose Sand	(SP)	115	15	-	-	33	40
Dense Sand	(SP)	125	10	-	-	40	80

Undrained shear strength profiles are provided in Figure 3.2-2 from triaxial shear tests as well as correlations from CPT and SPT. The undrained shear strength, s_u, of the upper 30 ft of the profile was calculated using CPT data in the program CLiq with equation 3-7,

$$S_u = \frac{q_t - \sigma_v}{N_{kt}} \qquad 3\text{-}8$$

where σ_v is the total vertical stress and N_{kt} is a paramter equal to 14. Race (2015) predicted the undrained shear strength using empirical values for unconfined compressive strength (qu) based on the corrected blow count (N) of a standard split spoon sampler modified from Vanikar (1986). The undrained shear strength is taken as 1/2 of the unconfined compressive strength. The CPT based strength profile and the results from the s_u correlations from the SPT blowcount from Race (2015) are compared to the test results from the undrained unconsolidated triaxial test results

performed by Race (2015) in Figure 3- 10. All three profiles show a similar pattern with higher undrained shear strength near the surface that decreases with depth. This is likely a result of dessication near the ground surface. The agreement between the undrained shear strength from the CPT and measured shear strength is very good; however, the shear strength from the SPT significantly overestimates the measured strengths until depths of about 20 feet. This suggests that the SPT correlation with undrained shear strength is relatively poor, as might be expected.

3.2 Preliminary Pile Capacity Calculations

With the data that was gathered from the site characterization studies, three different methods were used to calculate axial pile capacity. Two of the methods were performed with CPT data, which are (1) the LCPC method developed by Bustamante and Gianeselli (1982) and updated by Briaud and Tucker (1986), and (2) the Eslami and Fellenius method (1997). The results of these methods were then compared to the methods recommended by FHWA, see Hannigan et al. (2006) using basic soil properties such as friction angle and undrained cohesion.

As discussed subsequently, three test piles were ultimately installed at the site as discussed in Chapter 4. The test piles were a 78-foot long, 18-inch diameter, closed end, pipe pile, a 74-foot long, 18-inch by 18-inch square pre-stressed concrete pile, and a 92-foot long, 14x117 H-Pile. The steel pipe pile was subsequently filled with concrete. All piles were driven until four feet remained above the surface.

3.2.1.1 FHWA Method

The FHWA method uses the undrained shear strength and Tomlinson α (alpha) method in cohesive soils (Tomlinson 1957) and uses Nordland's method based on friction angle, wall friction, and pile displacement in the cohesionless soils. The Tomlinson alpha method in clay

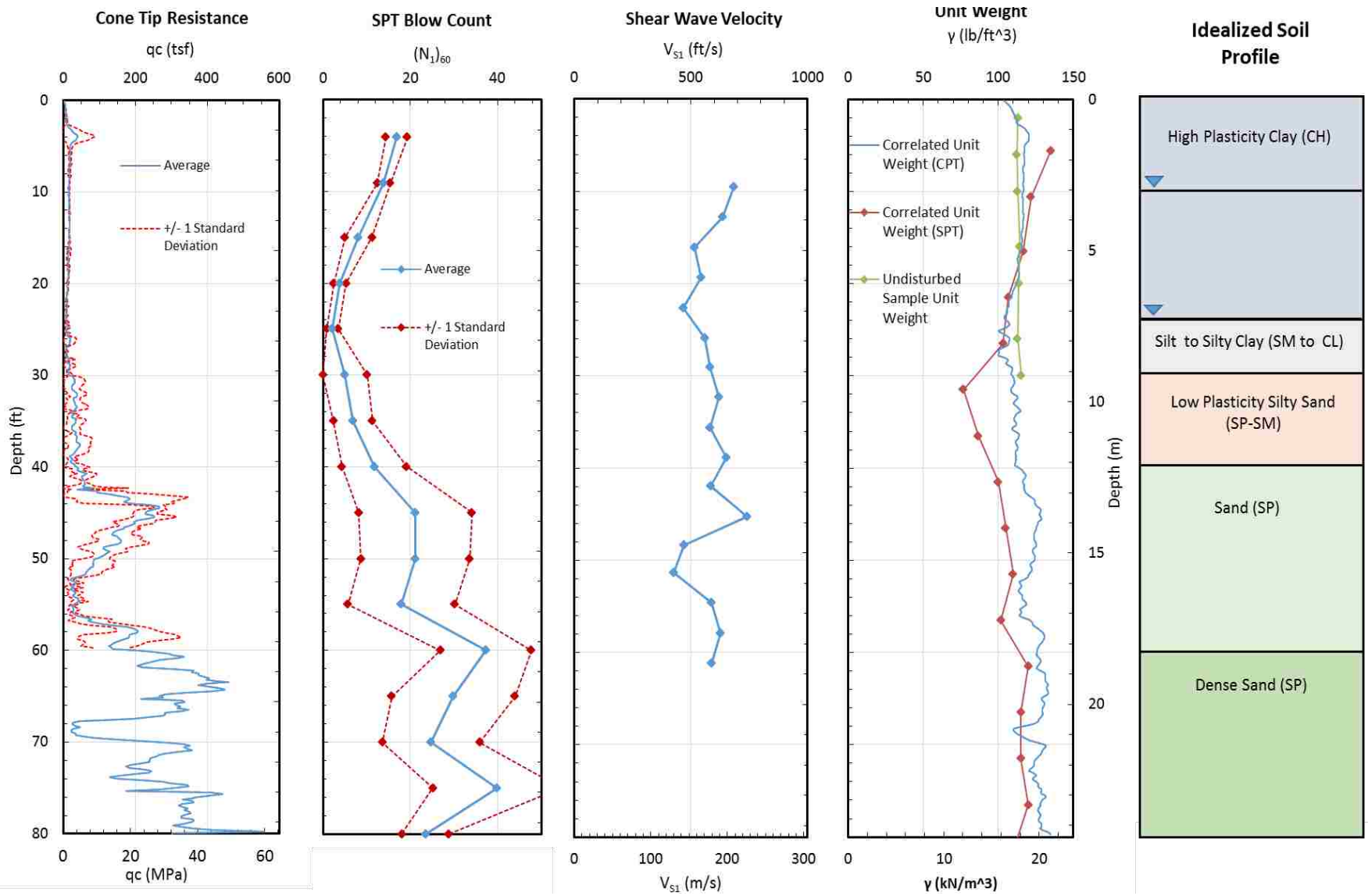

Figure 3.2-1 Plots showing profiles of cone tip resistance, SPT blow count, shear wave velocity, unit weight and the idealized soil profile.

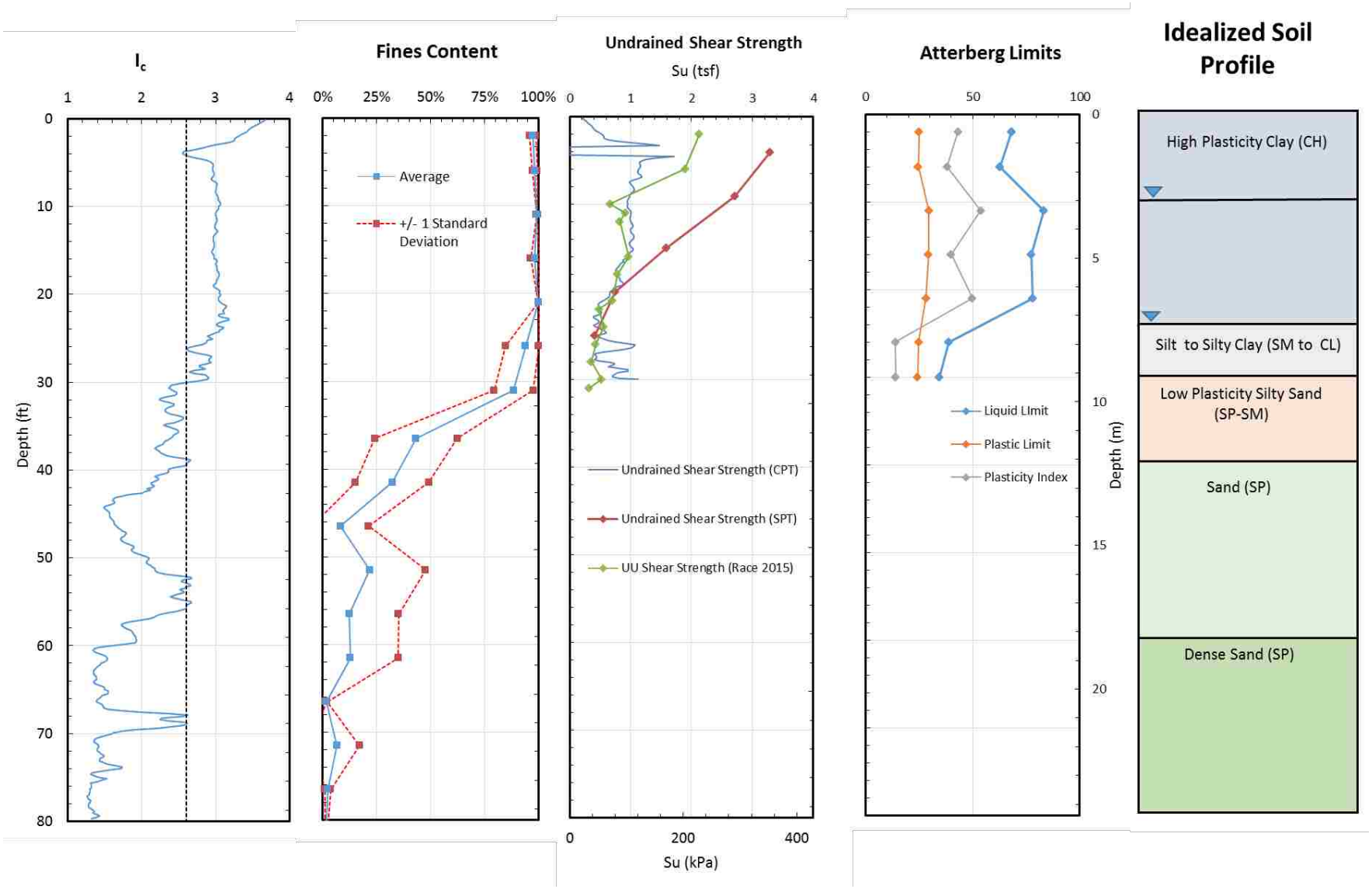

Figure 3.2-2 Plots showing profiles of I_{SBT} parameter, fines content, undrained shear strength, and Atterberg limits, along with the idealized soil profile.

involves determining an adhesion factor, α, based on the undrained shear strength, s_u. This alpha factor is then multiplied by the pile perimeter, the undrained shear strength, and the length of the section of the pile being analyzed. The various increments of the pile are added up to determine the total skin friction with the clay layers along the pile.

The end bearing is determined by multiplying the undrained shear strength of the soil at the toe by an end bearing capacity factor N_c, which is based on the ratio of the length of the pile to the base of the pile and will not exceed 9. It was 9 for all the piles as they were driven through the clay layers.

The skin friction in cohesionless soils was determined by using the Norland method (FHWA 2006). The equation used was the following

$$\mathbf{Q_s = \sum_{z=0}^{D}[K_\delta C_f \sigma_v' \sin \delta \, C_d \Delta z]} \qquad 3\text{-}9$$

where K_δ is a factor that is based on the soil friction angle φ and the volume of soil displaced per foot of driven pile, C_f is a correction factor based on the soil friction angle φ and the friction angle between the pile and the soil, δ. σ_v' is the vertical effective stress, C_d is the perimeter of the pile and Δz is the thickness of the layer of soil that is being evaluated.

The undrained shear strengths that were used were the strengths obtained from the undrained unconsolidated triaxial tests (Race 2015). The unit weights that were used for the FHWA method were the undisturbed unit weights obtained from samples for the clay layer (Race 2015) and the correlated unit weights for the sandy and silty sand layers (Race 2015). Friction angles were used from the calculations performed by Race as well.

The end bearing was calculated using the smaller of the two values predicted by the following two equations.

$$\mathbf{Q_p = \alpha N_q' A_t p_t} \qquad 3\text{-}10$$

$$\mathbf{Q_p = q_l A_t} \qquad \text{3-11}$$

where α is a dimensionless factor dependent on the pile depth-width relationship, N_q' is a bearing capacity factor which is based on the soil friction angle φ near the pile toe, A_t is the pile toe area, p_t is the effective overburden pressure at the pile toe, and q_l is the pile limiting capacity based on the soil friction angle φ near the pile toe. The ultimate capacity of the pile is the sum of the skin friction and the end bearing.

3.2.1.2 Eslami and Fellenius Method

The Eslami and Fellenius (1997) is a direct method of calculating shaft capacity and end-bearing using direct correlation with the cone tip resistance. The cone tip resistance is first transformed into the effective cone resistance q_E by subtracting the pore pressures, u_2, from the total cone tip resistance, q_t. The toe resistance is calculated by taking a geometric average of the q_E parameter over a zone extending from 8B above the toe when the pile goes from a weak soil to a dense soil or 2B above the pile toe when going through a dense soil to a weak soil to 4B below the toe of the pile. This results in the parameter q_{Eg} which is the geometric average of the cone point resistance over the influence zone after correcting for pore pressure and adjustment to effective stress. The value of q_{Eg} is then multiplied by the toe correlation coefficient, C_t, which is 1.0 to obtain the end-bearing pressure. Finally, the end-bearing pressure is multiplied by the area of the pile base resulting in the end bearing force.

The skin friction in the Eslami and Fellenius (1997) method is calculated in a similar manner. The effective cone resistance is calculated for each interval of cone data and multiplied by C_s, which is the shaft correlation coefficient. This coefficient is based on the soil type. The total skin friction force is then calculated by summing up the values of q_E times C_s at each CPT

interval, multiplied by the perimeter of the pile and pile length of the interval. For the H-Pile the perimeter of the square the H-Pile would make if it was solid was used for calculating skin friction assuming that the pile would plug during driving.

The CPT data collected before the design of the piles only extended down to 80 feet, while the SPT data extended down to 100 feet. Due to the lack of data from the CPT, the average of the last 6 feet of available data was taken and used for the parameters needed at depths greater than 80 feet. The extrapolated parameters were cone tip resistance and pore pressure.

3.2.1.3 LCPC Method

Also known as the French method, the LCPC method (Bustamante and Gianeselli, 1982; Briaud and Tucker, 1997) involves taking a mean of the tip resistance around the pile toe and calculating an end-bearing resistance. The end bearing is calculated by taking an average of the q_c in a zone extending 4B above the pile toe and 4B below the pile toe. This is then multiplied by an end bearing coefficient, k_c. The end bearing coefficient is determined by the type of soil and by pile type. This results in q_p, which is the end bearing pressure. The end bearing force is simply the end bearing press multiplied by the area of the pile toe.

Skin friction in the French method is calculated by taking the q_c value at each CPT reading and dividing it by an α_{LCPC} (alpha) factor that is specific to the LCPC method. The α_{LCPC} is determined based on the soil that surrounds the pile at this depth, and the pile type, the resulting value is f_p. Maximum f_p values are also found based on soil and pile type. These maximum values can change drastically in clay soils surrounding piles if the pile is given time to set up. Therefore, if test data is available, there is an exception written in the method that allows the engineer to use the higher values of f_{pmax} if test data is available. So, the skin friction of all the piles was calculated two ways with the LCPC method, one with the lower f_{pmax} in the clay

layer and one with the higher f_{pmax} in the clay layer. The lower f_{pmax} is designated as LCPC method low f_{pmax}, and the higher f_{pmax} value will be designated as LCPC method in the tables and figures presented subsequently. To get skin friction as a load the f_p value is multiplied by the perimeter and length of the pile. Once again, the perimeter of the H-Pile used in calculation was the perimeter of the square the H-Pile would make if it was solid assuming that the pile would plug during driving. Also, values of cone tip resistance had to be extrapolated for depths greater than 80 feet.

3.2.2 Pile Capacity Results

The first two figures (Figure 3.2-3 and Figure 3.2-4) compare the cumulative side friction and the ultimate capacity versus depth. Each chart provides results comparing the three design methods for one pile type. In contrast, the two subsequent figures (Figure 3.2-5 and Figure 3.2-6) compare the side friction and ultimate capacity versus depth, however, each chart compares the results for three different piles for one method.

When comparing the different methods for the same pile, shown in Figure 3.2-3, we see that the predicted skin friction values are generally quite consistent for the different methods for the pipe pile and the concrete square pile. The H-Pile also has similar predicted skin friction values for the LCPC method and the Eslami and Fellenius methods. However, the FHWA predicted skin friction value was much higher than the other two methods. This is probably due to the s_u values being determined by undrained unconsolidated triaxial tests, the results of which seemed high. The lowest value of side friction reported for every pile was the LCPC method when the lowest design curve was used in the absence of test data. This result is expected, as the lowest curve is meant to give conservative predictions in the face of uncertainty.

The ultimate capacity versus depth curves predicted for each pile with different methods, are shown in Figure 3.2-4. When end-bearing resistance is added to obtain the ultimate resistance versus depth, the FHWA and the LCPC methods are generally close for all three test piles. In contrast, the Eslami and Fellenius method predicts ultimate capacities that are much higher than the other methods, due to the higher predicted end-bearing values. Even though the Eslami and Fellenius method gave skin friction values that were similar to the other methods, the end bearing values were so large, that the ultimate capacity predicted using this method is also quite large. The FHWA method and the LCPC method give similar predicted ultimate capacities of the piles and were within 50 kips of each other for the H-pile and the pipe pile. The LCPC method with the conservative maximum skin friction once again predicted the smallest ultimate capacities and was quite a bit smaller for the H-pile and the pipe pile than the other methods. However, even though it was still the smallest, it was only 20 kips smaller than the FHWA method for the concrete pile. Comparisons of the skin friction, end-bearing and total pile capacities for each design method and each pile type are summarized in Table 3.2-1.

Table 3.2-1 Skin Friction, End Bearing, and Total Pile Capacity Computed Using the FHWA Method, Eslami and Fellenius Method, and LCPC Method

	FHWA Method		
	Skin Friction	End Bearing	Total Pile Capacity
Pipe Pile	476	258	735
Concrete Square Pile	601	85	686
H-Pile	948	77	1025

	Eslami and Fellenius Method		
	Skin Friction	End Bearing	Total Pile Capacity
Pipe Pile	435	833	1268
Concrete Square Pile	505	932	1437
H-Pile	642	861	1503

Table 3.2-1 Continued

	LCPC Method		
	Skin Friction	End Bearing	Total Pile Capacity
Pipe Pile	431	349	780
Low f_{pmax}	200	349	549
Concrete Square Pile	447	406	852
Low f_{pmax}	240	406	646
H-Pile	580	389	969
Low f_{pmax}	225	389	613

The comparisons of the cumulative side friction for various piles for each design method are shown in Figure 3.2-5, while comparisons of the total pile capacity for various piles for each method are shown in Figure 3.2-6. For the FHWA method the curves are close for all pile types. This makes sense as the methods do not vary according to pile type, if the H-pile is assumed to plug, because the pile geometries are similar. The Eslami and Fellenius method also has little variation between pile types, for the same reason, that is the method does not consider pile type. It does consider the effective cone resistance, which is a function of the normalized cone tip resistance adjusted for the pore pressure, which makes the pile capacities even more uniform. The LCPC method has larger variation between piles, and this makes sense, because the LCPC method does take into consideration the pile type as well as the method of installation.

The comparison of the total or ultimate capacity for various piles for a given design method on one chart is provided in Figure 3.2-6. The FHWA method once again has ultimate capacities that are very similar. Once again, the differences seem to only be geometry of the pile. As the end bearing values were added with depth. The end bearing values for the H-Pile and the concrete square pile are similar, while the pipe pile has a much larger value. This is because the

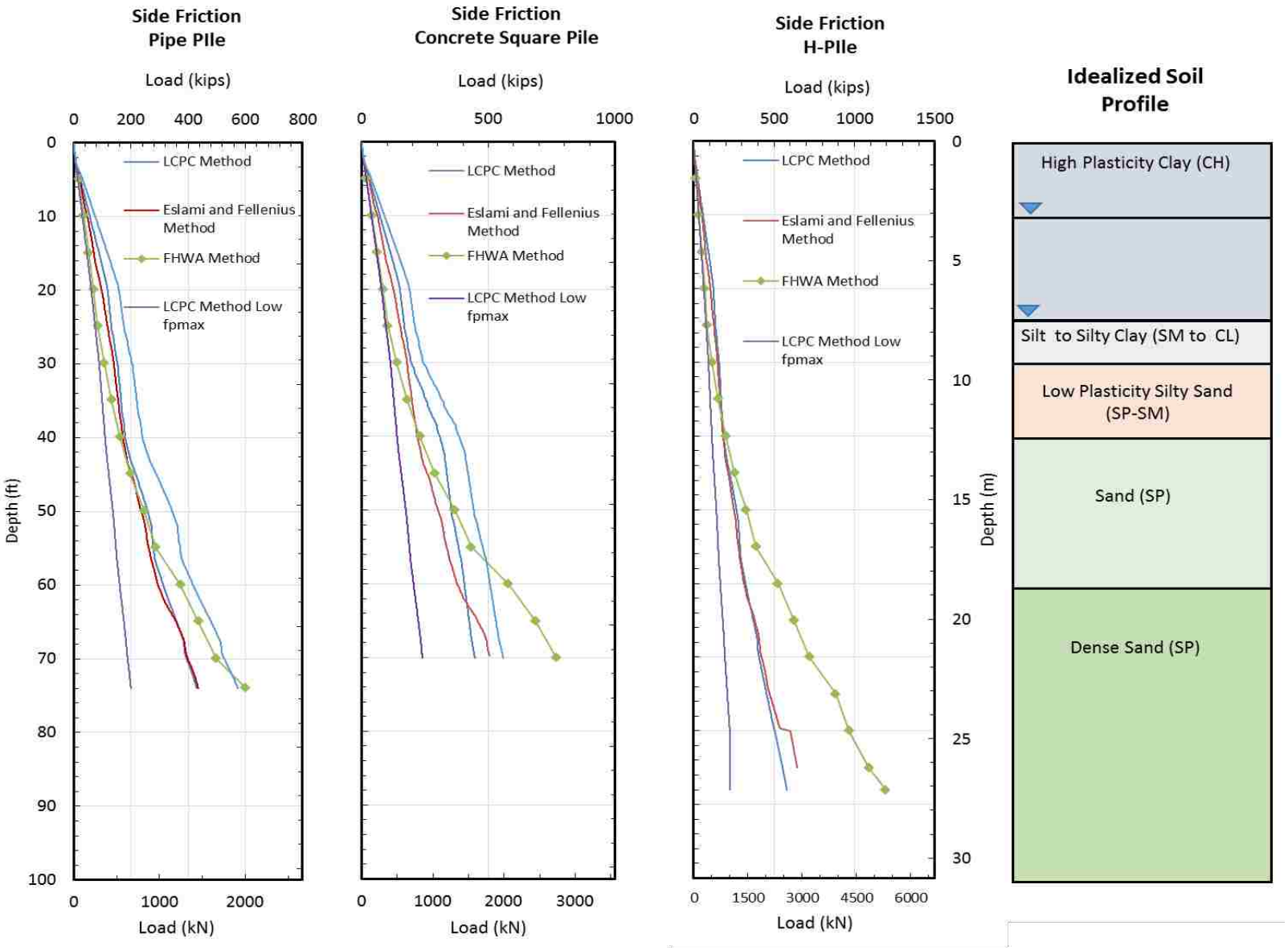

Figure 3.2-3 Charts comparing cumulative skin friction resistance for each pile based on the three methods of calculation used.

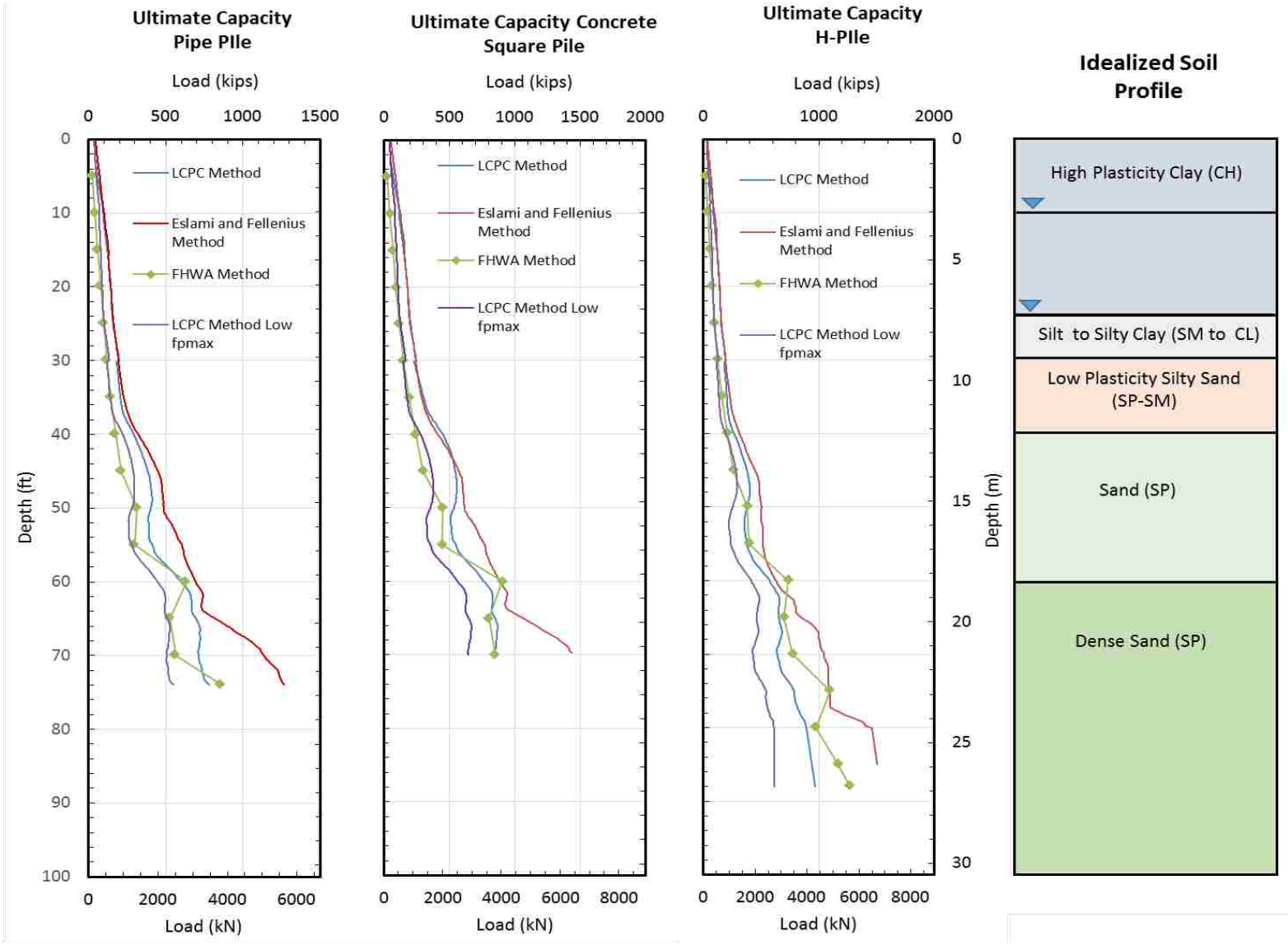

Figure 3.2-4 Charts comparing the ultimate capacity for each pile based on the three methods of calculation used.

pipe pile terminates in a denser stratum of soil, according to the SPT data. The H-pile and concrete square pile would both have much higher end bearing capacities if they ended at the same depth as the pipe pile. This can be determined by subtracting the skin friction from the ultimate capacity at that depth.

The Eslami and Fellenius method predicts very similar values for skin friction and for end bearing capacity for the various piles. This occurs because the method does not explicitly take the pile type into account, like the FHWA method. The end bearing capacities are very similar in all cases. They are only based on the area of the pile and the surrounding soil 4B below the pile and 8B above the pile. The geometric mean of the CPT cone tip resistance for the soil is taken so the toe capacities become more uniform. The soil surrounding the tips of the concrete pile and the pipe pile are similar, and the soil surrounding the H-pile tip is the extrapolation of the soil surrounding the other piles, so there will be little variation from the soil type. Thus, the main difference for ultimate capacity in this method would be the area of the pile toe.

The largest variation between piles comes from the LCPC method. Once again this is because the LCPC method considers the pile type where the other methods do not. The H-pile and the pipe pile are similar; however, the concrete pile is much different. This is because the LCPC method has slightly different parameters for a concrete pile. This would make sense because concrete is rougher and would have more friction generated between the pile and the soil. The end bearing capacities of the piles are similar, and the primary difference between toe capacity is due to the surface area. Because the soil effects are averaged out 4B above the pile type and 4B below, the soil does not play a large factor in the different pile capacities.

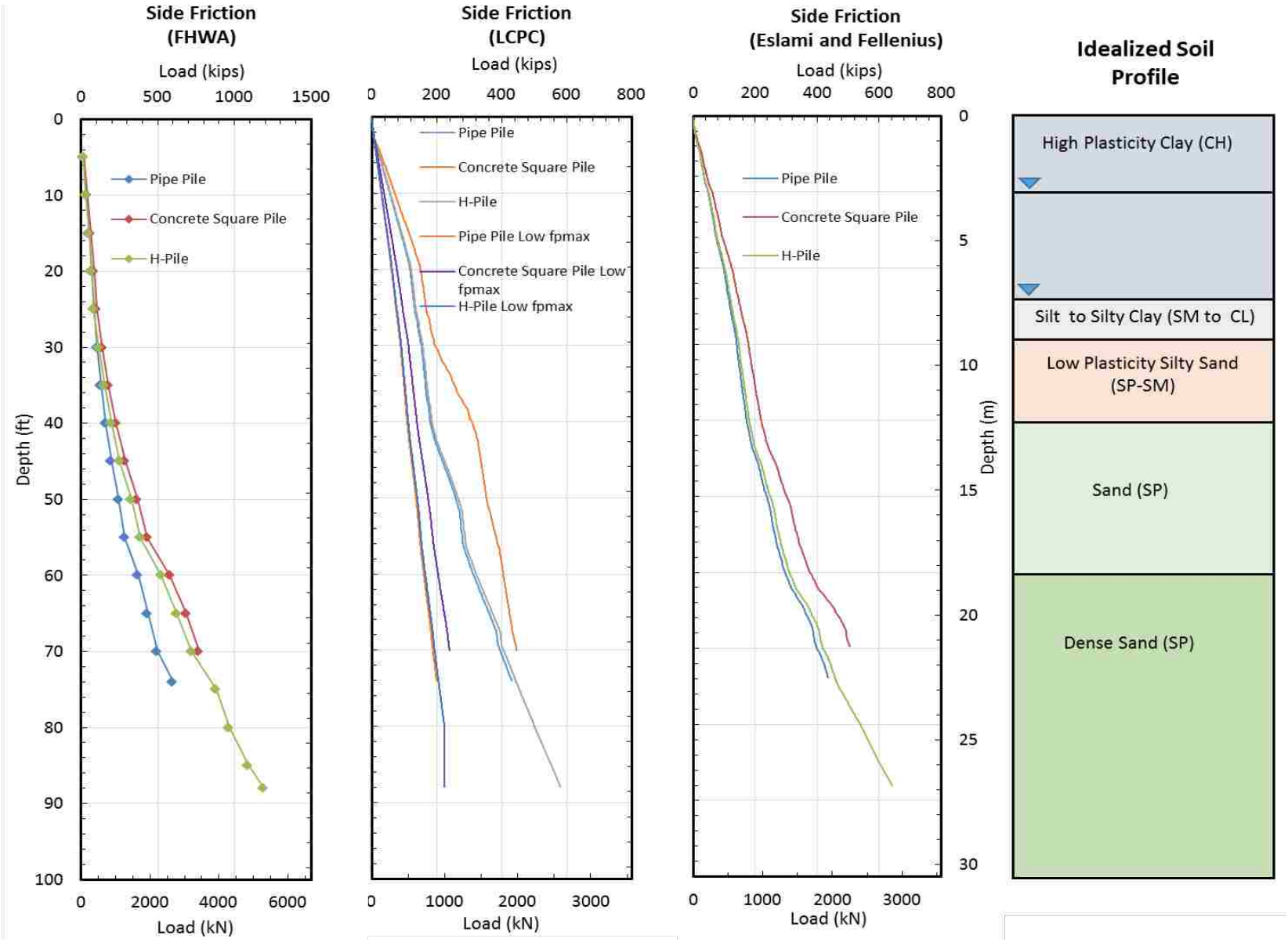

Figure 3.2-5 Charts comparing the expected side friction based on the LCPC method, the Eslami and Fellenius method, and the FHWA method.

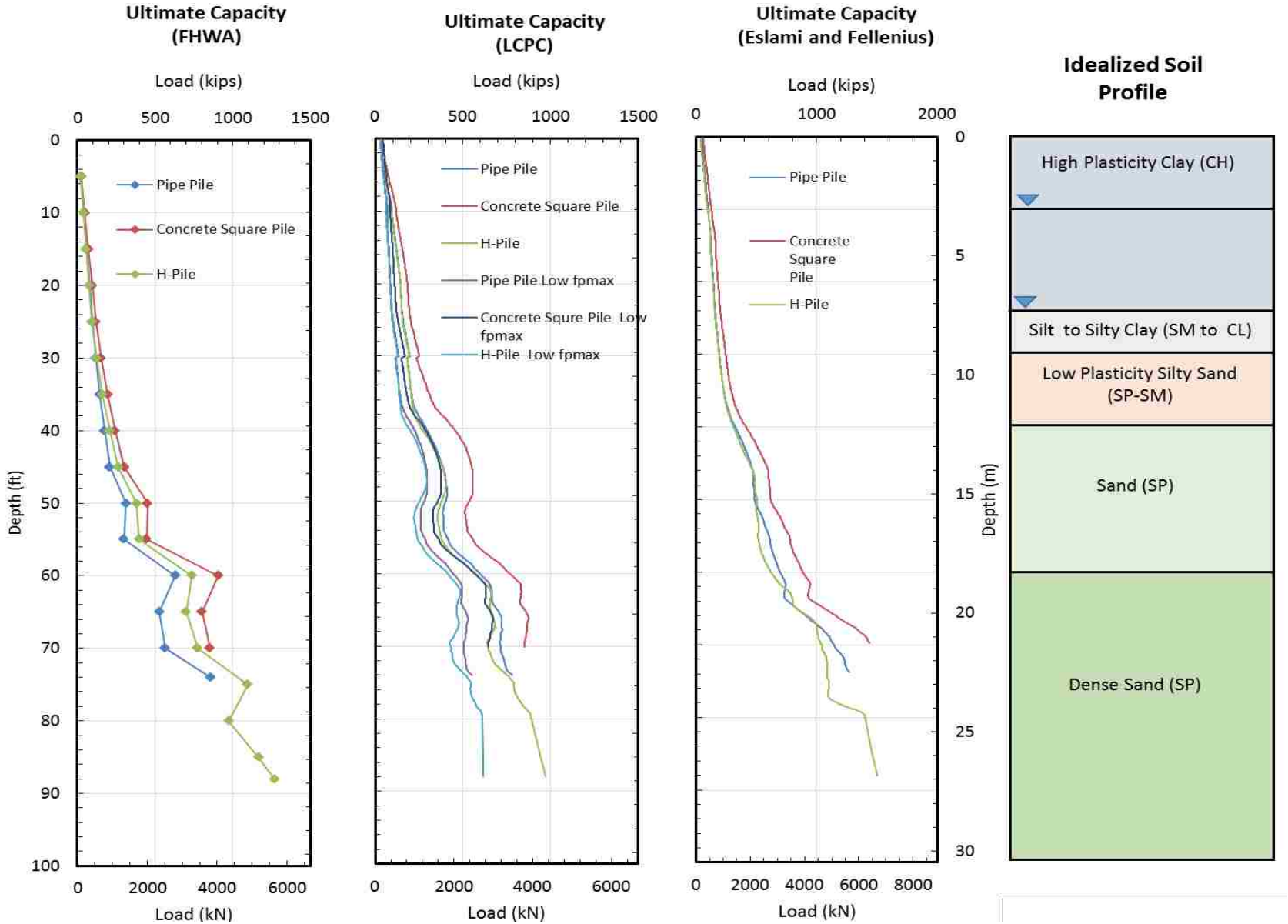

Figure 3.2-6 Charts comparing expected ultimate capacity based on the LCPC method, the Eslami and Fellenius method, and the FHWA method.

3.2.3 Preliminary Liquefaction and Settlement Calculations

Liquefaction occurs when the excess pore pressure produced by earthquake shaking equals the vertical effective stress. The progress towards liquefaction can be expressed using an excess pore pressure ratio, R_u defined by the equation where Δu is the excess pore pressure

$$Ru = \frac{\Delta u}{\sigma'_o} \qquad 3\text{-}12$$

above the static water pressure and σ'_o is the initial vertical effective stress prior to shaking. R_u becomes equal to 1.0 when the soil liquefies. As described previously, liquefaction is known to occur in sands and silty sands similar to those in the soil profile found at the TATS. Liquefaction, and settlement from liquefaction cause significant damage during earthquakes. Many engineers have developed methods to calculate the factor of safety against liquefaction, as well as the amount of settlement. In this experiment, settlement due to liquefaction is important to see downdrag loads form on the driven piles.

The factor-of-safety (FS) against liquefaction is defined by the equation

$$\mathbf{FS} = \frac{\mathbf{CRR_{M=7.5}}}{\mathbf{CSR_{M=7.5}}} \qquad 3\text{-}13$$

where CSR is the cyclic stress ratio or the average cyclic shear stress generated by an earthquake and CRR is the cyclic resistance ratio, which is a measure of liquefaction resistance. It should be noted that the 7.5 subscript means the calculations are performed for an earthquake with a magnitude of 7.5. The soil is expected to liquefy when the factor of safety against liquefaction, is less than one (Youd et. al. 2001).

Using the simplified method originally developed by Seed and Idriss (1971), the CSR is typically computed using the equation

$$\mathbf{CSR = 0.65 * \frac{\tau_{av}}{\sigma_{vo}} = 0.65 * \left[\frac{a_{max}}{g}\right] * \left(\frac{\sigma_{vo}}{\sigma'_{vo}}\right) * r_d} \qquad 3\text{-}14$$

where r_d is the depth factor, a_{max} is the peak horizontal acceleration at ground surface, g is the acceleration of gravity, σ_{vo} is the total overburden stress, and σ'_{vo} is the effective overburden stress. CRR was computed using two methods. The first was a method presented by Idriss and Boulanger (2010) in which CRR is given by the equation

$$\mathbf{CRR_{M=7.5}} = \mathbf{exp}\left(\frac{(N_1)_{60cs}}{14.1} + \left(\frac{(N_1)_{60cs}}{126}\right)^2 - \left(\frac{(N_1)_{60cs}}{23.6}\right)^3 + \left(\frac{(N_1)_{60cs}}{25.4}\right)^4 - 2.8\right) \quad \text{3-15}$$

where $(N_1)_{60cs}$ is the SPT blow count normalized to an overburden pressure of 1 ton/ft^2 (atmospheric pressure) and adjusted for a hammer energy of 60%, and to clean sand conditions.

The second method for computing CRR was originally developed by Robertson and Wride (1998) and is based on the normalized cone tip resistance and is given by the equation

$$\mathbf{CRR_{M=7.5}} = 0.833 * \left[\frac{Q_{tn,cs}}{1000}\right]^3 + 0.05$$

3-16

where $Q_{tn,cs}$ is the normalized cone tip resistance adjusted for pore pressures and clean sand conditions. The liquefaction analysis for the CPT results was performed using the computer program CLiq developed by (Robertson and Cabal 2015).

The results of the liquefaction factor of safety calculations are presented in Figure 3.2-7. In each method, the factor of safety against liquefaction was computed assuming a peak ground acceleration of 0.64 g produced by a magnitude 7.5 earthquake. These seismic inputs were chosen for this project based on the region's past seismic history. The method proposed by Idriss and Boulanger (2010) indicates that sand will liquefy from 35 to 55 feet, in a magnitude 7.5 earthquake. It is important to note, however, that these simplified procedures become less applicable below depths of about 40 feet.

The Robertson and Wride (1998) method predicted consistent liquefaction from 30 feet to 50 feet, with a few thin layers where liquefaction would not occur. Generally, liquefaction is not

predicted from 50 to 60 feet. The Robertson and Wride (1998) approach also suggests that liquefaction may occur in small lenses from 20 feet to 30 feet, however, these are layers where the soil exhibits claylike behavior and will not liquefy in the traditional sense because they are too plastic. Therefore, based on the results from the two different methods it is expected that the zone from 30 to 50 feet is susceptible to liquefaction for a large magnitude earthquake. It should be noted; however, that the soil profile from 30 to 40 feet is a silty sand, so it is possible that some of the soil at that depth range may not liquefy if the plasticity index of the fines is too high and went undiscovered based on limitations of field and lab testing. It should also be noted that these calculations are based on a 7.5 magnitude earthquake and explosives may not fully simulate the effects of a large earthquake. As a result, the zone of liquefaction for the blast testing contemplated in this study will likely be smaller than for an earthquake.

After calculating the liquefaction potential, the total settlement was calculated using a method by Tokimatsu and Seed (1987) based on the SPT blow count and a method presented by Zhang, Robertson, and Brachman (2002) based on CPT test results. These methods use correlations to compute the post-liquefaction volumetric strain in each layer, ε_{vi}, and then the total settlement, S, is summed up for the entire profile using the equation

$$\mathbf{S} = \sum_{\mathbf{i}}^{\mathbf{j}} \boldsymbol{\varepsilon}_{\mathbf{vi}} \mathbf{\Delta z_i}\, \mathbf{DF_i} \qquad 3\text{-}17$$

where Δz is the layer thickness, i is the layer being analyzed and j is the total number of layers. In both these methods the settlement was reduced using a depth weighting factor, DF, proposed by Cetin et al. (2009) shown in equation 3-16 where the depth weight factor is given by the equation 3-17.

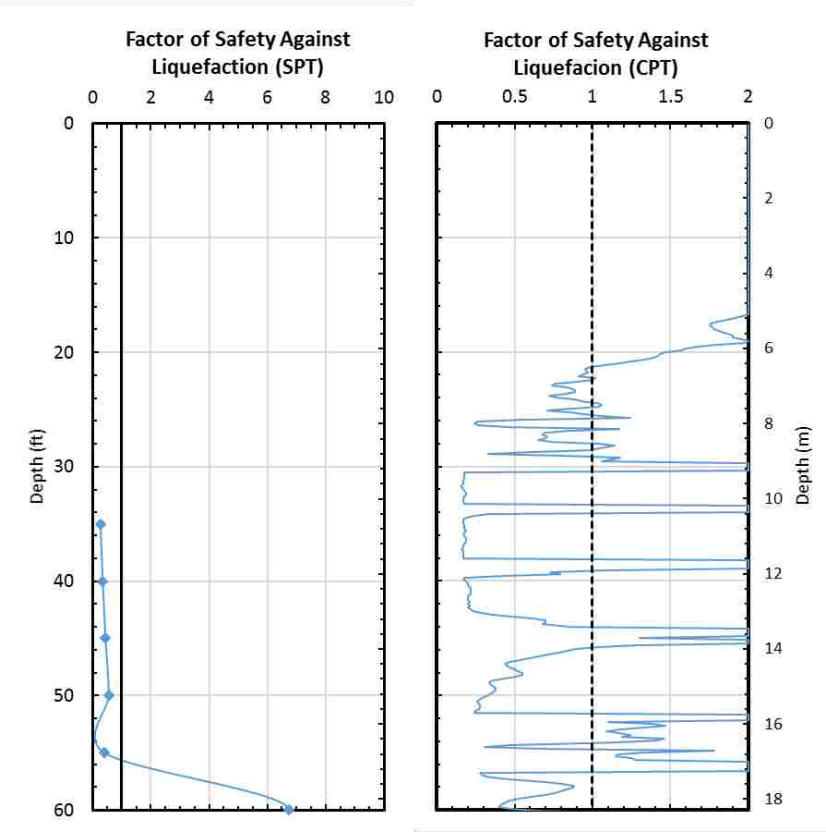

Figure 3.2-7 Plots showing the factor of safety against liquefaction with depth for both the SPT-based Idriss and Boulanger (2010) method and the CPT-based Robertson & Wride (1998) method.

$$DF = 1 - \frac{d}{18} \qquad 3\text{-}18$$

where d is the depth below the ground surface in meters.

The total expected settlement for a moment magnitude 7.5 earthquake and a peak ground acceleration of 0.64 g. was predicted to be about 7.1 inches using the SPT based approach while the settlement calculated using the CPT data in the program CLiq with the same seismic parameters was 7.5 inches. Assuming a liquefied layer thickness of about 20 feet, this amounts to an average volumetric strain of approximately 3%.

Once again, these calculations were made assuming a magnitude 7.5 earthquake with a peak ground acceleration of 0.64g. Explosives, however, do not necessarily reproduce an

earthquake of this magnitude and may not liquefy the same volume of soil that an earthquake would liquefy depending on the charge weight and charge location.

3.2.4 Preliminary Blasting and Blasting Calculations

A preliminary blast experiment was performed at the Turrel Arkansas Test Site in May of 2015 to determine how susceptible the soils would be to liquefaction during blasting. Unfortunately, the test blast area was located some distance away from where the full-scale blasting testing around the piles later took place and CPTs in this area indicated that the sand was significantly denser than the sand in the final test area. A total of 12 pore pressure transducers embedded into cone tips were installed at depths of 25, 31, 37, 43, 49, 59, and 67 and 79 ft at the center of the test area to monitor the generation and dissipation of excess pore pressures. Because of the density of the sand below about 43 feet it was often necessary to hammer the cone tips into the ground.

A total of 16 charges were placed in 8 blast holes located around the periphery of a circle of with an approximate radius of 26.5 feet (8.07 meters). In each blast hole, there were two decks of explosives, one at a depth of 38.1 feet (11.6 meters), and one at a depth of 47.9 feet (14.6 meters). The weight of each blast charge was 2 pounds. The blasts were detonated one at a time around the bottom ring with a delay of 500 milliseconds followed by sequential detonation of the charges in the upper ring. Three of the upper charges failed to detonate.

Excess pore pressure generation was minimal in the cohesive layers above 30 ft and in layers below 50 feet as anticipated. However, within the target zone from 30 to 50 ft, liquefaction (R_u = excess pore pressure ratio = $\Delta u/\sigma'_o = 1.0$) was only achieved at a depth of 37.1 feet (11.3 meters). Excess pore pressure ratios of 45 and 30%, were achieved at depths of 31 and 43 feet, respectively.

To produce a thicker zone of liquefaction at the site, a correlation equation developed by Eller (2011) was used to predict the excess pore pressure ratio (R_u) as a function of charge weight, SPT blowcount and vertical effective stress. According to Eller (2011), R_u can be computed using the equation

$$R_{u_{multipe_{log}}} = 1.747 - 0.512 \ln\left(\frac{R}{W^{0.33}}\right) - 0.032(N_1)_{60} - 0.002\sigma'_{vo} \text{ (kpa)} \qquad 3\text{-}19$$

where R is the distance from the charge to the point of interest in m, W is the sum of all the charge weights in kg, $(N_1)_{60}$ is the normalized SPT blowcount defined previously, and σ'_{vo} is the initial vertical effective stress at the depth of interest in kPa. Based on equation 3-18 and a radius of the blast charges of 6.5 meters, two blast charges totaling 6.5 pounds (3 kg) in each blast hole, for a total weight of 52 pounds (23.6 kg) would be needed to create an R_u of 1.0 for a blowcount of 8 at a vertical effective stress of 100 kPa (a depth of 35 feet). R_u versus scaled distance is shown in Figure 3.2-8.

Unfortunately, 6.5 pounds of explosives per charge is so large that concerns about soil heaving, damage to pore pressure transducers, and damage to pile strain gauges become concerns. As a compromise, a charge weight of 4.5 pounds per blast was chosen (2.04 kg) and then analyzed as a maximum charge size that would not likely cause heave or instrumentation damage, based on past experience. Using equation 3-16 again an excess pore pressure versus depth profile was developed using a charge weight of 4.5 pounds (2.05 kg) at distance of 6.5 meters from the explosive to the piezometer, and correlated N values from CPT q_c based on a correlation by Robertson and Cabal (2015) see Figure 3.2-9.

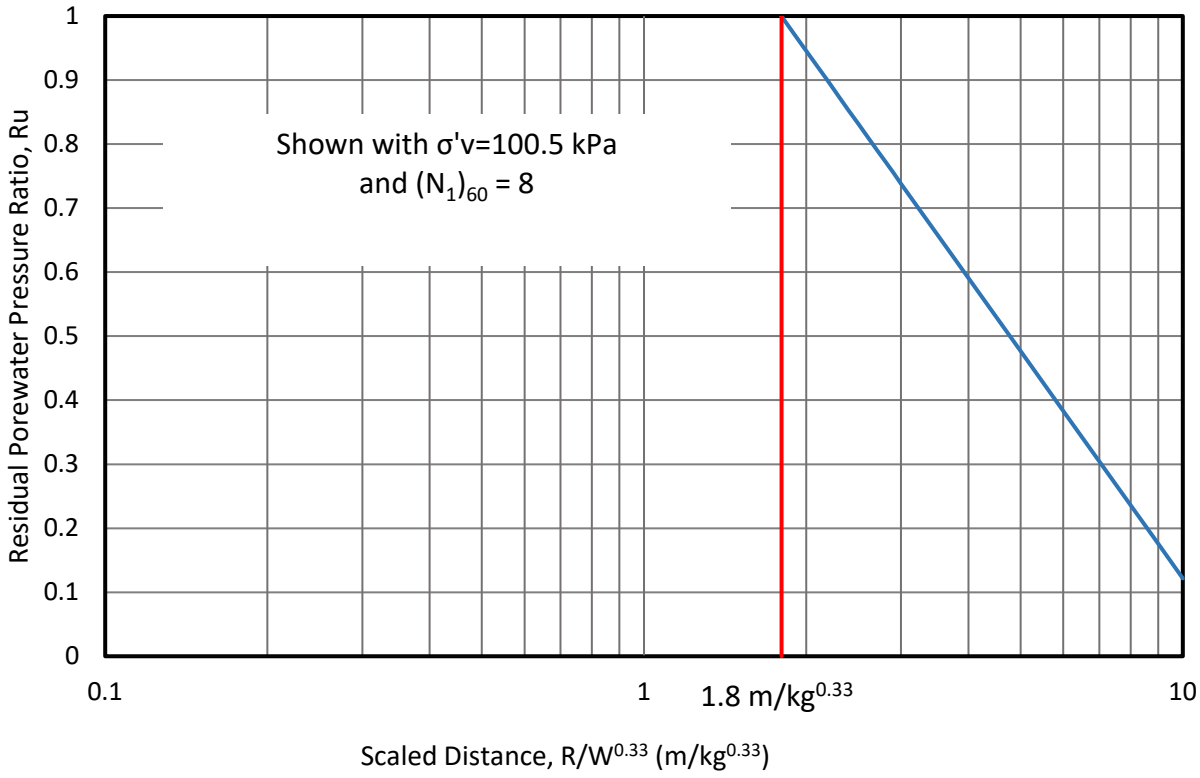

Figure 3.2-8 The scaled distance versus residual pore water pressure.

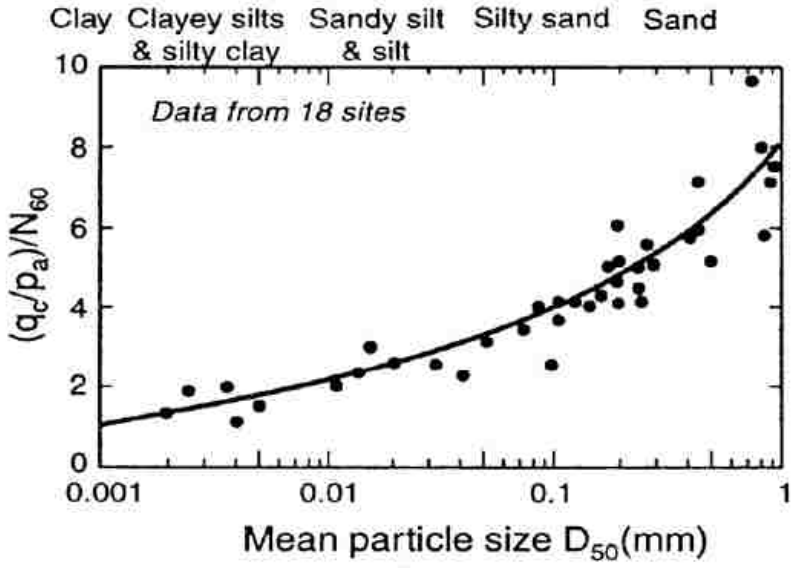

Figure 3.2-9 Correlation between Soil type, mean particle size and the ratio $(q_c/p_a)/N_{60}$, see Robertson and Cabal (2015).

Figure 3.2-10 provides a plot of the predicted R_u versus depth profile for the 4.5 lb charge case. The predicted excess pore ratios are greater than 0.9 from 30 to 40 feet (9.1 to 12.2 meters). These values are not quite 1.0 however the soil has essentially liquefied for practical purposes at values greater than about 0.8. Below 40 feet, the R_u values drop below 0.8 and do not surpass this value again. The decrease in R_u with depth is a result of the combination of increased vertical stress, increased soil penetration resistance and increased distance from the blast charge with depth.

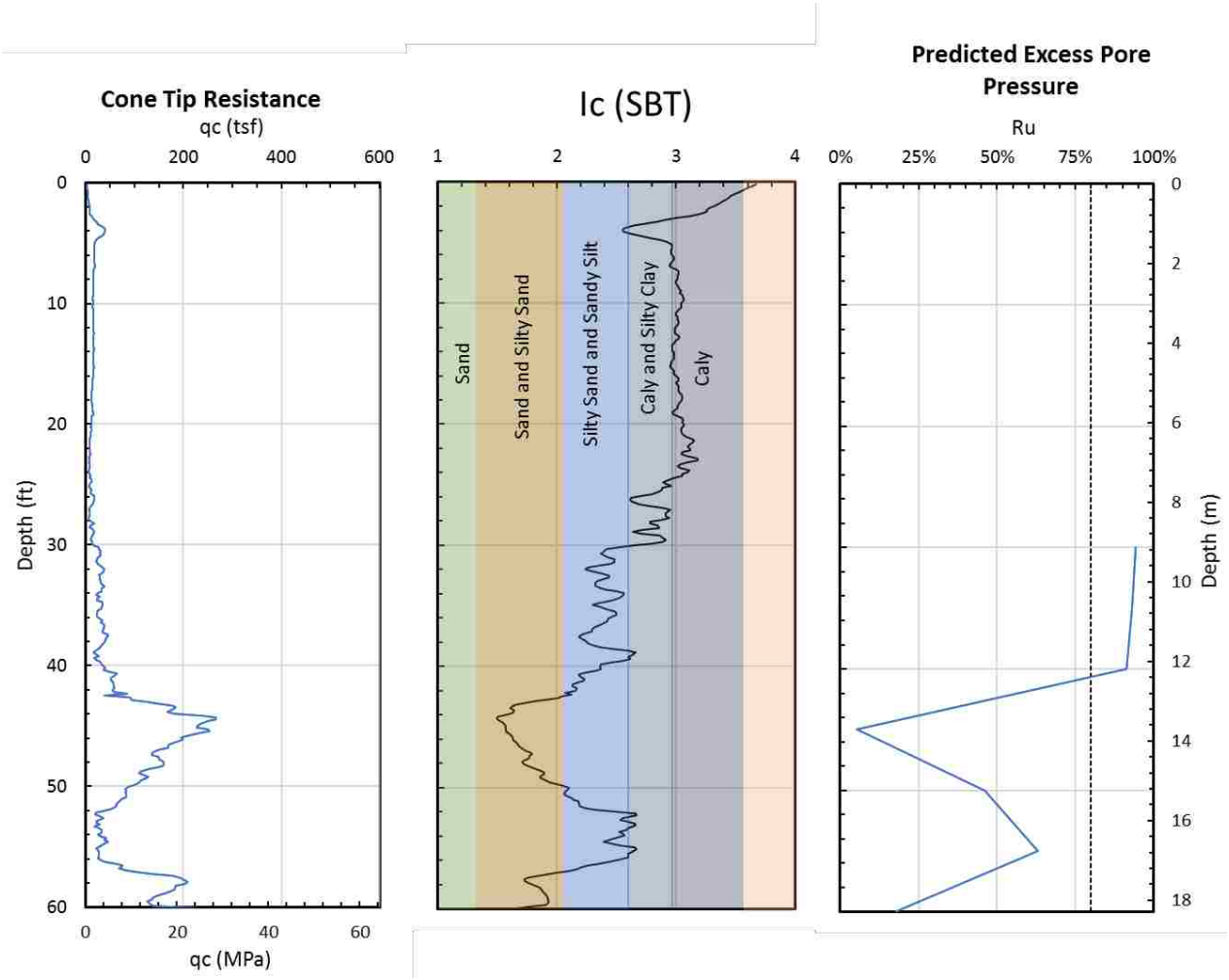

Figure 3.2-10 Cone tip resistance, soil behavior type Ic, and predicted excess pore pressure. Preliminary Pile Downdrag Calculations Following Blast Liquefaction

The goal of this experiment is to measure the load in the piles and resulting pile settlement after blast induced liquefaction. Total settlement was predicted to be about 7.5 inches in section 3.2; however, if it is only possible to liquefy the zone from 30 to 40 feet for blast induced liquefaction, the settlement should only be about 3 inches. This was determined by summing the settlements calculated for a M7.5 earthquake from 30 to 40 feet only and assuming settlement will not take place anywhere else in the soil profile during blasting. Using the three design approaches (the method used for the LCPC method was the one that used the higher f_{pmax} values) to compute side friction and end-bearing in test piles described previously, along with predicted soil settlement, an iterative approach was employed to predict pile load distribution and pile settlement prior to the testing. The steps in the procedure are as follows:

1. Compute a soil settlement profile in the liquefied zone (30 to 40 ft)
2. Assume a neutral plane location
3. Compute load distribution in the pile assuming negative skin friction above the neutral plane and positive skin friction below the neutral plane. (Note: Skin friction in the liquefied zone was assumed to be equal to 50% of the pre-liquefaction design value.)
4. Determine the end-bearing resistance, Q_p required to produce static equilibrium
5. Determine the settlement at the toe of the pile
6. Use Q-z curves proposed by O'Neil and Reese (1999) as shown in Figure 3.2-11 to determine if mobilized Q_p is compatible with settlement.
7. Revise the location of the neutral plane and repeat the process until the required Q_p is compatible with the settlement necessary to mobilize Q_p

The results of the calculations are presented in Figure 3.2-12, Figure 3.2-13, and Figure 3.2-14. Soil settlement and pile capacity prediction calculations were described in previous sections of this report. Liquefaction-induced soil settlement is assumed to increase linearly within the layer from 30 to 40 ft. and the overlying clay layers are assumed to settle with the underlying sand. Applied axial load was assumed to be 200 kips. Ultimately the load applied to the pile was only 120 kips, which according to these predictions would results in zero settlement.

The results of the analysis for the pipe pile in Figure 3.2-12 show negative friction developing from the top of the pile to nearly the bottom of the liquefied zone. The LCPC and the Eslami and Fellenius methods predict end-bearing resistances of 120 to 80 kips, respectively. The FHWA method predicted that the mobilized negative skin friction would not be enough to mobilize end bearing and settlement. Maximum load in the pile varied from 280 to 360 kips. The predicted pile settlement for each method was only about a tenth of an inch.

The concrete square pile results are shown in Figure 3.2-13. Once again, negative skin friction develops from the ground surface to near the bottom of the liquefied layer. Maximum axial force in the pile is predicted to reach between 320 to 450 kips. Neither of these capacities come close to failing the pile. Both the LCPC and Eslami and Fellenius methods predicted the development end bearing. The settlement of the pile predicted using the Eslami and Fellenius method was about 0.1 inch, and the settlement with the LCPC method was about 0.4 inch. However, the FHWA method predicted no pile settlement.

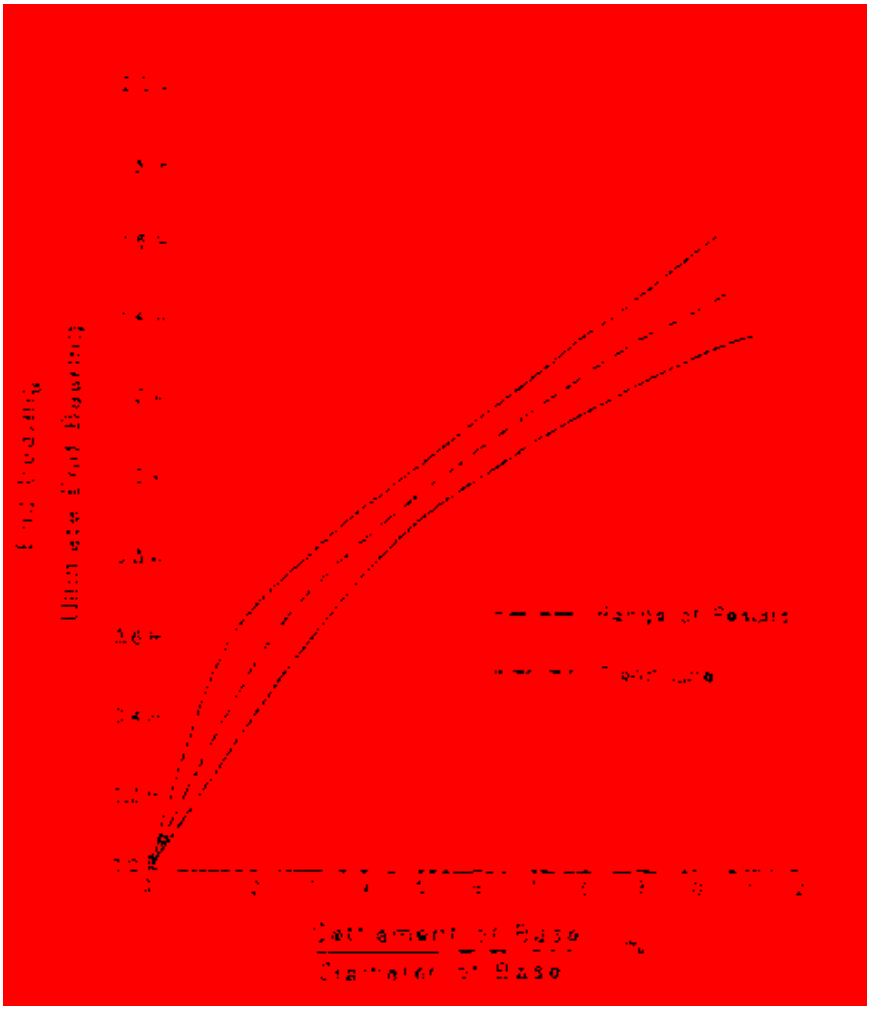

Figure 3.2-11 Normalized end-bearing versus normalized settlement for cohesionless soil

Results for the H-Pile, shown in Figure 3.2-14, indicate that no design method predicted mobilized end bearing or pile settlement for any of the three methods. This is due to the length of the H-pile. There is so much length below the neutral plane that the pile comes into equilibrium for all three methods before end bearing is mobilized. Nevertheless, the maximum axial force is predicted to be between 320 and 370 kips. It is also important to note that the expected settlement of the piles relative to the soil is very small even for the cases where end bearing was predicted to be mobilized. Also, the FHWA method did not predict pile settlement for any of the piles. This is most likely due to the larger skin friction values predicted.

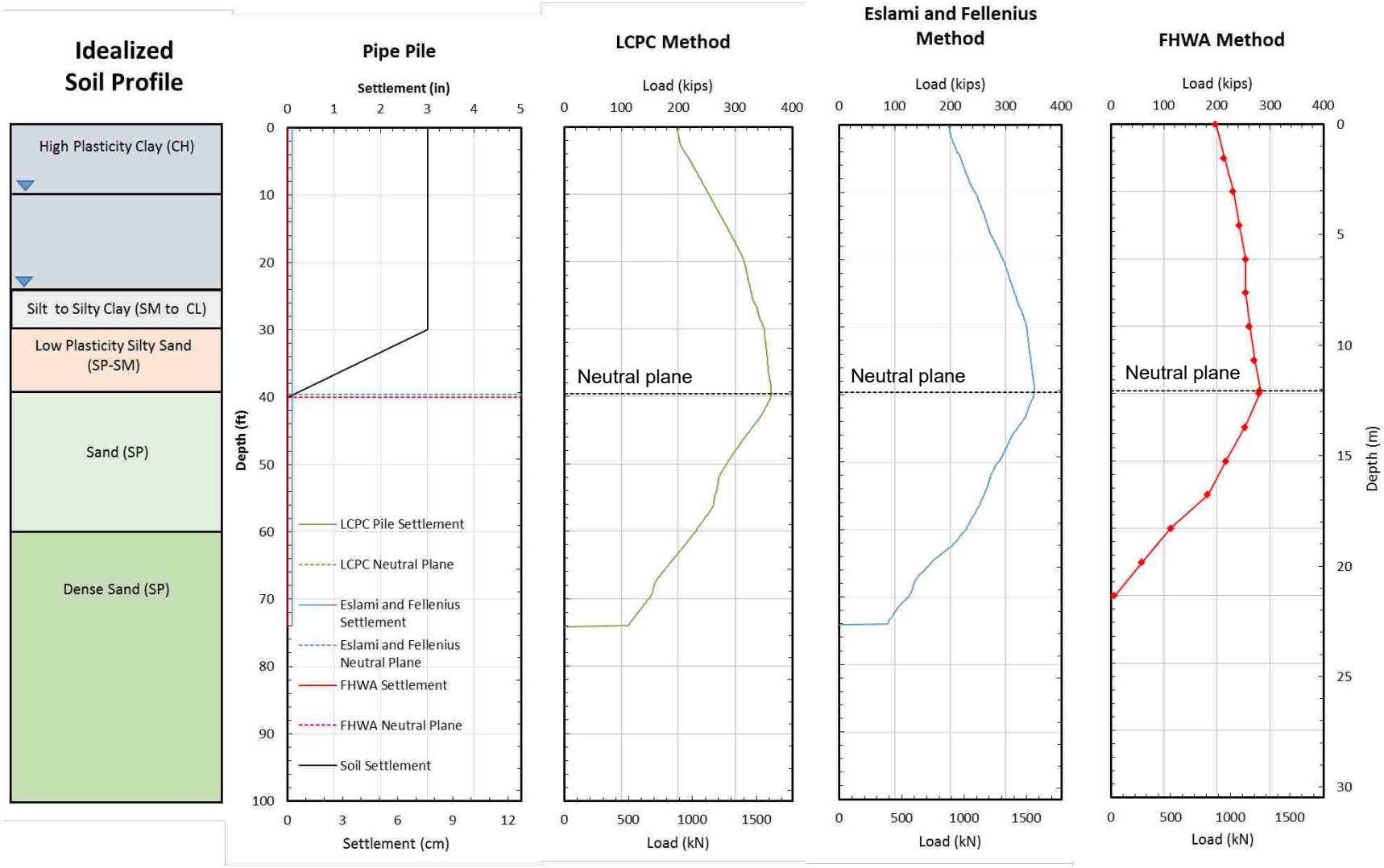

Figure 3.2-12 Plots showing the neutral plane calculations using the three pile capacity prediction methods (Pipe Pile).

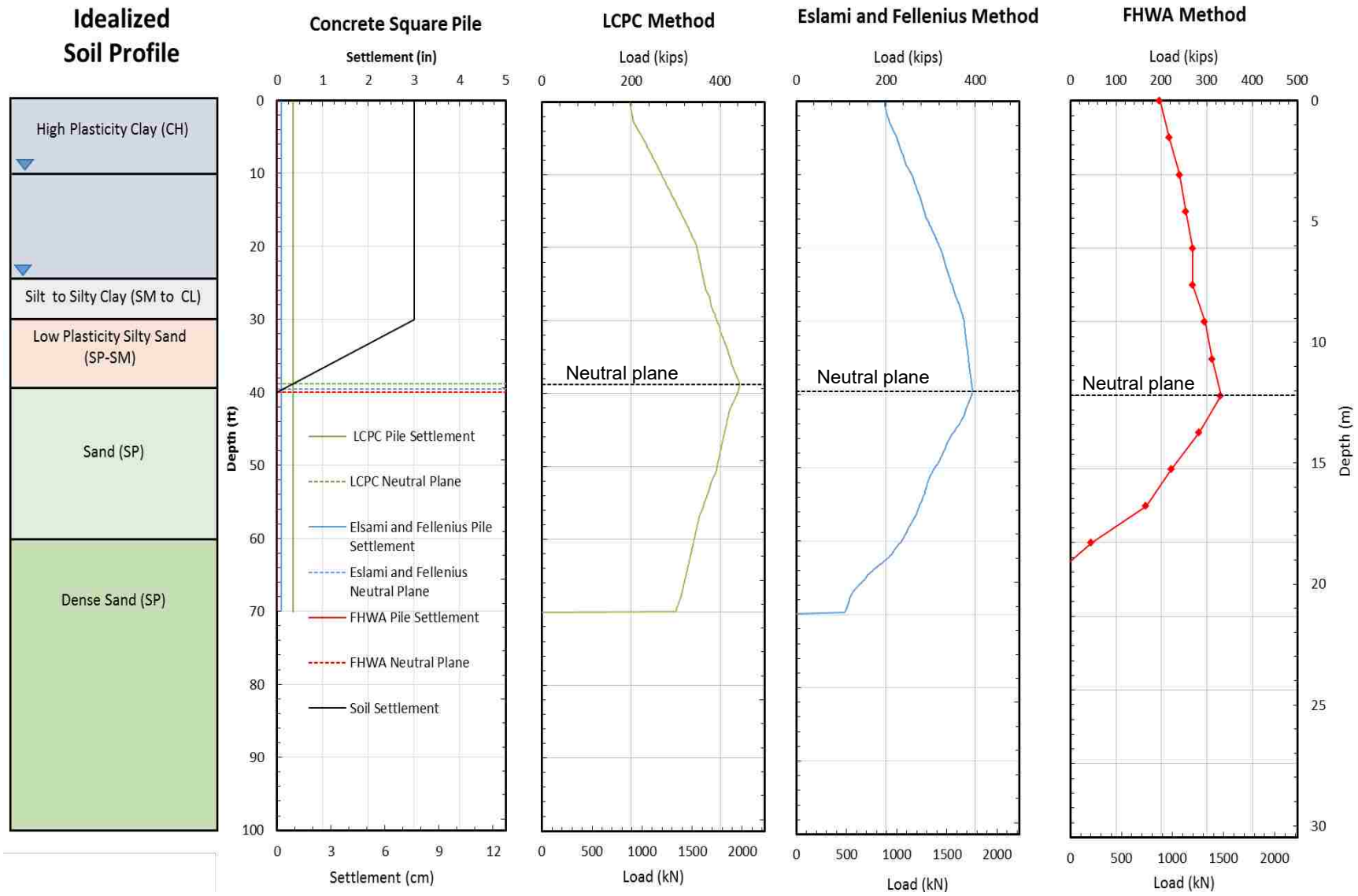

Figure 3.2-13 Plots showing the neutral plane calculations using the three pile capacity prediction methods (concrete pile).

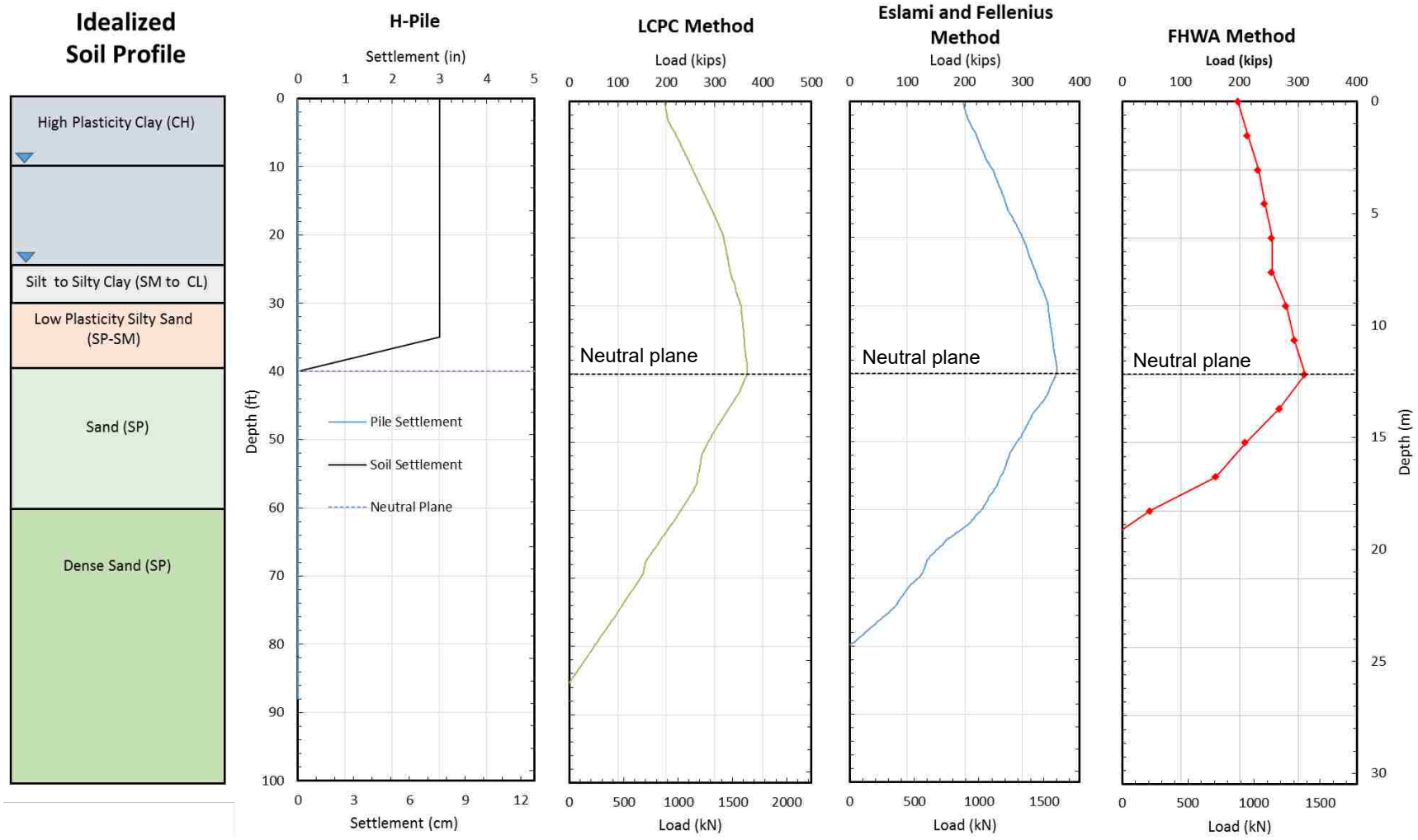

Figure 3.2-14 Plots showing the neutral plane calculations using the three pile capacity prediction methods (H pile).

4 AFT CELL-TEST, STATIC LOAD TEST, AND PILE DRIVING ANALYSIS, AND TEST LAYOUT

4.1 Overview

This chapter describes the layout of the test foundations and the instrumentation involved for both the static pile load testing and the subsequent blast liquefaction testing. Prior to blasting, axial pile capacity was evaluated using three techniques. First, during pile driving a Pile Driving Analyzer or PDA was used to evaluate pile capacity along with a CAPWAP analysis technique. Secondly, sacrificial bi-direction load cells (AFT cells) were placed at depth in two test piles and inflated so that skin friction on the top part of the pile could be reacted against side friction and end-bearing on the bottom part of the pile. Finally, dead weights were stacked on top of three test piles to partially develop the axial capacity of the piles. After the three test piles were loaded with dead weights, controlled blasting was carried out to liquefy a layer of soil along the test piles so that the resulting pile load distribution and pile settlement could be evaluated relative to the soil settlement. The results from the blast liquefaction testing will be presented in chapter 5.

4.2 Test Layout

The testing of the driven piles took place at an interchange where Interstate 555 crosses interstate 55 as shown previously in Figure 3.4-1. As shown in Figure 4.2-1, five test piles were driven near the three drilled shafts that were previously constructed as a part of another

experiment (Race 2015). During the blast testing, blast holes were placed around a pile and a shaft thereby reducing the number of blasts from six to three making instrumentation easier. Companion concrete and pipe piles, driven 55 feet to the northeast of the test piles used in the blast tests, were used to perform AFT cell tests without disturbing the test piles that would subsequently be used in the blast liquefaction tests.

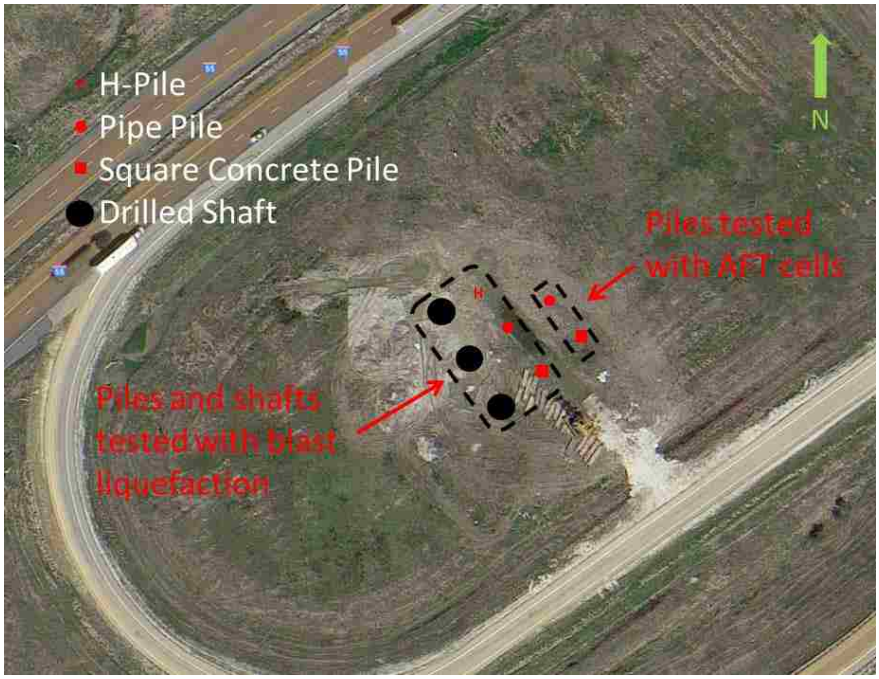

Figure 4.2-1 Approximate locations of the driven piles and drilled shafts at the Turrell Arkansas Test Site.

4.3 Test Pile Cross Sections and Instrumentation

As illustrated in Figure 4.2-1, there were three piles tested by blast induced liquefaction and two piles tested with AFT cells. Test piles consisted of two companion 18-inch diameter closed end steel pipe piles, one 14x117 H-Pile, and two companion 18-inch by 18-inch square pre-stressed concrete piles. Cross-sections showing dimension for the pipe piles and the H pile are provided in Figure 4.3-1 while a cross-section for the concrete piles is provided in Figure 4.3-2. One of the pipe piles and one of the concete square piles was fitted with an AFT Cell.

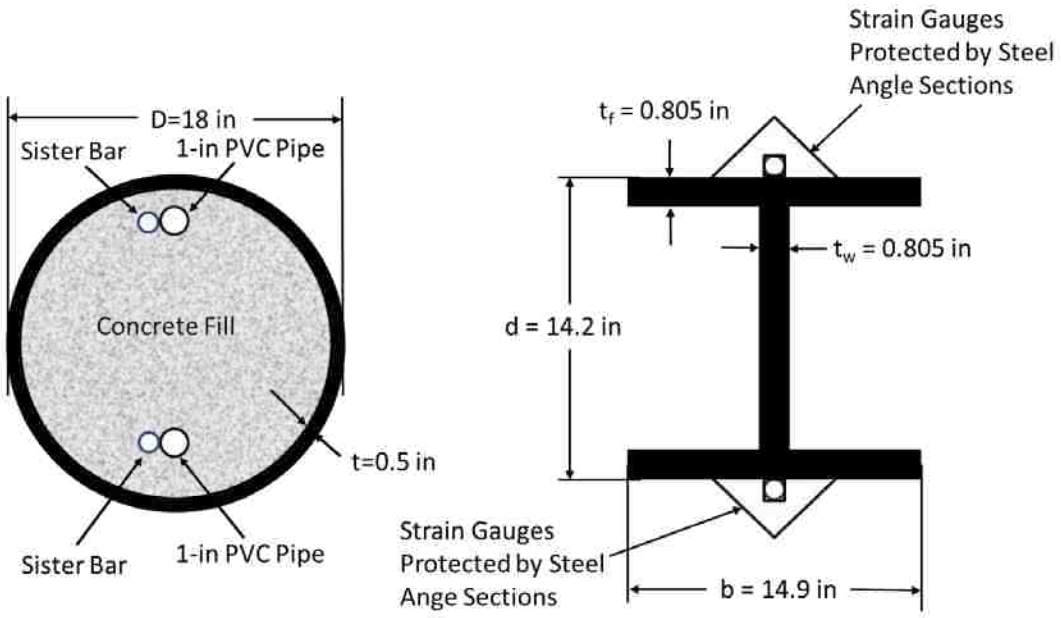

Figure 4.3-1 Cross sections for the 18-inch diameter pipe pile and the HP14x117 H-pile.

The two 78-foot long steel pipe piles were instrumented with strain gages and driven until four feet of the pile remained above the surface. One pipe pile was driven in two sections to install an AFT cell. It was initially driven to a depth of 30 feet, attachments were made to help install the AFT cell, and then it was driven to a final depth of 74 ft. Both pipe piles were fitted with strain gauges at depths of 2, 10, 17, 25.5, 29, 38, 41.5, 45, 51.5, 58, 66 and 74 feet below the ground surface. The strain gauges were attached to sister bars, which were zip-tied to 1-inch PVC pipe and lowered into the pile as shown in Figure 4.3-1. The piles were then backfilled with concrete, which had a compressive strength of 8000 psi and a slump of 3.5 inches. The AFT-Cell pipe pile was independently connected to the top and bottom pile sections by four rectangular pieces of steel about 2 inches thick, 4 inches wide and 8 inches long welded to the inside of the pipe. This was to support the AFT-Cell as it sat within the pile.

The 92-ft long H-Pile was pre-fabricated into two 46-foot long sections so it could be transported on a semi-truck. The strain gauges were installed on site to be located at depths of

20, 29, 36, 40, 45, 51, 59, 66, 76, and 88 feet below the ground surface after driving the pile to a depth of 88 ft. The strain gauges were fastened with a bolt to metal pieces that were tac welded to the H-Pile flange. The gauges were then covered by an angle section that was welded to the flange as shown in Figure 4.3-1. This was done to protect the strain gauges during driving.

The 74-foot long square pre-stressed concrete piles were made with 0.5 inch 270 ksi low lax 7-wire pre-stressing strand as shown in Figure 4.3-2. They were each instrumented with strain gauges starting at 4 (ground level), 12, 20, 26.5, 33, 39.5, 46, 52.5, 60.5, 65.5, and 72 feet below the top of the pile. The strain gauges were attached to sister bars, which were tied to the pre-tensioned cables using rebar tie wire. The slump of the concrete was measured twice. The average slump of the concrete was 6 inches. The concrete had an average compressive strength of about 8000 psi (55.2 MPa).

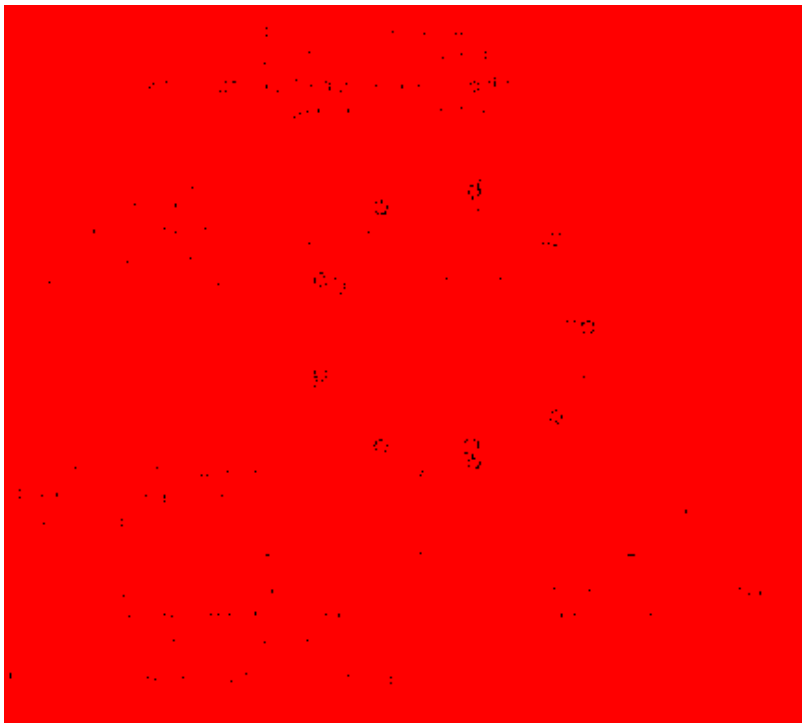

Figure 4.3-2 Cross section of the pre-stressed concrete square pile.

4.4 Load Testing to Evaluate Static Capacity Prior to Blasting

As indicated in Chapter 3, there is significant variation in predicted pile capacity using static equations. To provide better understanding of the static axial pile capacity for each test pile, three different tests were employed prior to blast liquefaction. First, PDA measurements were made on five of the driven piles and CAPWAP analyses were performed to estimate side resistance and end-bearing. Secondly, after driving, Osterberg type load tests were performed on one pre-stressed concrete pile and one pipe pile driven near the test piles used in the blast as indicated in Figure 4.2-1. Finally, dead weights were placed on top of each test pile immediately prior to blast testing.

A pile driving analysis predicts the capacity of a driven pile by measuring the response of the pile head for each hammer blow and then back-calculating the side resistance and end-bearing resistance of the pile using equations developed by Goble et al. (1975). This impact is measured by sensors that record strain and acceleration near the pile head during driving and are shown in Figure 4.4-1. The measured parameters are then converted to force and velocity using a PDA data acquisition system shown in Figure 4.4-2. Measured force and velocity time histories are then compared with computed time histories using the program CAPWAP to better determine the distribution of side friction and end-bearing for the driven pile.

This experiment had a total of five test piles that were driven into the ground. All of them had analysis performed at the End of Initial Driving (EOID). Two of them, the pipe pile that was tested with blasting and the concrete pile that contained an AFT cell, had restrikes performed on them, to see what the capacity of the pile would be after the soil had time to set up. Ideally, restrike analysis would have been performed for all test piles but the pile driving equipment had

to move onto another project. The decisions regarding which piles to perform restrikes on was at the discretion of the field engineer.

Figure 4.4-1 Accelerometer and strain gauges connected to the top of a pipe pile at the end of driving in connection with PDA measurements.

Figure 4.4-2 Pile Driving Analyzer device.

The piles were driven into the ground with an ICE Model I-30^{V2} single-acting diesel pile hammer with specifications shown in Figure 4.4-3. The stroke height of the hammer was adjusted as it passed through the different layers of soil to increase effiency. A cushion was built and placed between the hammer and the pile to soften impact and to prevent damage to the pile.

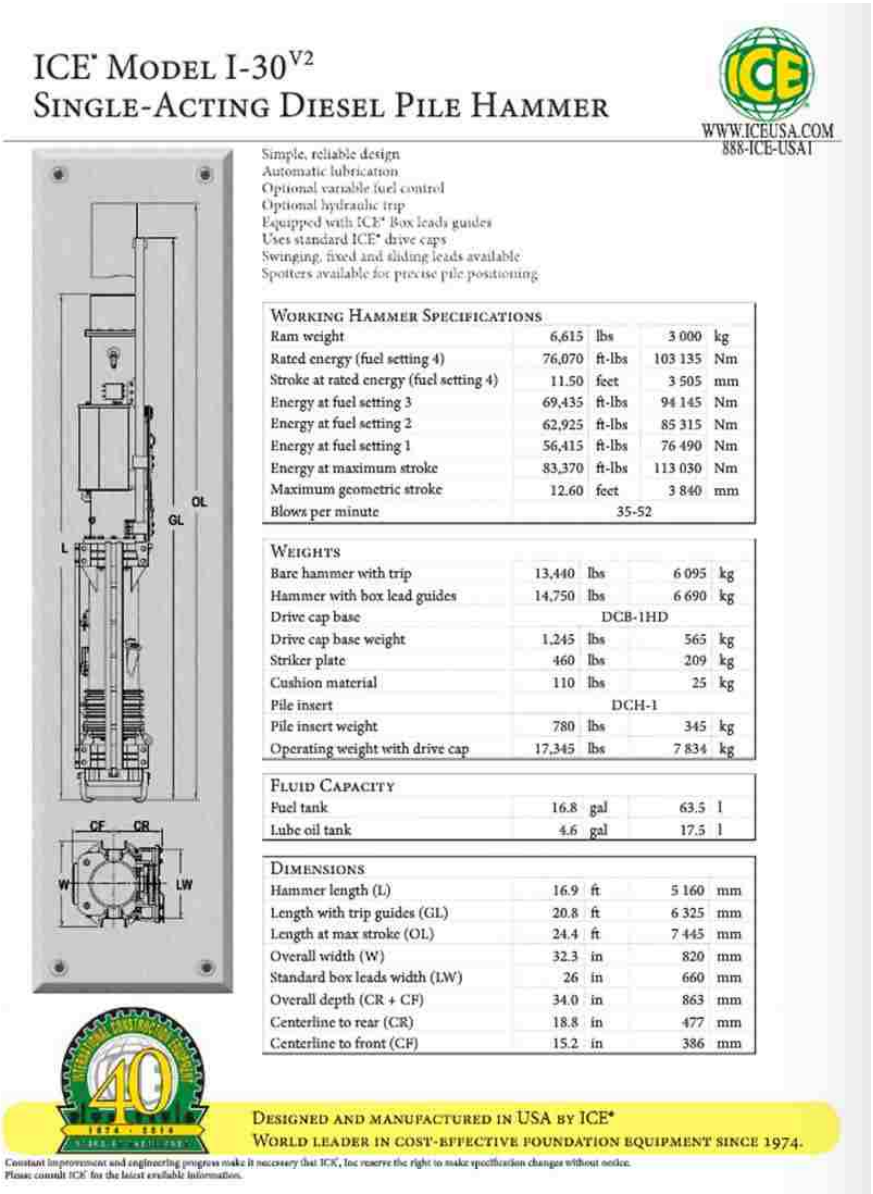

ICE® MODEL I-30^{V2}
SINGLE-ACTING DIESEL PILE HAMMER

WWW.ICEUSA.COM
888-ICE-USA1

Simple, reliable design
Automatic lubrication
Optional variable fuel control
Optional hydraulic trip
Equipped with ICE® Box leads guides
Uses standard ICE® drive caps
Swinging, fixed and sliding leads available
Spotters available for precise pile positioning

OL
GL
L
CF
CR
W
LW

WORKING HAMMER SPECIFICATIONS				
Ram weight	6,615	lbs	3 000	kg
Rated energy (fuel setting 4)	76,070	ft-lbs	103 135	Nm
Stroke at rated energy (fuel setting 4)	11.50	feet	3 505	mm
Energy at fuel setting 3	69,435	ft-lbs	94 145	Nm
Energy at fuel setting 2	62,925	ft-lbs	85 315	Nm
Energy at fuel setting 1	56,415	ft-lbs	76 490	Nm
Energy at maximum stroke	83,370	ft-lbs	113 030	Nm
Maximum geometric stroke	12.60	feet	3 840	mm
Blows per minute	35-52			

WEIGHTS				
Bare hammer with trip	13,440	lbs	6 095	kg
Hammer with box lead guides	14,750	lbs	6 690	kg
Drive cap base	DCB-1HD			
Drive cap base weight	1,245	lbs	565	kg
Striker plate	460	lbs	209	kg
Cushion material	110	lbs	25	kg
Pile insert	DCH-1			
Pile insert weight	780	lbs	345	kg
Operating weight with drive cap	17,345	lbs	7 834	kg

FLUID CAPACITY				
Fuel tank	16.8	gal	63.5	l
Lube oil tank	4.6	gal	17.5	l

DIMENSIONS				
Hammer length (L)	16.9	ft	5 160	mm
Length with trip guides (GL)	20.8	ft	6 325	mm
Length at max stroke (OL)	24.4	ft	7 445	mm
Overall width (W)	32.3	in	820	mm
Standard box leads width (LW)	26	in	660	mm
Overall depth (CR + CF)	34.0	in	863	mm
Centerline to rear (CR)	18.8	in	477	mm
Centerline to front (CF)	15.2	in	386	mm

DESIGNED AND MANUFACTURED IN USA BY ICE®
WORLD LEADER IN COST-EFFECTIVE FOUNDATION EQUIPMENT SINCE 1974.

Constant improvement and engineering progress make it necessary that ICE, Inc reserve the right to make specification changes without notice.
Please consult ICE for the latest available information.

Figure 4.4-3 Cross section, plan view and specifications on the hammer used.

The load cells for the Osterberg type load tests were manufactured by Applied Foundation Testing and will be referred to as AFT cells in this thesis. In the AFT tests, a bi-directional hydraulic jack in the cell loads the pile evenly above and below the cell. The jack was inserted into the pre-stressed concrete pile during construction as shown in the photo in Figure 4.4-4. It was placed at 42.5 feet from the top of the pile or 38.6 feet below the ground surface as shown in Figure 4.4-5. The AFT Cell in the pipe pile was placed at a distance of 42 feet from the top of the pile (38 feet below ground) and 36 above the toe of the pile.

Figure 4.4-4 Photo of the AFT cell installed in the pre-stressed concrete pile.

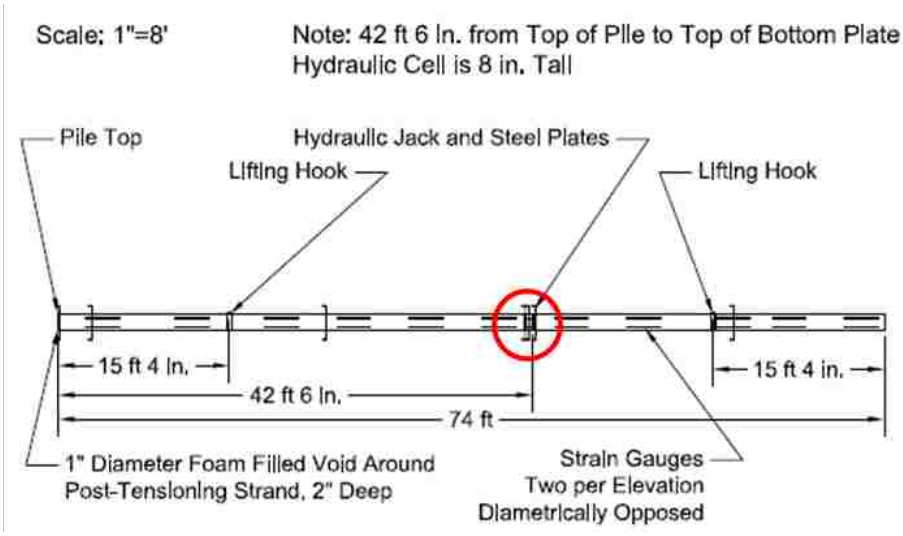

Figure 4.4-5 Drawing showing the location of the Osterberg (AFT) Cell in the pre-stressed concrete pile.

Finally, dead weights were applied to the test piles immediately prior to blasting to provide some idea of the side resistance in the top section of the piles as illustrated in Figure 4.4-6. This approach simulates a static load test is some respects, but the loads were too small to reach ultimate capacity. The loads were designed to simulate a static load that might be in place on the piles prior to an earthquake event which caused liquefaction. To support the load, a circular pile helmet cap was placed on top of the pile protruding from the ground. A six foot by six foot by two-inch thick metal plate was then welded on top of the pile cap. Then steel weights consisting of H-Pile blanks, weighing 12.58 kips each, were placed on top of the metal plate in three rows. Each row had three blanks for a total of nine blanks and a total load of 118.26 kips, including the helmet and plate which weighed 5 kips. A schematic plan view drawing is shown in Figure 4.4-7. The blanks were added to the pile one at a time with an approximate 5-minute time interval between each one. A photo of the pile cap with all the blanks loaded is shown in Figure 4.4-8. Considerable effort was expended to ensure that the weights were centered on the test pile.

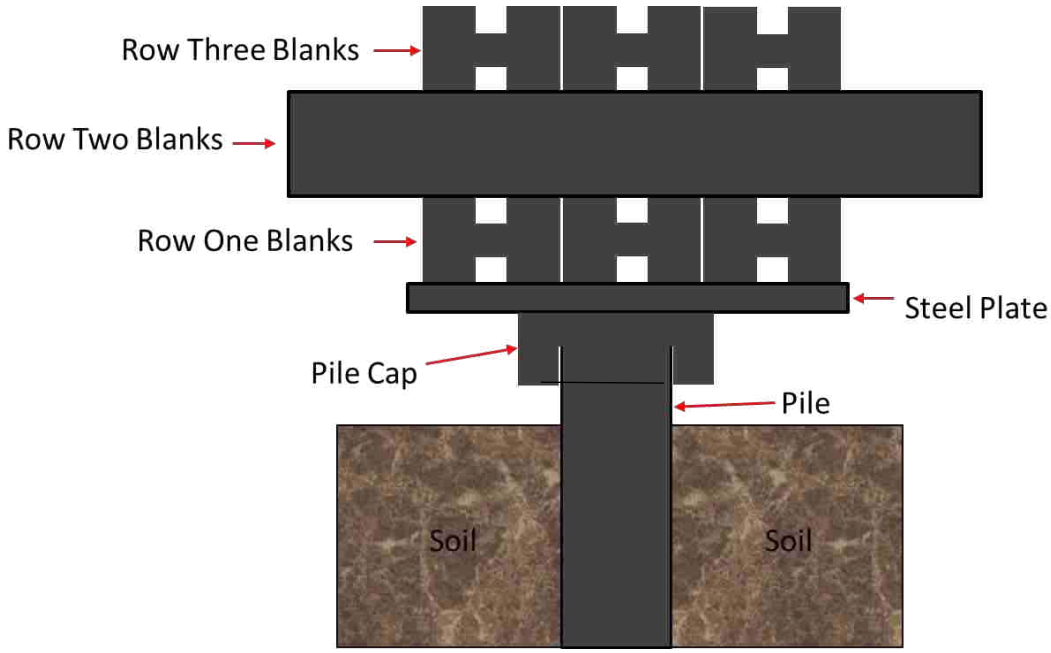

Figure 4.4-6 Schematic elevation view of the static loading of the test piles (Not to scale).

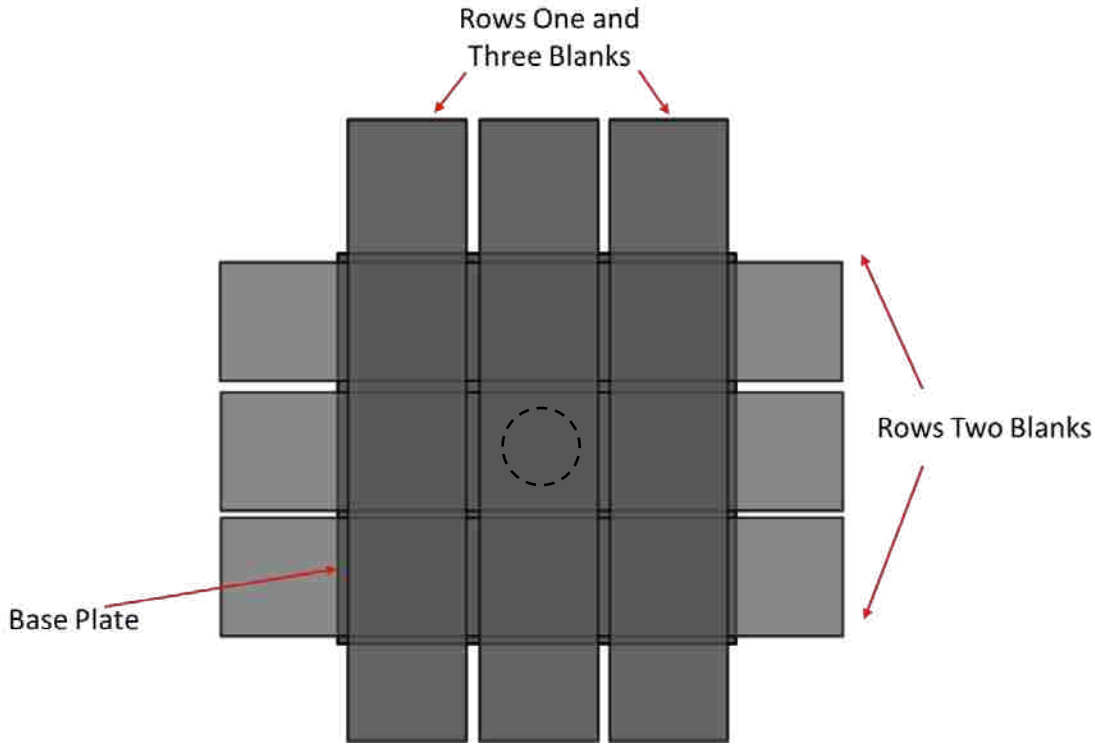

Figure 4.4-7 Schematic Plan view of the static loading of the test pile (not to scale).

Figure 4.4-8 Photo of the loading configuration completed.

4.5 Results of the CAPWAP Analysis

All five piles driven as part of this experiment had PDA instrumentation attached to them during driving, and all of them had CAPWAP analysis thereafter. The H-pile was subject to an End of Initial Driving (EOID) analysis, but not a restrike. The pipe pile used for blasting was subject to an EOID analysis as well as a restrike while the pipe pile with the AFT-Cell was subject to an EOID analysis. The 18-inch square concrete pile was subject to an EOID analysis and the 18-inch AFT-Cell concrete pile was subject to an EOID analysis and a restrike. Both restrikes were performed 24 hours after initial driving and were performed to assess strength gain strength with time. The majority of the strength gain typically takes place in the clay layer and can be substantial. Some strength gain can also occur in the sandy layers, but it is less likely to

be significant. The shaft resistance, toe resistance and total pile capacity for each pile based on the CAPWAP analyses are summarized in Table 4.5-1.

Table 4.5-1 Pile, Pile Shaft, Toe and Total Capacity

Pile	CAPWAP Capacity (kips)		
	Shaft	Toe	Total
HP 14x117	187	30	217
18 Inch Pipe Pile EOID	152	305	457
18 Inch Pipe Pile Restrike	327	256	583
18 inch AFT-Cell Pipe Pile EOID	87	285	372
18 inch Concrete Pile EOID	228	236	464
18 inch AFT-Cell Concrete Pile EOID	213	245	458
18 inch AFT-Cell Concrete Pile Restrike	480	268	748

The shaft capacity of the H-pile for EOID conditions was 187 kips and the total capacity was 217 kips. Based on what we know from the results of the other piles the shaft capacity of 187 kips seems reasonable, however, the end bearing was only 30 kips which seems unreasonably low. FHWA (2016) design guidance indicates that H piles often remain unplugged during driving but subsequently plugs after pile set-up. This means that an H pile will have a higher end bearing capacity after it has been driven and set up. During driving end-bearing would only be developed on the relatively small cross-section of the steel.

Intuitively, 30 kips seems small when compared to the capacities of the pipe pile and the concrete pile. The recorded blow count during driving at the bottom of the H-Pile was approximately 62. In contrast, the blow counts for the pipe pile and the concrete pile were 28 and 38, respectively which represents a resistance per blow of 7.4 kips and 8.9 kips, respectively. If the end-bearing resistance for the H pile was proportional to the blow count, it would be about 16 kips per blow. Because the area of the H-pile was one tenth of the other piles, the end-bearing resistance would be 16 kips/blow divided by 10. This would yield an end-bearing resistance of

about 99 kips. The pile capacity provided by end-bearing and side resistance for the H-pile at EOID conditions is plotted as a function of depth in Figure 4.5-1. In addition, an estimate of the end-bearing resistance after re-strike is presented based on previous discussion. Increases in side resistance have been neglected because an H-pile is a low-displacement pile and should produce therefore develop less set-up.

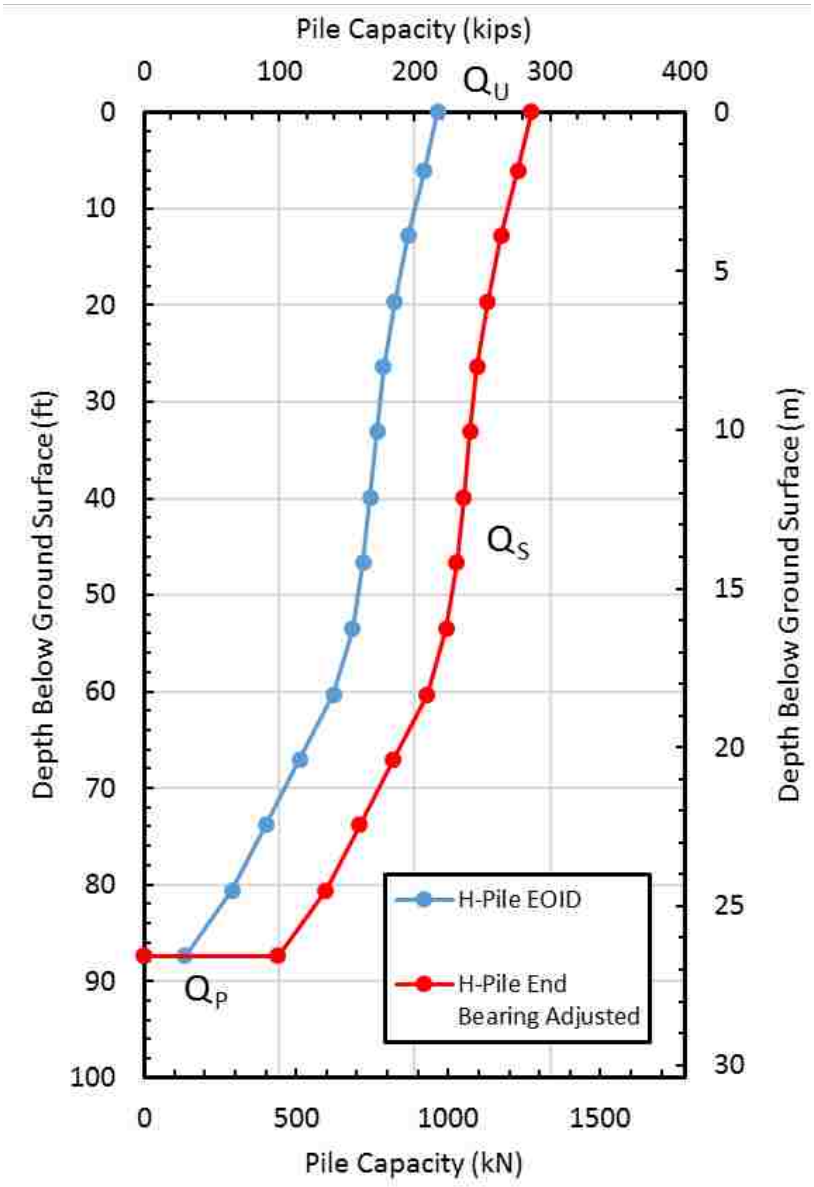

Figure 4.5-1 Pile capacity versus depth curves for the H-Pile from CAPWAP analysis.

The shaft capacity of the pipe pile for EOID was 152 kips, the toe capacity was 305 kips, and the total capacity was 457 kips. The restrike was performed the following day, approximately 24 hours after initial driving. The shaft, toe and total capacities were 327, 256 and 583 kips, respectively. The increase in axial capacity was primarily a result of increased shaft capacity, which increased by 115%. The EOID analysis for the AFT-Cell pipe pile gave a shaft capacity of 87 kips, a toe capacity of 285 kips and a total capacity of 372 kips. While the end-bearing resistance is similar to the other pipe pile, the side resistance is somewhat lower. These discrepancies might be expected because the piles were driven in different locations and the pile was installed in two separate pieces with a discontinuity in the middle. The PDA instrumentation had to be removed from the bottom piece of the pile and moved to the upper piece after attaching the two pieces together. Because of the discontinuity in the pile, stress waves may have been distorted. For these reasons, the predicted capacity was likely lower than it was. For these reasons, the results from the pile used in the blast test appears to be most representative. The end-bearing and side resistance versus depth curves for the pipe piles obtained from EOID and restrike are shown in Figure 4.5-2.

The end-bearing and side resistance versus depth curves for the concrete piles obtained from EOID and restrike are shown in Figure 4.5-3. The square concrete pile used for blasting had a shaft capacity of 228 kips, a toe capacity of 236 kips and a total capacity of 464 kips. This was very similar to the concrete AFT-Cell pile, which had a shaft, toe and, total capacity of 213 kips, 245 kips and 458 kips, respectively. The restrike performed on the latter of the two piles had a total capacity of 748 kips. The pile capacity is higher due to higher side resistance, which increased by about 125%, similar to that for the H pile. The restrike was performed approximately 24 hours after initial driving.

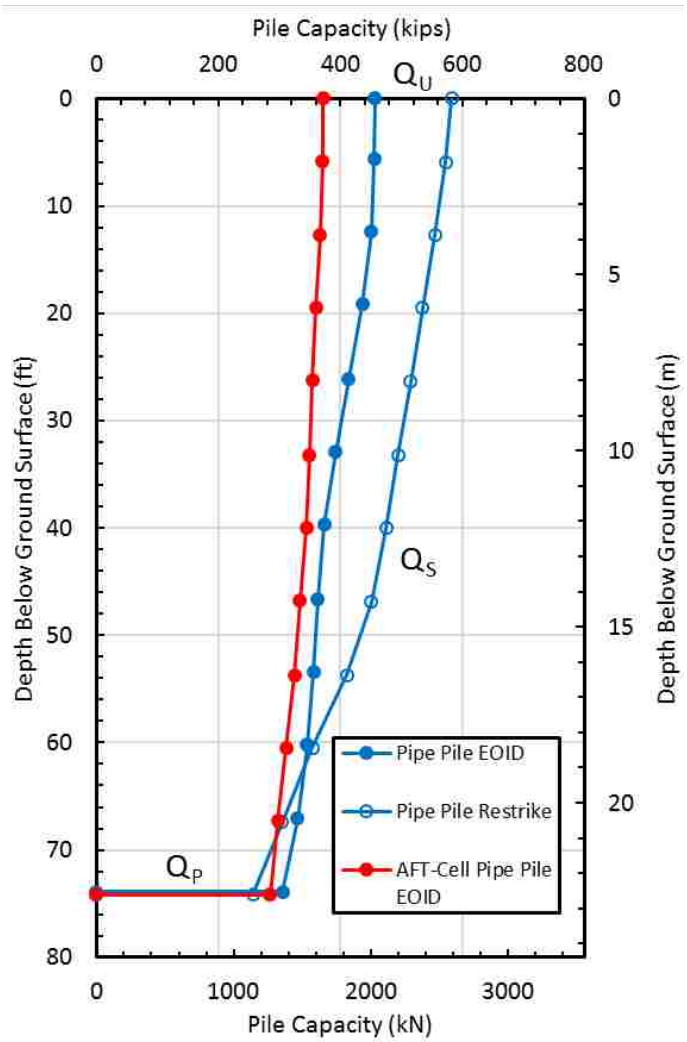

Figure 4.5-2 Pile capacity versus depth curves for the pipe piles from CAPWAP analysis.

The concern with the concrete AFT-Cell is that while driving the top eighteen inches of the pile were damaged and broke off the top. In addition, it was necessary to drill holes into the pile and use an acetylene torch to cut the pre-tensioned cables at the location of the AFT-Cell so that it could expand and function without issue. This caused significant drying of the concrete and as a result cracking. Cracking does affect the capacity of the pile, so the AFT-Cell CAPWAP analysis is not as reliable, although it is comparable. For these reasons, the EOID results from the test pile used in the blast test is considered the most representative and will be used in subsequent analyses.

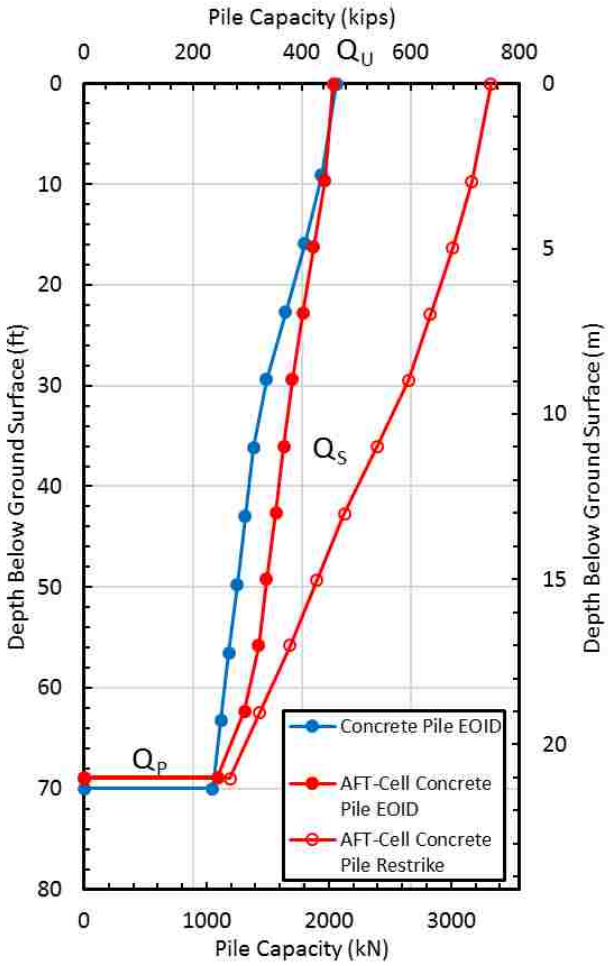

Figure 4.5-3 Pile capacity versus depth for the concrete piles from CAPWAP analysis.

Figure 4.5-4 provides plots of the cumulative skin friction versus depth curves for each of the piles based on CAPWAP analyses. This chart makes it possible to compare the different values of skin friction calculated from the different piles to determine if the results are consistent and reasonable. The H pile yields the lowest skin friction except for the AFT Cell pipe pile which is suspiciously low, as discussed previously. This makes sense because it has the smallest perimeter when based on the rectangular perimeter, and the soil-steel interface friction should be lower, therefore it should develop the least amount of resistance per unit length. The pipe pile has the second largest diameter, and is also made of steel, thus it should develop more resistance

per unit length, than the H-Pile, but less than the concrete square pile. This is indeed the case. The concrete square pile developed the greatest skin friction. It also has the largest perimeter and because it is concrete it should develop more load per unit length than a steel pile.

However, in both piles where restrikes were performed, the shaft capacity more than doubled. In the pipe pile, it went from 152 kips to 327 kips growing by 115%. The shaft capacity of the AFT-Cell Concrete Pile went from 213 kips to 480 kips growing by 125%.

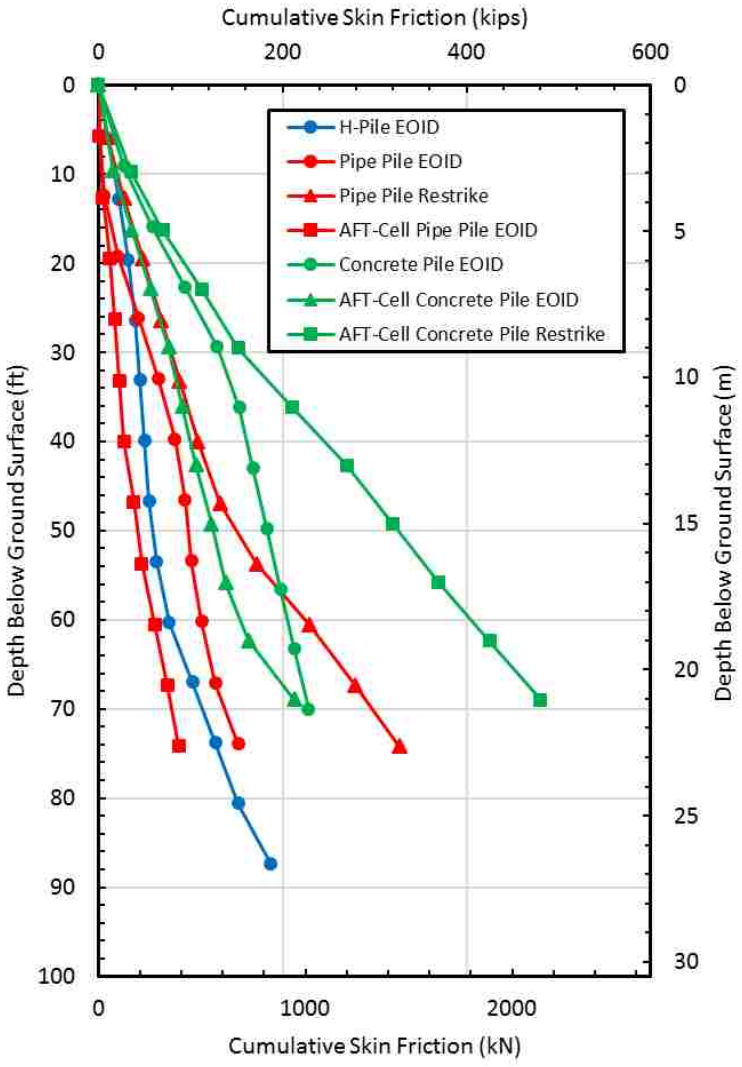

Figure 4.5-4 Load in the pile versus depth for all the piles.

4.6 AFT Cell Test Results

The AFT bi-directional hydraulic jacks were expanded until the piles were loaded to 176 kips for the concrete pile and 160 kips for the pipe pile. These load values were relatively low considering the capacity of the piles from the re-strikes and from preliminary static capacity equations. The low load values were due to the fact that the AFT load cells had a capacity of only 200 kips. Furthermore, because the AFT cells were placed at relatively shallow depths, the piles failed in skin friction in the upward direction and weren't able to mobilize all the side resistance and end bearing of the lower portion.

Load versus depth plots are important in this experiment because they make it possible to determine the side friction prior to liquefaction. The values after liquefaction can then be compared with the values prior to liquefaction. Load in the pile, P, was computed from the strain gauge data at each depth using the equation

$$P = \varepsilon E_s A \qquad 4\text{-}1$$

where ε is the average strain, E_s is the secant modulus, or the modulus of elasticity of the pile, and A is the cross-sectional area of the pile. Average strain was found at each individual depth by taking the average of the strain of the two strain gauges located at that depth. When a strain gauge was damaged, then the value from the one strain gauge was used, if both were damaged or malfunctioning, then the depth was skipped.

The steel piles have a constant modulus of elasticity, however for concrete this is not the case. The elastic modulus for a concrete pile tends to decrease with increasing load. The difference in initial and final modulus can be large, so it is important that it is correctly represented. However, to correct this modulus in the driven piles, more information would be

needed than what was available, so in this report the modulus of concrete was calculated using the equation

$$\mathbf{E = 57,000 * \sqrt{(f'_c)}} \qquad 4\text{-}2$$

where f'_c is the unconfined compressive strength of the concrete. The compressive strength was found by performing compressive strength tests on concrete cylinders. The strain gauges in the pipe pile were embedded in the concrete grout used to fill the pipe piles. Thus, the modulus of elasticity of the pipe pile was calculated using a combined modulus of the concrete and steel sections of their respective piles. The modulus of the concrete was calculated using the equation 4.2 and the modulus of steel was assumed to be 29,000 ksi. Then a weighted average was taken based on the cross-sectional area of each material.

Plots showing the load in the pile interpreted from the strain gauges during the AFT cell tests for the pipe pile and the concrete pile are found in Figure 4.6-1 and Figure 4.6-2, respectively. The maximum load in the pile occurs at the point where the AFT cell is located, and could be as high as the maximum cell capacity of 200 kips. The max load in the pipe pile was about 160 kips and the max load in the square concrete pile was about 176 kips. The load cell never quite made it to 200 kips, this is most likely due to the pile failing upward in skin friction.

The difference in load between the two strain gauges indicates the incremental skin friction for that section of the pile. The load at the ground surface was assumed be zero, and the load at the pile toe was determined by extrapolating the skin friction from the previous two strain gauges and cutting it off at the pile tip. End bearing was mobilized in both tests but was only about 15 kips for the concrete pile and 30 kips for the pipe pile. Such small amounts of mobilized end bearing didn't cause the base of the pile to settle a significant amount.

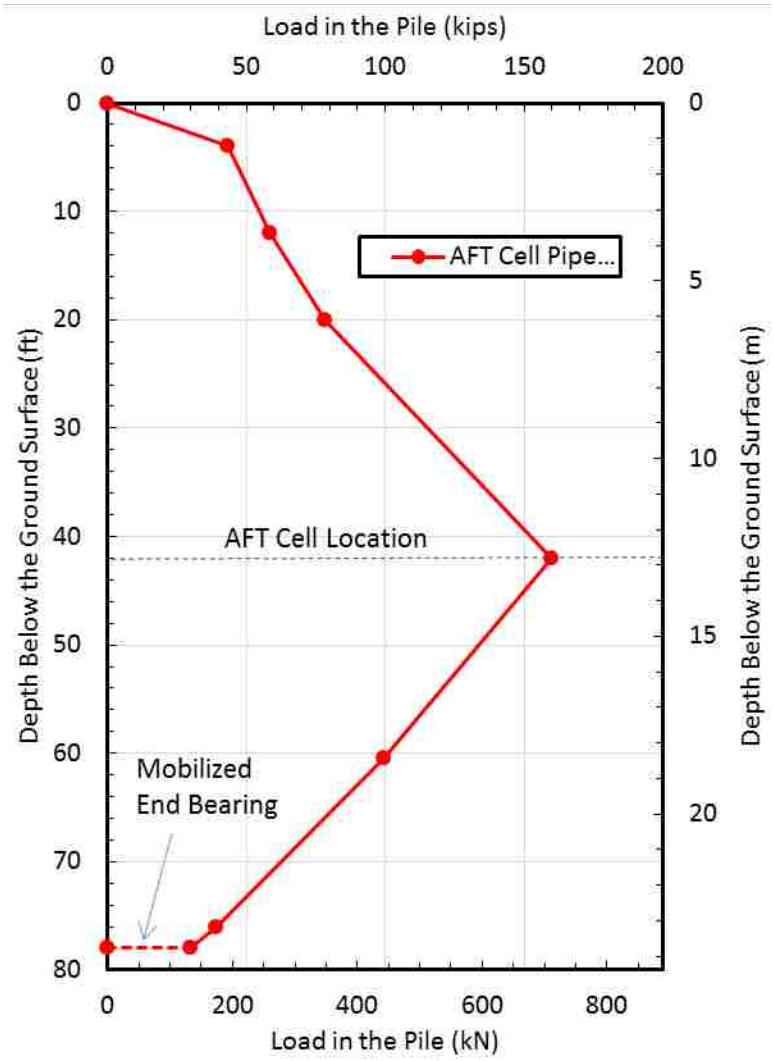

Figure 4.6-1 Load versus depth curve for the AFT cell test performed on the pipe pile.

A comparison of the CAPWAP data is made with the AFT Cell data for the pipe pile and the concrete is shown in Figures 4.6-3 and 4.6-4, respectively. This makes it possible to determine if the results are comparable to what was seen with the CAPWAP data and paints a better picture of what the actual pile capacity should be. The comparison charts were made by taking the 118-kip load that would be placed on the pile prior to blasting and then subtracting the side resistance measured by each test, respectively. This procedure was followed for both the concrete and pipe piles.

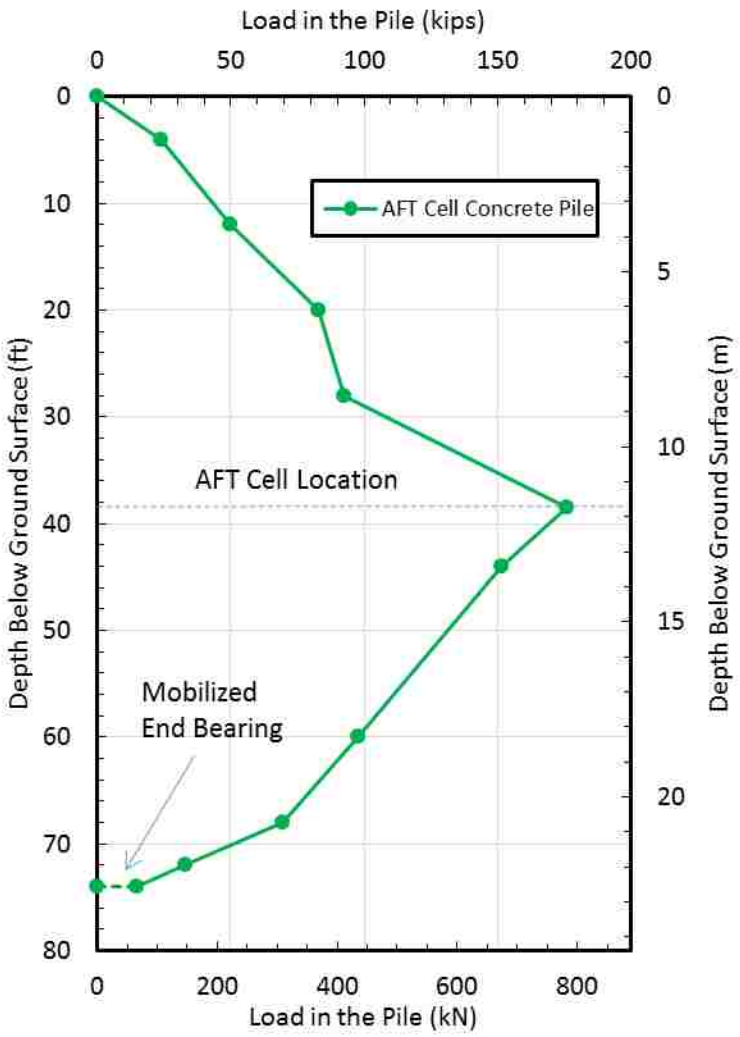

Figure 4.6-2 Load versus depth curve for the AFT cell test performed on the concrete pile.

As shown in Figure 4.5-3, the AFT Cell load test results for the pipe pile agree well with the test results from the PDA and subsequent CAPWAP analysis for the restrike test. Except for the first two feet, the slopes of the two curves are quite similar. However, the pile test with the AFT cell sheds load due to skin friction faster for any of the EOID test results. This could be explained by the soil gaining strength in the clay layers with time because the AFT Cell test was performed several weeks after pile driving.

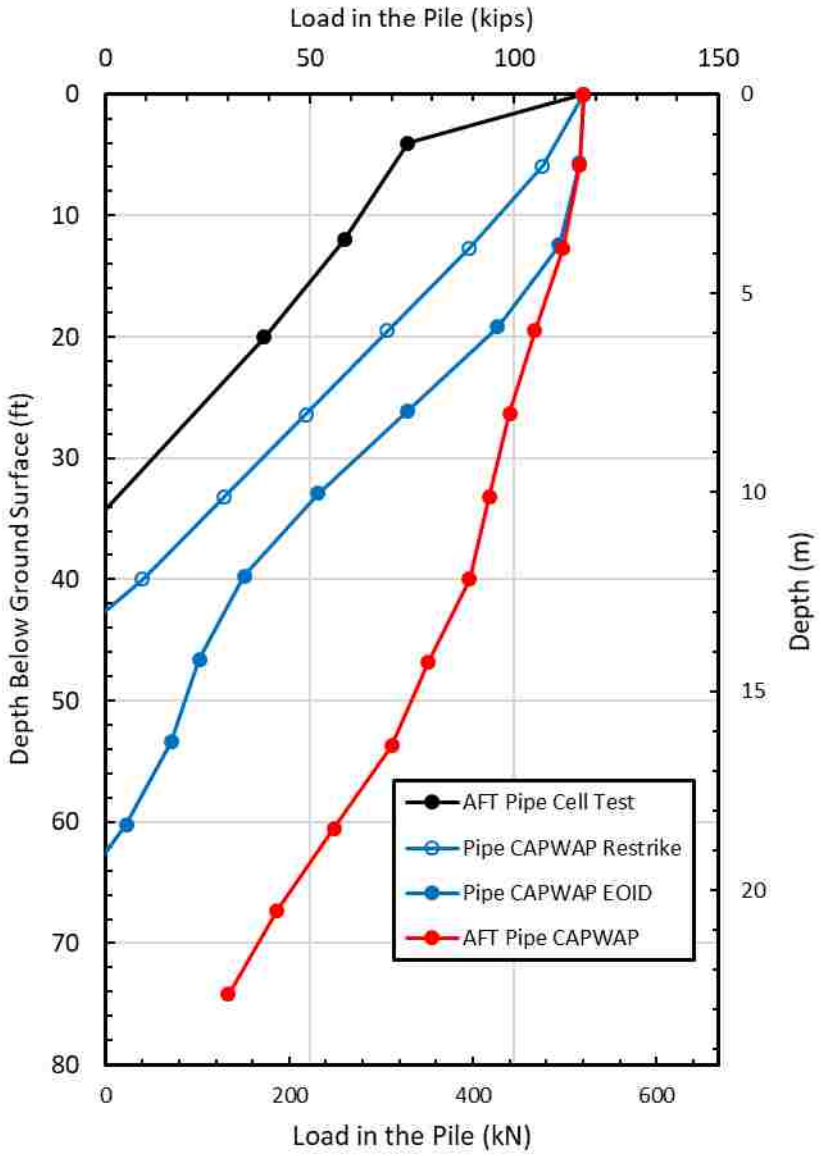

Figure 4.6-3 Load in the pile versus depth comparing the results of the PDA to the AFT Cell test for the pipe pile.

As shown Figure 4.6-4, the AFT Cell test results for the concrete pile agree well with the results obtained from the CAPWAP analysis. It is particularly close to the EOID analysis performed on the concrete square pile used in the blast test, which suggests that the load distribution is realistic.

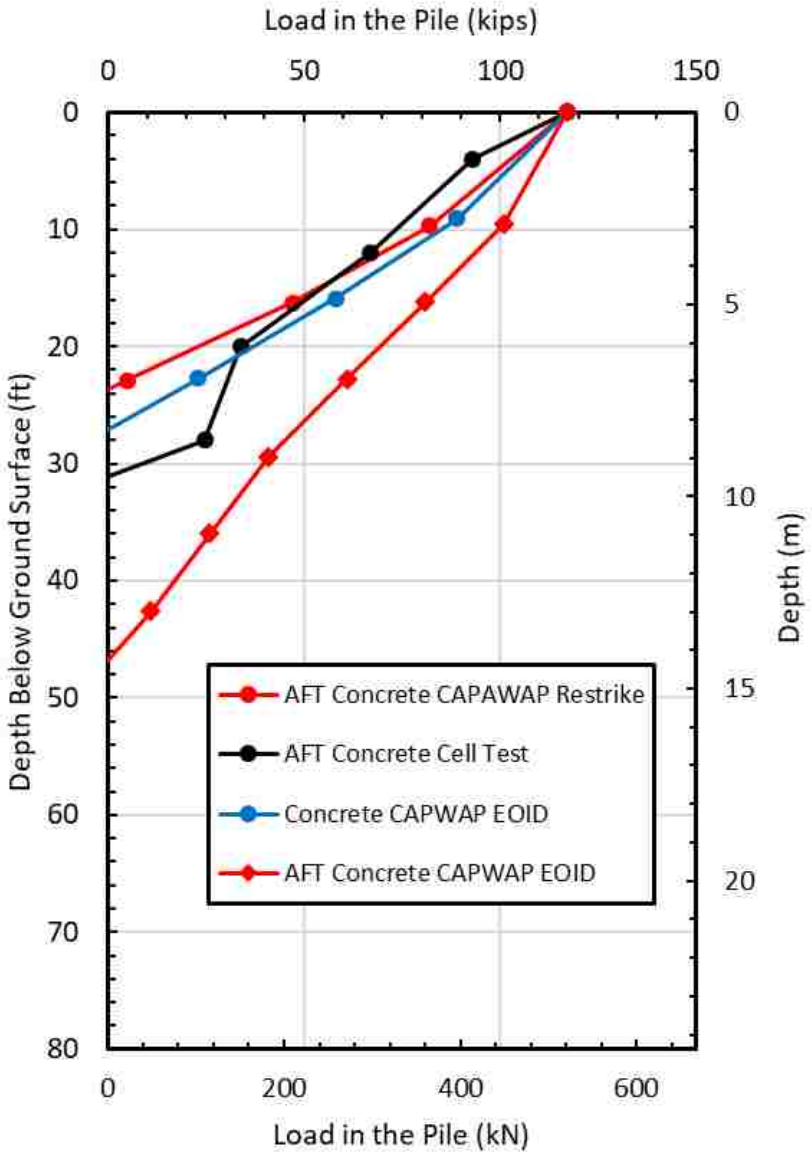

Figure 4.6-4 Load felt in the pile versus depth comparing the results of the PDA to the AFT Cell test for the pipe pile.

4.7 Results from the Static Load Testing

Pile head load versus deflection curves from all three static load tests are shown in Figure 4.6-1. All three piles were loaded to 118.5 kips using the steel blanks as discussed previously. Applied pile head load was based on the weight of each steel blank and the helmet, while pile head settlement was measured using laser level readings. The purpose of the loading was not to

fail the pile, but to measure the side resistance that developed as the pile was loaded, and to have weight on the pile to simulate structural load during blast induced liquefaction. The displacement of the H-Pile was one tenth of an inch while the displacements of the pipe and concrete square piles were less than 0.05 inches, which is negligible. Due to the settlement of the H-Pile it was possible to fully mobilize skin friction and even mobilize some of its end bearing as shown subsequently. Higher settlement for the H-pile is consistent with the lower capacity of the H-pile estimated from the PDA testing as shown in Figure 4.5-4.

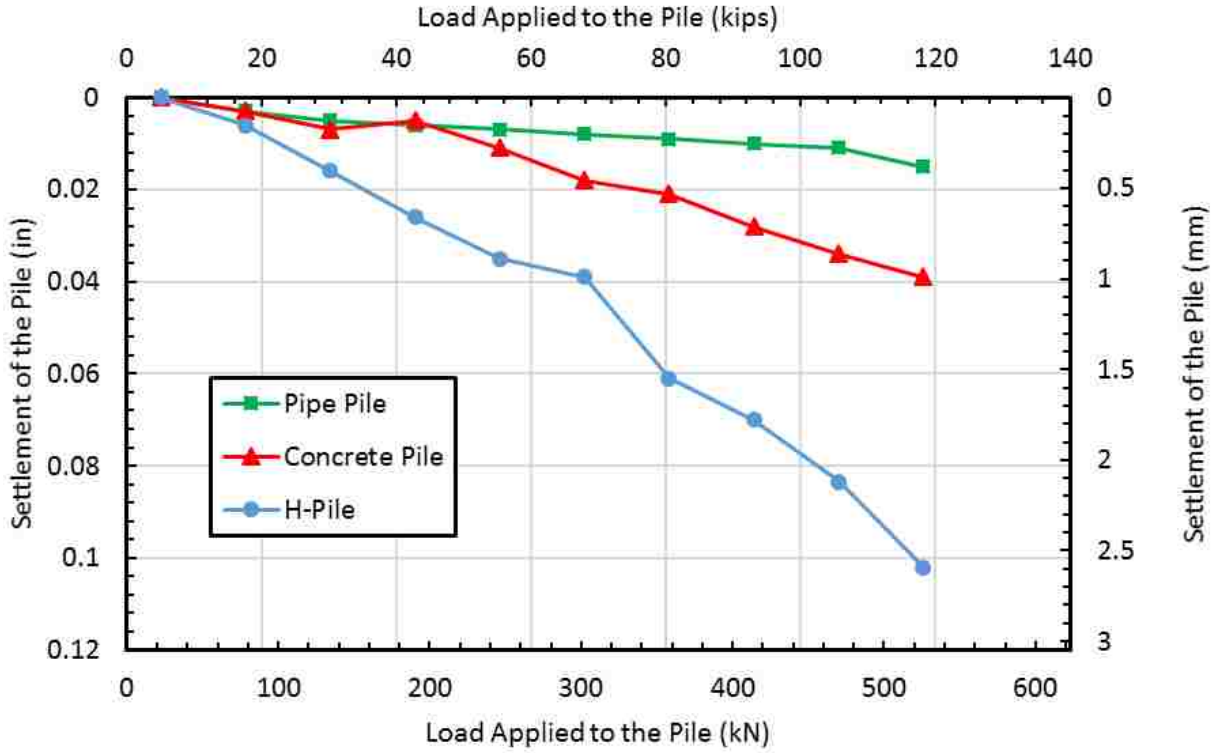

Figure 4.7-1 Pile head load versus deflection curves for each test pile during the static load testing.

The load in the pile before blasting is essential as it will allow us to determine how much the load changed in the liquefied zone after blasting. The load in the H-Pile versus depth from the strain gauge data is presented in Figure 4.7-2, along with the load expected in the pile when

taking the total load of 118 kips and subtracting the side friction predicted from the CAPWAP analysis. Comparing these two load versus depth profiles, it can be seen that they are generally quite similar.

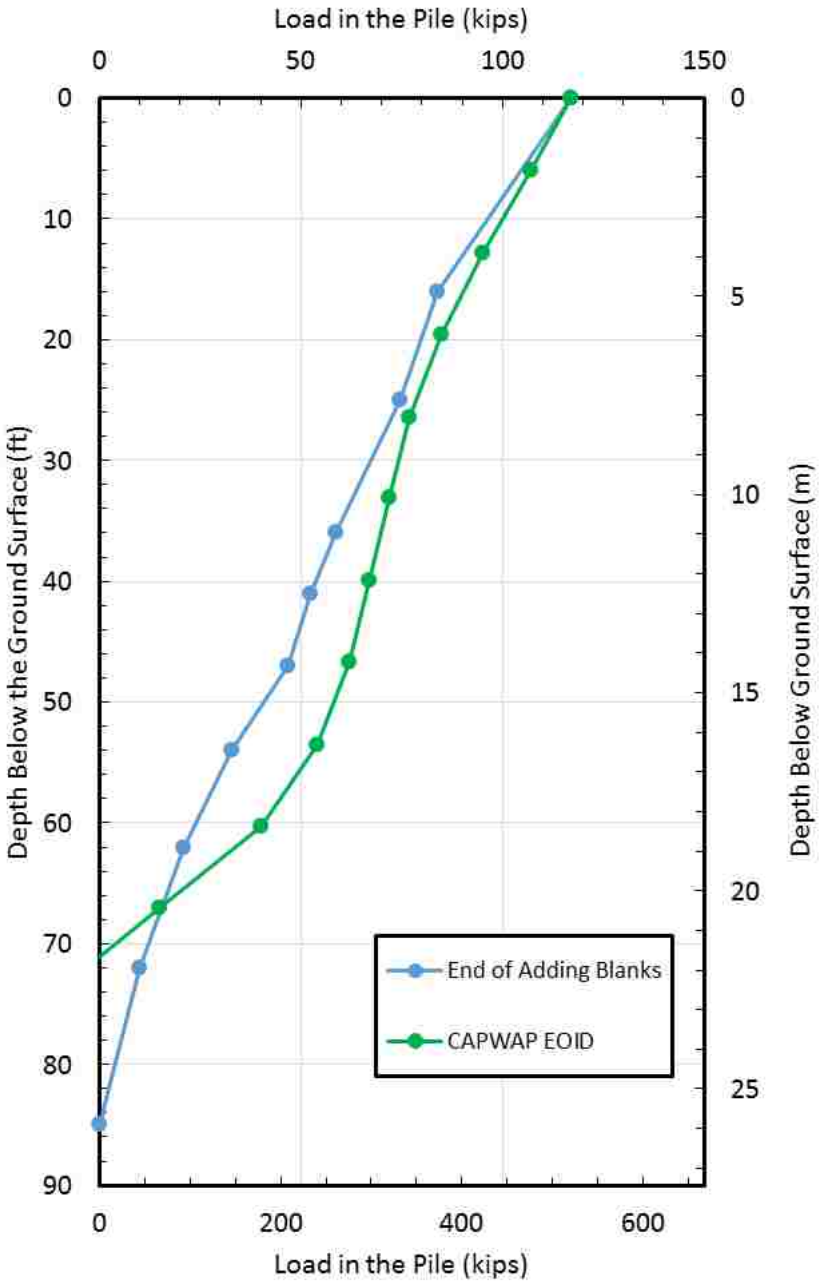

Figure 4.7-2 Load in the pile versus depth in the H-Pile.

Based on the static load test, the skin friction was fully mobilized by the adding of the dead weight. However, based on the CAPWAP analysis skin friction wasn't completely mobilized near the bottom of the pile and end bearing wasn't mobilized at all.

Figure 4.7-3 compares the load versus depth in the pile after application of the static load, with all three CAPWAP analyses performed on pipe piles subtracted from the total load on the pile. This makes it possible to compare various test results and determine what the load is most likely to be prior to blasting.

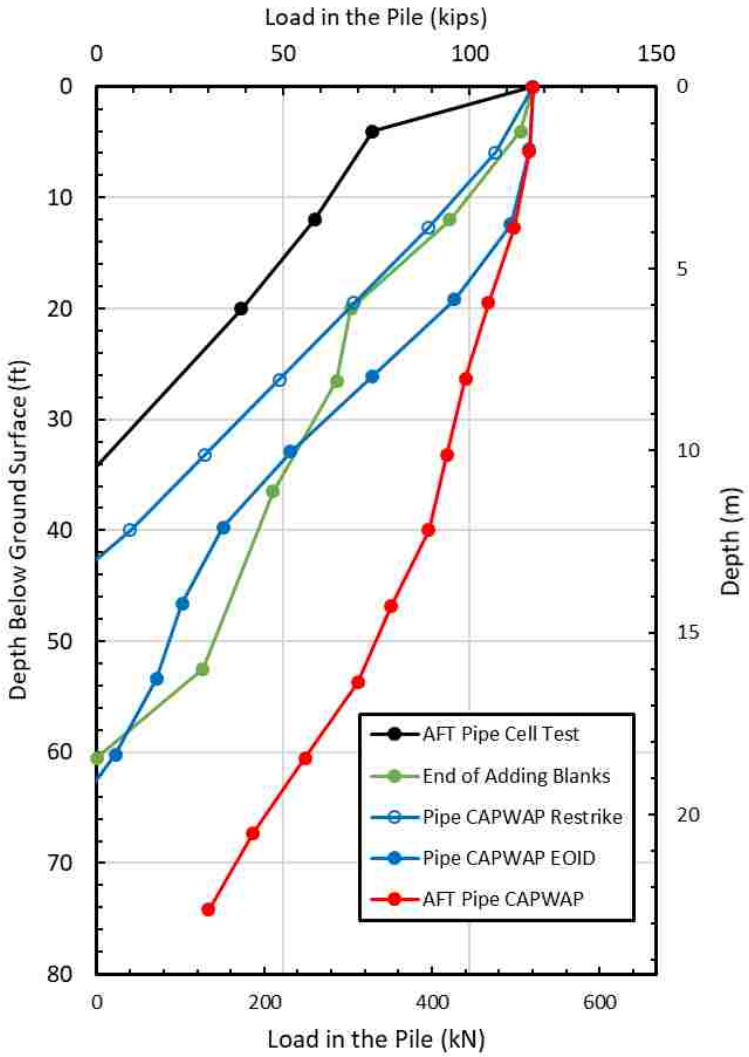

Figure 4.7-3 Load in the pile versus depth for the Pipe Pile.

The load in the pile interpreted from the strain gauges during the static load test generally falls between the CAPWAP results for the EOID and restrike conditions. The load curve from the static load is closer to the restrike curve from CAPWAP in the upper 20 feet of the profile which is composed of clay and would be expected to gain strain with time after pile driving. In the deeper portion of the profile where the soil is primarily sandy, the load curve from the static tests more closely follows the CAPWAP EOID curve. The EOID performed on the pipe pile with the AFT cell shows lower side friction and indicates that end bearing was mobilized, but this isn't reliable as discussed previously. These results suggest that the actual load the pile is feeling is similar to what was obtained from the CAPWAP analyses and this is what will be used later in this document.

Unfortunately, the data collected from the strain gauges in the square concrete pile after loading were unreliable or inoperable and therefore provide little guidance. Nevertheless, Figure 4.7-4 compares the results of the three CAPWAP analyses. Based on these results we can expect that the side resistance on the pile increased with time because the load is shed faster when the restrike data is analyzed. We expected the actual load in the pile to be similar to that obtained from the AFT-Cell restrike pile and the EOID of the concrete square pile later used in the blast test.

A plan view drawing of the drilled shafts, driven piles, and the blast rings surrounding them is shown in Figure 4.8-1. Each of the blast circles has a radius of 8 m (26.5 ft) and shares blast holes with the adjacent circles. This is in order to reduce the number of blast holes per pile. The blast circles were detonated two at a time with a figure 8 sequence starting with the northern pair of piles and drilled shafts. Once blast charges in the top (northern) two rings were detonated,

the instrumentation for the first pile and drilled shaft was disconnected. Then the instrumentation for the next pile and drilled shaft was connected and so forth until all the rings were detonated.

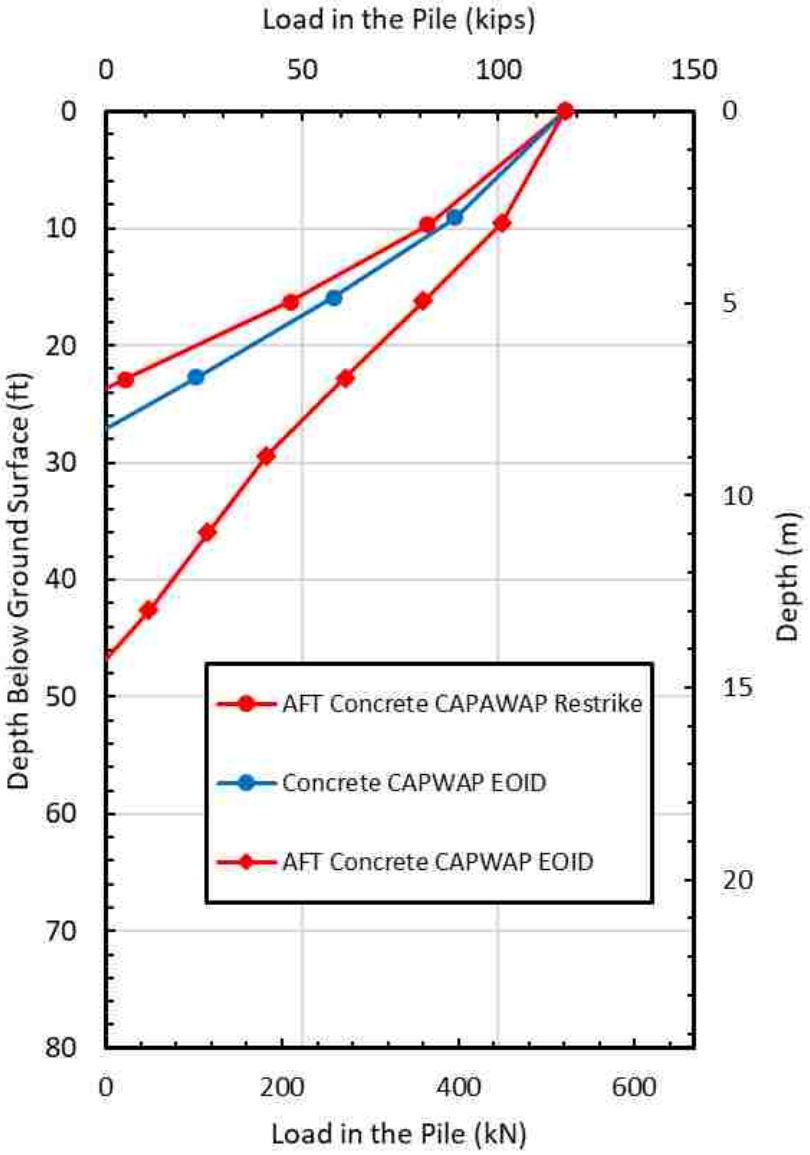

Figure 4.7-4 Load in the pile versus depth in the Concrete Pile.

4.8 Layout and Instrumentation of Blast Tests

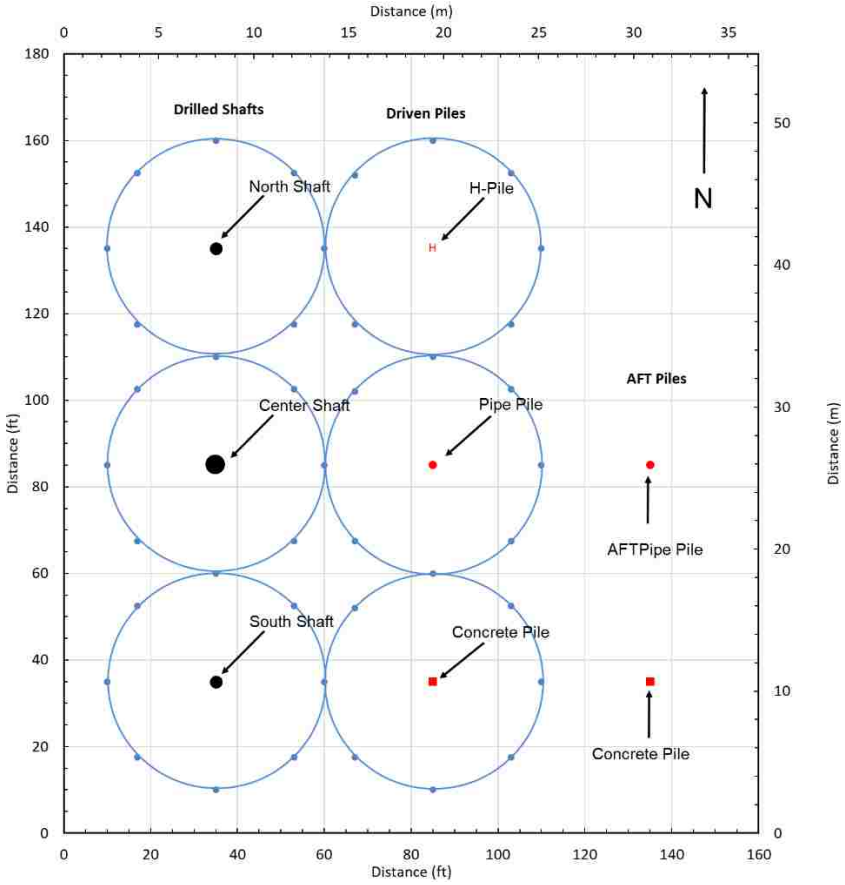

Figure 4.8-1 Plan view showing the overall layout of the blast rings, drilled shafts and driven piles.

A plan view drawing of the test piles, blast holes, and instrumentation around a drilled shaft and driven pile for a typical blast test is presented in Figure 4.7-2. In addition, a profile view of a single pile/drilled shaft within a single blast circle with parts of the adjacent circles is shown in Figure 4.8-3.

Each blast ring typically consists of eight blast holes, eight pore pressure transducers, a line of wooden survey stakes and a Sondex profilometer tube. Up to eight pore pressure transducers (PPTs) were located around a ring approximately two meters away from the center of the test foundation and about six meters inside the blast ring. The pore pressure transducers were

used to measure the generation and dissipation of pore pressure in the soil during blasting and to determine the maximum excess pore pressure ratio produced by the blast. The transducers could measure excess pore pressure with an accuracy of 0.1 psi but had a maximum range of 1000 psi and could survive a transient pressure of 3000 psi. Target depths for the transducers were 30, 33, 36, 39, 42, 46, 56 and 62 feet below the ground surface around both the drilled shaft and the driven pile. These depths were selected so the majority of the transducers were in or around the suspected liquefied zone (30-40 feet), and the rest were spread out to a depth of 60 feet to monitor possible liquefaction at larger depths.

The transducers were installed by drilling a hole filled with drilling mud to a depth about 1 feet above the target depth for the transducer. The transducers, which were mounted in a nylon cone, were then pushed a distance of one foot into the sand. A wire rope was attached to the cone housing so that it could be retrieved after a test blast, re-saturated, and re-installed for a subsequent blast test. Pore pressure data was recorded by a computer data acquisition system at a sampling rate of 20 samples per second.

The wooden survey stakes were used to measure the total settlement at the surface of the soil along a cross-section through the driven piles and drilled shafts. The survey stakes, spaced at 3 ft intervals, typically extended about 70 ft outward from the driven pile and often extended to the drilled shaft or beyond. Liquefaction induced settlement was monitored by comparing the survey stake elevations before and after blasting using an automatic level with an accuracy of 0.001ft. Soil settlement as a function of depth was monitored using a Sondex profilometer probe installed near the test pile. Prior to blasting, stainless steel rings were fixed around a 3-inch diameter corrugated PVC drain pipe at approximately 2 feet depth intervals and the pipe was installed within a bore hole to a depth of 60 ft. Although the sand below the water table generally

flowed in against the corrugated pipe, a gap existed between the drain pipe and the clay in the upper 30 feet of the profile. This gap was filled by pouring pea gravel into the annular space. Prior to blasting, the Sondex probe was inserted through a PVC access pipe inside the drain pipe to determine the depths to the stainless-steel rings relative to a fixed reference point. After blasting, the soil settlement around the drain pipe caused the pipe to move downward with the soil and subsequent Sondex readings were taken to measure the difference in depth to the stainless-steel rings. This procedure made it possible to determine the soil settlement as a function of depth after each test blast.

Unfortunately, as discussed subsequently, it appears that there were gaps in the pea gravel backfill or perhaps loosely placed pea gravel zones that settled following blasting and caused somewhat erratic settlement of the drain pipe, particularly in the upper 30 feet of the profile. In addition, the sand below 30 feet may not have always flowed in tightly adjacent to the drain pipe leading to some erratic settlement readings in this zone.

More detailed plan views of each pile are shown in Figure 4.8-6 which show the depth of each pore pressure transducer and its location around the driven piles. A number of transducers were damaged or became inoperable in the process of installing and extracting them. As a result, fewer transducers were available in subsequent blast tests. Although the Sondex profilometer was located within the blast ring for the drilled shaft in each case, its location relative to the center of the blast area is shown in these figures for reference. It has been assumed that the settlement within the blast ring for the drilled shaft would be comparable to that which would have occurred around the test pile considering that blast charges were comparable.

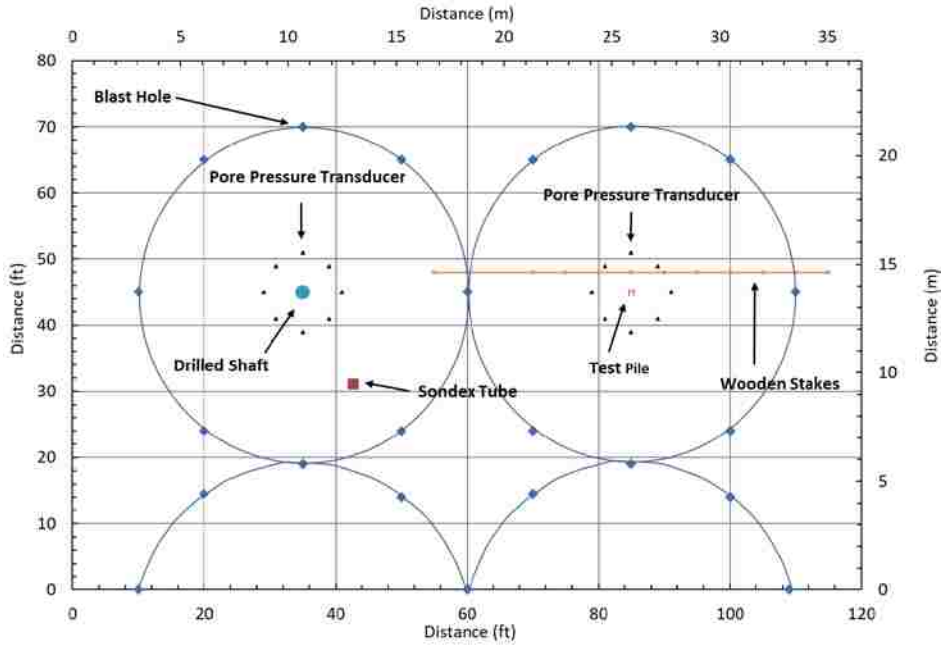

Figure 4.8-2 Plan view drawing for a typical test blast showing drilled shaft and driven test piles, blast holes, and instrumentation.

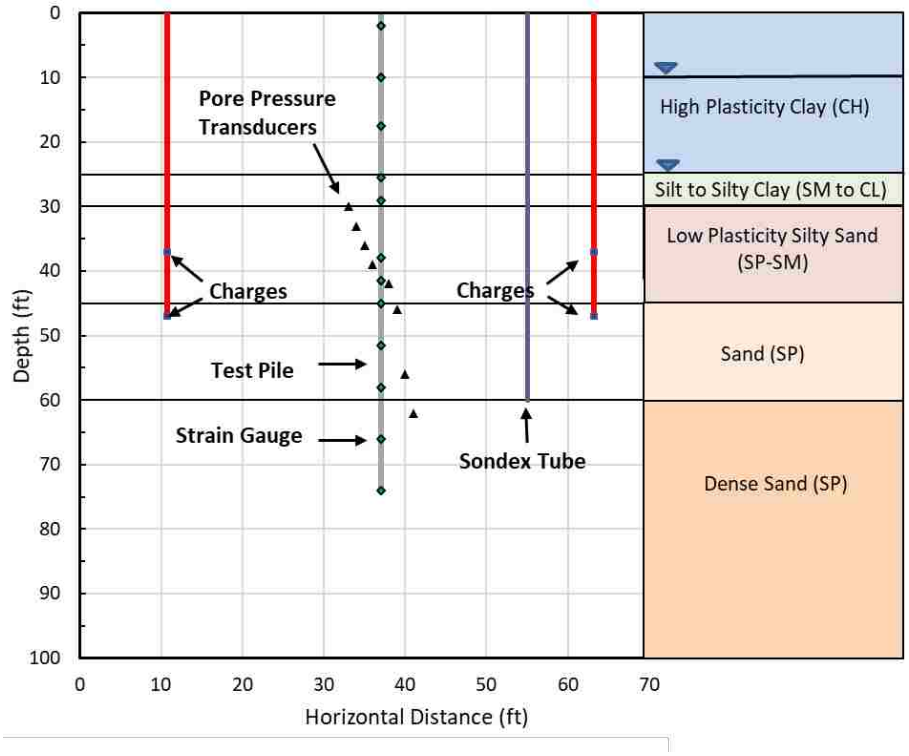

Figure 4.8-3 Profile drawing of test pile, blast holes, and instrumentation for a typical test pile/drilled shaft at the test site.

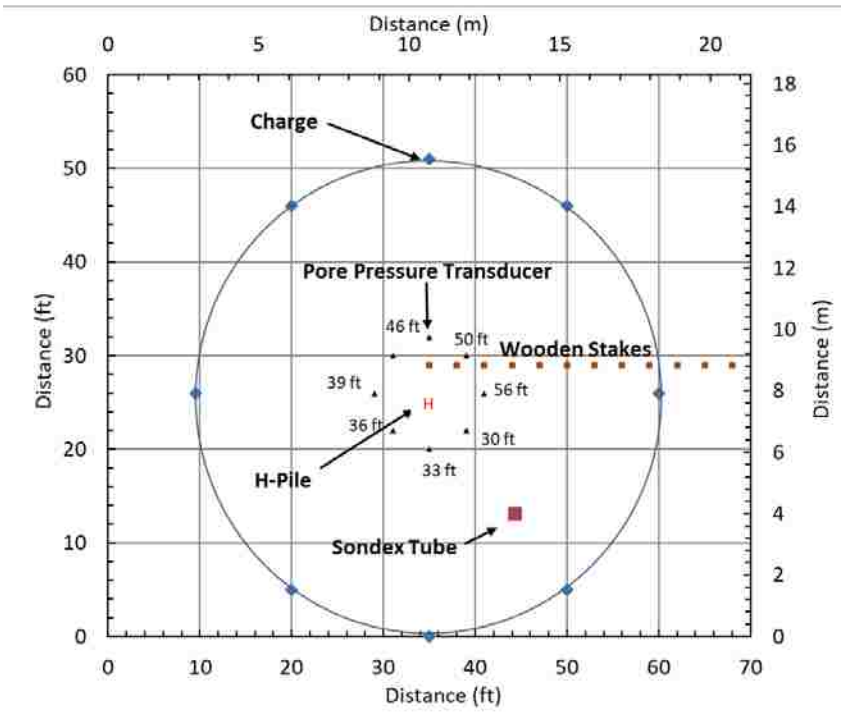

Figure 4.8-4 Detailed plan view drawing of the H-pile with blast holes and instrumentation.

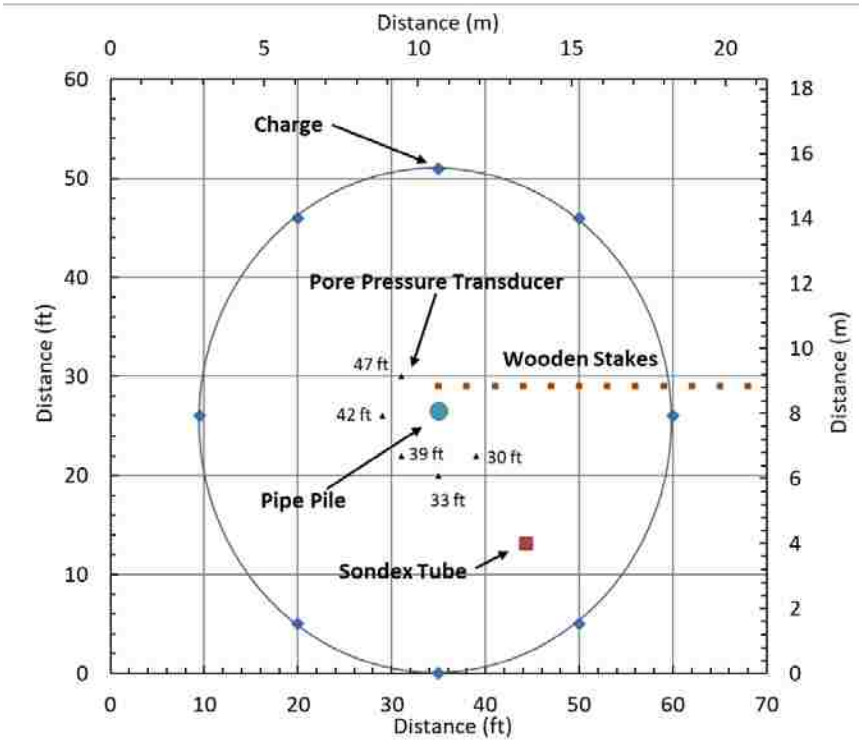

Figure 4.8-5 Detailed plan view drawing of the pipe pile with blast holes and instrumentation.

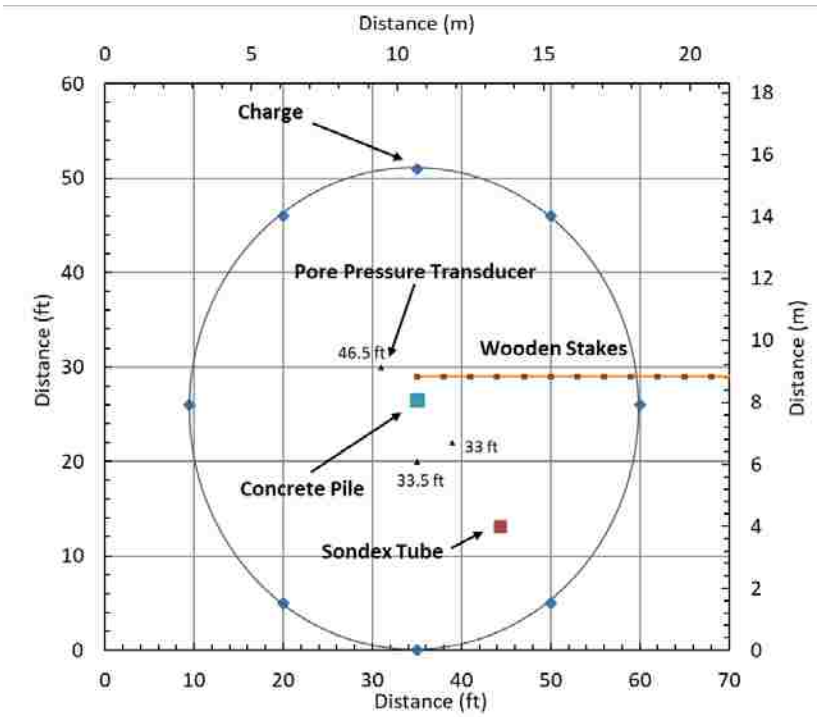

Figure 4.8-6 Detailed plan view drawing of the square concrete pile with blast holes and instrumentation.

5 BLAST-INDUCED LIQUEFACTION TEST

5.1 Overview

As discussed in the literature review, blast induced liquefaction has been used in the past to evaluate downdrag loads on piles (Rollins and Strand 2006, Rollins and Hollenbaugh 2015). In addition, blast liquefaction has been used to determine lateral resistance of pile in liquefied sand (Rollins et al 2005), and the effectiveness of earthquake drains (Rollins et al, 2006). The objectives of this experiment are to measure the drag loads that developed in pre-loaded piles following liquefaction along with the settlement of the pile relative to the surrounding soil. To achieve these objectives, the experiment was designed to measure load in the pile and pile settlement along with excess pore pressures and settlement of the soil around each pile during their respective blast tests.

This chapter describes the procedures used to conduct the blast test along with the results of the testing for each pile type. Blast test results include: (1) pore water pressure measurements, (2) soil and pile settlement measurements, (3) load and skin friction developed in the pile, and (4) neutral plane evaluation methods.

5.2 Blast Test Procedures and Results for the H-Pile

5.2.1 Blast Test Procedures

Prior to blasting, a dead weight of 118.5 kips was applied to the H-pile as discussed in Chapter 4. Based on the CAPWAP capacity of 285 kips (after adjustment for end-bearing increase), the factor of safety against axial compression failure of the pile prior to liquefaction was about 2.4. However, if the sand were to liquefy from 30 to 60 feet and the liquefied sand had no skin friction, the axial capacity would drop to 235 kips and factor of safety would be about 2.0.

The blast test for the H-pile and the adjacent 4 foot-diameter drilled shaft involved 15 blast holes evenly spaced around two rings each centered on the test foundations as shown in Figure 4.7-2. Within each blast hole, four pounds of explosive charges were placed with their centers at 37 and 47 feet below the ground surface, respectively. Gravel stemming was placed to the top of each blast hole to separate the charges and prevent sympathetic detonation as well as to direct the blast pressure to expand radially rather than simply vertically. In addition, three gravel-filled bags were placed atop each blast hole.

The charges in each blast hole were detonated sequentially in a figure eight pattern around the two rings. Within each blast hole the bottom charge was first detonated while the upper charge was detonated after a delay of 176 milliseconds. The charges in the next blast hole were then detonated after a delay of 500 milliseconds. Thus, 120 pounds of explosives (8 pounds in each blast hole) were detonated in a total time of 9.46 seconds. Following blasting, the dissipation of pore pressure was monitored for approximately 180 minutes. There were no physical signs of liquefaction such as sand boils, observed during this blast test. This could be a

result of the 30-foot thick layer of cohesive soil overlying the liquefiable sands at this site that likely restricted the upward flow of water and sand. Owing to the tight time schedule for completing the tests, the pile was then unloaded and the data collection system was disconnected although excess pore pressure ratios had not yet dissipated to less than 10% of the vertical effective stress at all depths, as discussed subsequently.

5.2.2 Pore Pressure Response Following Blasting

Based on the measured pore water pressure at each transducer, the excess pore pressure ratio (R_u) was calculated at depths of 30, 33, 36, 39, 42, 46, 50 and 56 feet below ground surface. Plots of peak R_u versus depth for the driven pile and companion drilled shaft are while peak R_u values are plotted versus depth in Figure 1.1-1Figure 5.2-1.

The pore pressure transducers (PPTs) were located approximately 2 meters away from the center of the H-Pile and about 6 meters inside the blast ring. The excess pore pressure ratio is a function of effective stress and is calculated using the equation

$$\mathbf{R_u} = \frac{\mathbf{u - u_o}}{\mathbf{\sigma_o'}} \qquad 5\text{-}1$$

where u is the pore pressure at the depth in question after blasting, u_o is the initial pore pressure at the depth in question prior to blasting, and σ_o' is the initial vertical effective stress prior to blasting. As mentioned in section 3.1, there was some confusion as to the appropriate depth for the water table, and even though some pre-blast calculations were made with a water table at 10 feet, post blast calculations were made with the water table at 25 feet. This included recalculating the vertical effective stresses and calculating the pore pressure ratios with a water table at a depth of 25 feet. For comparison purposes the effective stress was calculated three different ways. One was using the unit weight in chapter 3 correlated from N values (denoted as SPT Data), another

was using correlations with CPT data from chapter 3 (denoted as CPT Data), and the third way was using a single average unit weight in the clay layer based on the undisturbed samples and an average unit weight value in the sand based on the SPT correlations (denoted as Average Unit Weight SPT). The third method was also the method used in the field to provide a quick check on whether the soil had liquefied.

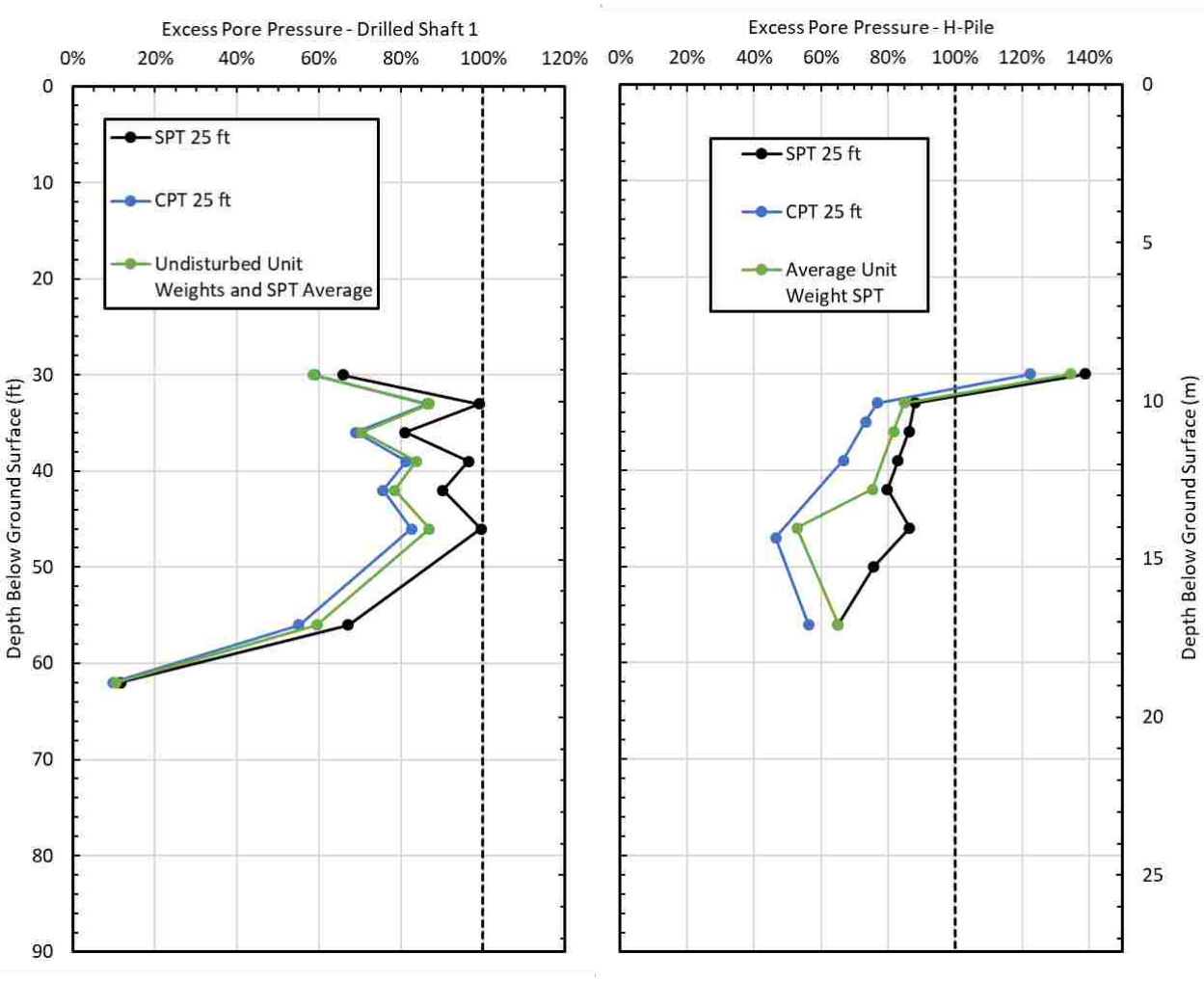

Figure 5.2-1 Excess pore pressure ratio versus depth (a) around the 4-ft diameter drilled shaft and (b) driven H-pile following the first blast.

The excess pore pressure ratio around the H-Pile was above 0.8 from 30 feet below the ground surface until about 40 feet below the ground surface. The results are compared to the

excess pore pressure ratios surrounding the drilled shaft that was blast tested at the same time. The results from the drilled shaft indicate liquefaction to at least 40 feet and even down to 46 feet. They differ drastically at 30 feet, but this may be due to clays extending a little deeper around the drilled shaft. Based on the results from the two deep foundations it is reasonable to say the soil was essentially liquefied to a depth of about 46 to 50 feet. Thus, about 16 to 20 feet of soil was liquefied.

There is some discrepancy in the pore pressure data around 46 feet. The excess pore pressure calculated using CPT data and an average SPT value both drop, however the R_u value at this depth for the SPT data does not drop. This could be that the SPT data indicated that the soil was not as dense as the CPT data read at this depth. Also, it was likely averaged out in the Average SPT curve, and therefore went overlooked. Further, it seems strange to have an excess pore pressure ratio of 1.4 at the depth of 30 feet. This is most likely due to the soil layering not being completely even and the pore pressure transducer remained in cohesive soil, and therefore read higher excess pore pressures than if it had been in sand.

R_u versus time curves at each pore pressure transducer location are presented in Figure 5.2-2. In this case, the vertical effective stress was based on the unit weights from correlations with CPT data from Chapter 3. The excess pore pressure dissipated slowly. At 180 minutes after the blast, the pore pressure ratios had not fully dissipated at 30, 33 and 36 feet, but were typically about 40%. However, at depths, 46 and 56 feet the excess pore pressures had dissipated to less than 10% after 30 minutes while the transducer at 42 feet required 140 minutes to reach this level.

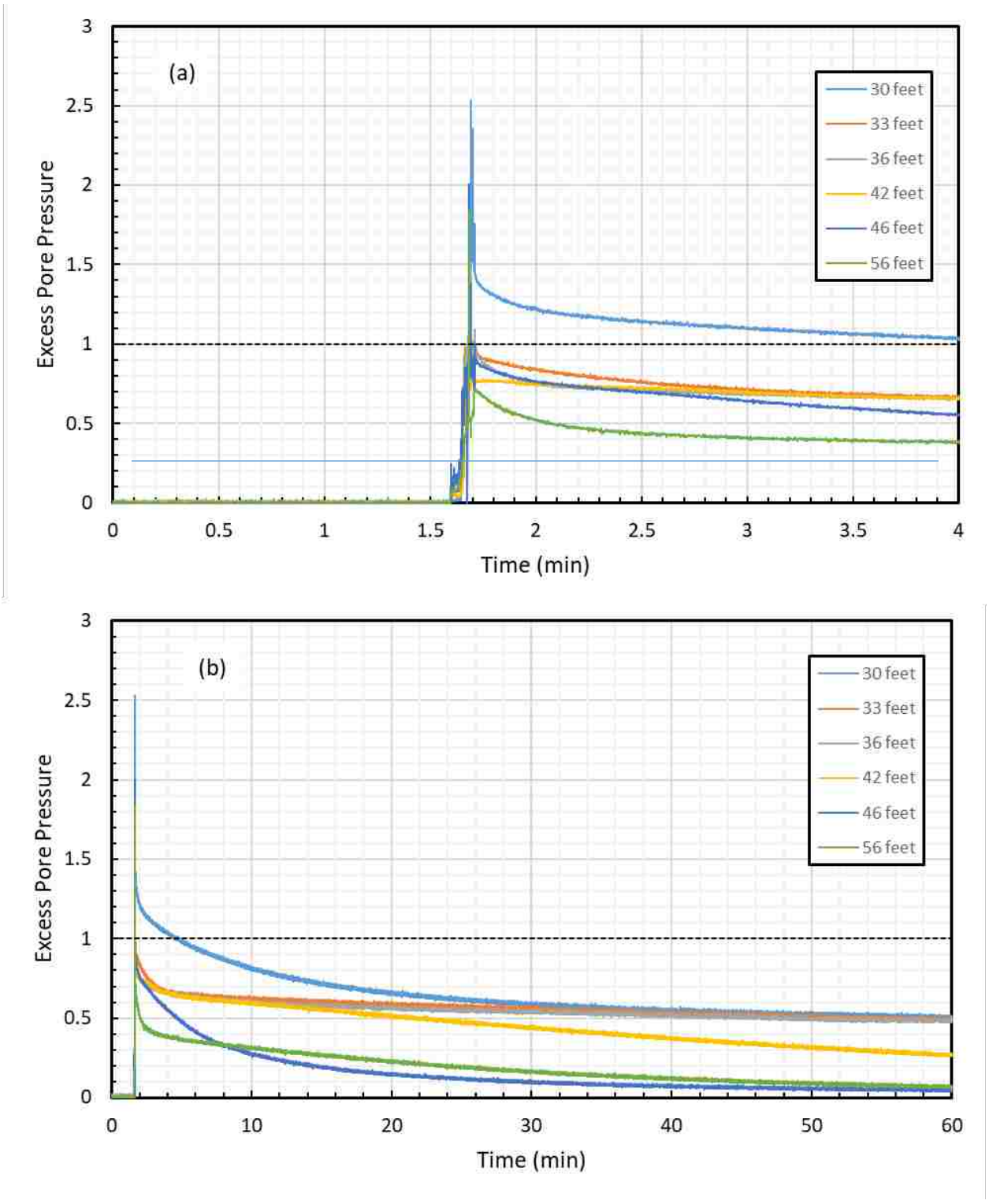

Figure 5.2-2 Excess pore pressure ratio versus time curves in the soil surrounding the H-pile (a) for 180 minutes following the blast and (b) immediately following the blast.

5.2.3 Soil and Pile Settlement Following Blasting

As indicated previously, the total ground surface settlement across the site was measured by placing a line of survey stakes adjacent to the two deep foundations at approximately 3-foot intervals extending about 75 ft eastward from the H pile. The line was located about 4 ft to the North side of the test foundations. The elevation of the top of the stakes was measured before the blast, 40 minutes after the blast, and 150 minutes after the blast. The settlement profile across the site is presented in Figure 5.2-3. Settlements became negligible at a distance of about 65 ft from the center of the test pile.

After 150 minutes, the settlement of the ground near the pile was about 1.8 inches while maximum settlement between the H pile and the drilled shaft was about 2.25 in. However, the excess pore pressures from the blast had not completely dissipated and some additional settlement may have occurred. The settlement near the pile itself may have been somewhat higher than at 4 ft from the pile where the survey line was positioned. Nevertheless, the offset between the soil and the H-pile was also measured and the difference was approximately 2.25 inches. The total ground surface settlement of the profile was estimated from the Sondex tube measurements. Sondex measurements were taken well after excess pore pressures had dissipated, more than 12 hours after the blast. The total ground settlement was estimated to be about 2.5 inches, based on an average determined from the Sondex data.

A settlement versus depth profile near the test pile was developed using data from the Sondex tube. This profile makes it possible to compare the soil settlement to the settlement of the pile, thus providing an independent estimation of the location of the neutral plane. As noted previously, the neutral plane is typically defined as the depth where the settlement of the pile is the same as the settlement of the soil. The raw settlement vs. depth data points collected from

the Sondex tube are shown in Figure 5.2-4. Because of difficulties during installation of the Sondex pipe, discussed in Chapter 4, it appears that the soil surrounding the Sondex pipe was not in uniform contact with the pipe. As a result, the settlement readings are somewhat erratic. Despite the scatter, there was a clear pattern to the data.

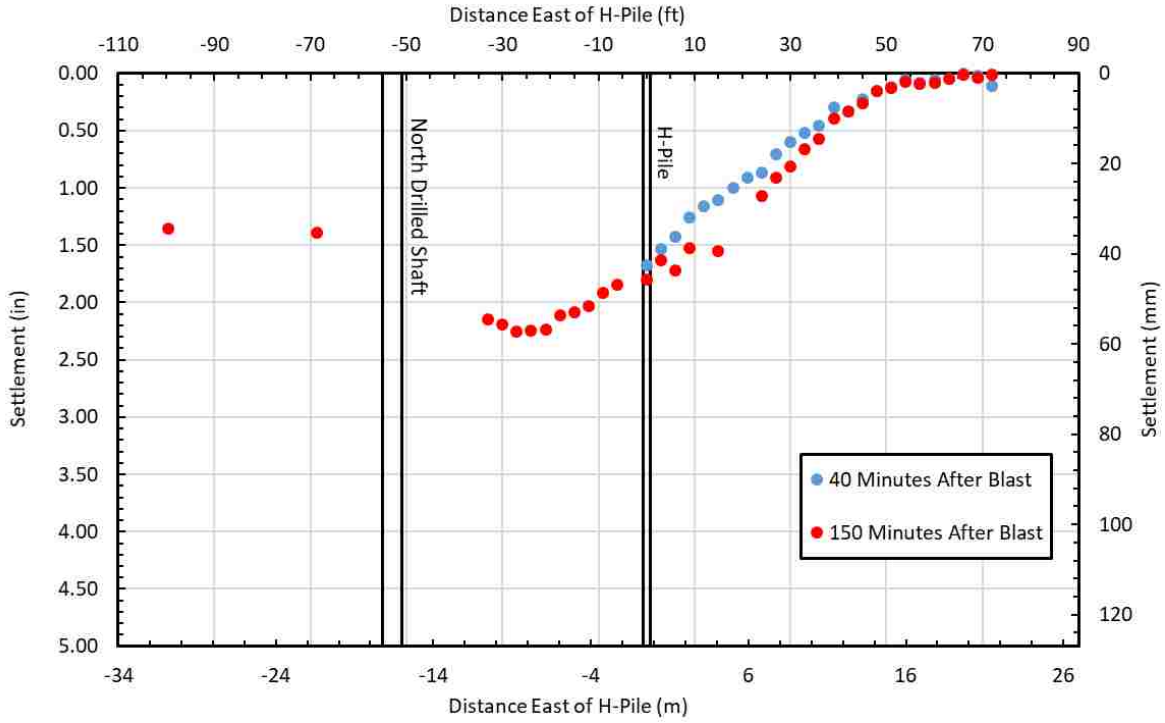

Figure 5.2-3 Liquefaction induced ground surface settlement versus horizontal distance along a line adjacent to the H Pile and a companion drilled shaft following blasting.

To develop a more reliable settlement profile, the average Sondex settlement was used in the clay layer down to 30 feet, and a regression equation was used to create a best fit curve for the cohesionless soil below 30 feet. This presumes that the cohesive layer essentially settled on top of the sand layer as it re-consolidated following liquefaction. The regression equation that provided the best fit curve was an exponential equation. For settlement below 54 feet, where data points ended, the line regression line was extrapolated. The settlement profile from the developed exponential function is also shown in Figure 5.2-4. The settlement profile is

consistent with the measured R_u values. The greatest settlement occurred in the layer from about 30 to 40 ft where R_u was highest, although significant but somewhat lower settlement occurred from 40 to 50 ft. Settlement was minimal below this depth which is consistent with the relatively low R_u values.

The settlement of the H-Pile during the blast was about 0.28 inches based on auto-level measurements. The elastic distortion that would be produced over the length of the pile for the 118.5-kip static load is negligible, therefore the pile settlement is plotted as a constant value along its length in Figure 5.2-4. Taking into account the pile settlement and the settlement of the soil, the neutral plane is at about 52 feet where the settlements are the same.

The total volumetric strain developed in the soil as a result of liquefaction was calculated by taking the total settlement of the liquefied layer and then dividing it by the thickness of the liquefied layer. This strain was then compared to expected volumetric strain from earthquakes based on SPT $(N_1)_{60}$ values determined by Tokimatsu and Seed (1987). The volumetric strain generated by blast induced liquefaction was determined to be 1% for the layer from 30 to 46 feet. The expected strain based on the average blowcount over the 16 feet of liquefied soil was about 2%. Initially, this would suggest that the soil did not strain as much as expected in an earthquake. However, recent studies recommend that the computed strain be reduced using a depth reduction factor proposed by Cetin et al. (2009) (see Eq. 3-17). Using this depth reduction factor, the computed volumetric strain would be reduced from 2% to about 0.7%. Therefore, considering the depth of the liquefied layer, the measured volumetric strain is comparable to that expected from an earthquake.

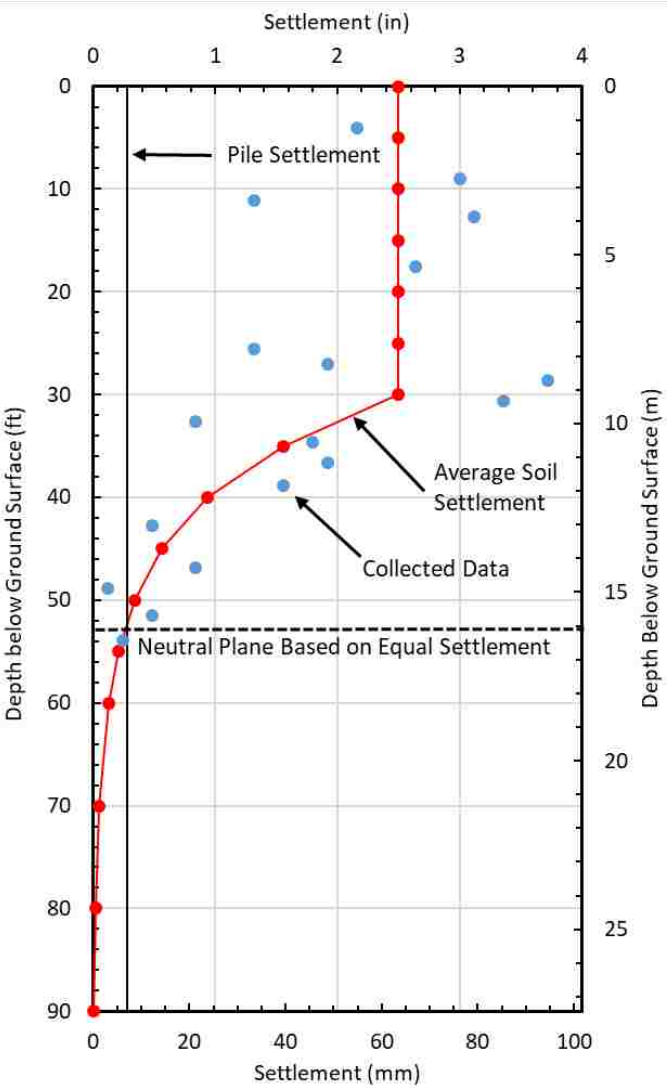

Figure 5.2-4 Settlement of the H-Pile and the surrounding soil during the first blast.

5.2.4 Load in the Pile Following Blasting

The load in the pile versus depth following blasting was computed using strain gauge readings with Equation 4-1 as was done when the blanks were applied to the H-Pile during static loading. The load in the pile versus depth curve resulting from liquefaction induced settlement is presented in Figure 5.2-5. This curve represents the load that developed about 100 minutes after blasting when the excess pore pressures were largely dissipated. The load in the pile clearly

increases with depth from the ground surface to a depth of 62 ft indicating that the soil is settling relative to the pile and inducing negative skin friction or dragload on the pile. Below this depth the load in the pile decreases indicating that load in being transferred from the pile to the surrounding soil by positive skin friction.

The load in the H-Pile was zeroed out before blasting because the blast liquefaction test was carried out the day after the static load test described previously in section 4-6. Due to concerns about equipment theft and the difficulty of maintaining power over night, the data acquisition system had to be disconnected and then reconnected the next day. Thus Figure 5.2-5 does not show the total load in the pile from static loading and downdrag loading, it shows the load in the pile minus the load induced from static loading.

To determine the total load in the pile versus depth it was necessary to add the load in the pile from the applied load. This was done using the CAPWAP pile resistance data at the end of initial driving displayed in Figure 4.7-2 and adding it to the load measured after liquefaction induced settlement in Figure 5.2-5. CAPWAP load vs. depth data was chosen as it was considered the most reliable data and generally fit reasonably well with the measured load from the static load test. Furthermore, CAPWAP data was available for all piles whereas static load test data was not.

Figure 5.2-6 shows the combined pre-blast (CAPWAP curve) and post-blast load versus depth curves added together. The load increases in the pile from the applied load at the top moving down the pile as negative skin friction is mobilized. The slope of the load versus depth curve changes at about 32 feet and becomes steeper. The liquefied zone was from about 30 to 46 feet; therefore, the slope would be expected to become steeper in this zone due to smaller skin

friction forces in the liquefied sand. It is also important to note that the slope of the curve is not vertical, therefore negative skin friction is developing in the liquefied layer and is not zero as some have speculated (Fellenius and Siegel, 2008).

The maximum load in the pile after blast liquefaction was about 175 kips at a depth of 55 feet. This would indicate that the neutral plane would be at this depth as well. It is important to note that this is very close to the 52-foot depth determined for the neutral plane from the settlement versus depth data. End bearing was mobilized and was about 60 kips. This is significant, because it will allow the pile to be analyzed using settlement versus end bearing mobilization curves.

Figure 5.2-7 compares the load in the pile versus depth curves for static loading before blasting and then after blast induced liquefaction and reconsolidation. Under static loads, before blasting, the load in the pile decreases with depth as load in the pile is transferred to the soil by positive skin friction. After blasting, the load in the pile increases as negative skin friction increases the load in the pile. If skin friction is the same before and after liquefaction the two curves would be mirror images of each other relative to the load at the top of pile. This appears to be the case for the top 30 feet of the soil profile which consists of cohesive soil and the load-transfer from skin friction is about the same. However, the load versus depth curve in the liquefied zone is steeper after the blast, meaning that the pile sheds less load in this zone and therefore has less skin friction. There is, however, a definite change in load versus depth present in the liquefied zone. Below about 60 feet, where liquefaction did not occur, the slopes of the two curves once again appear to be similar.

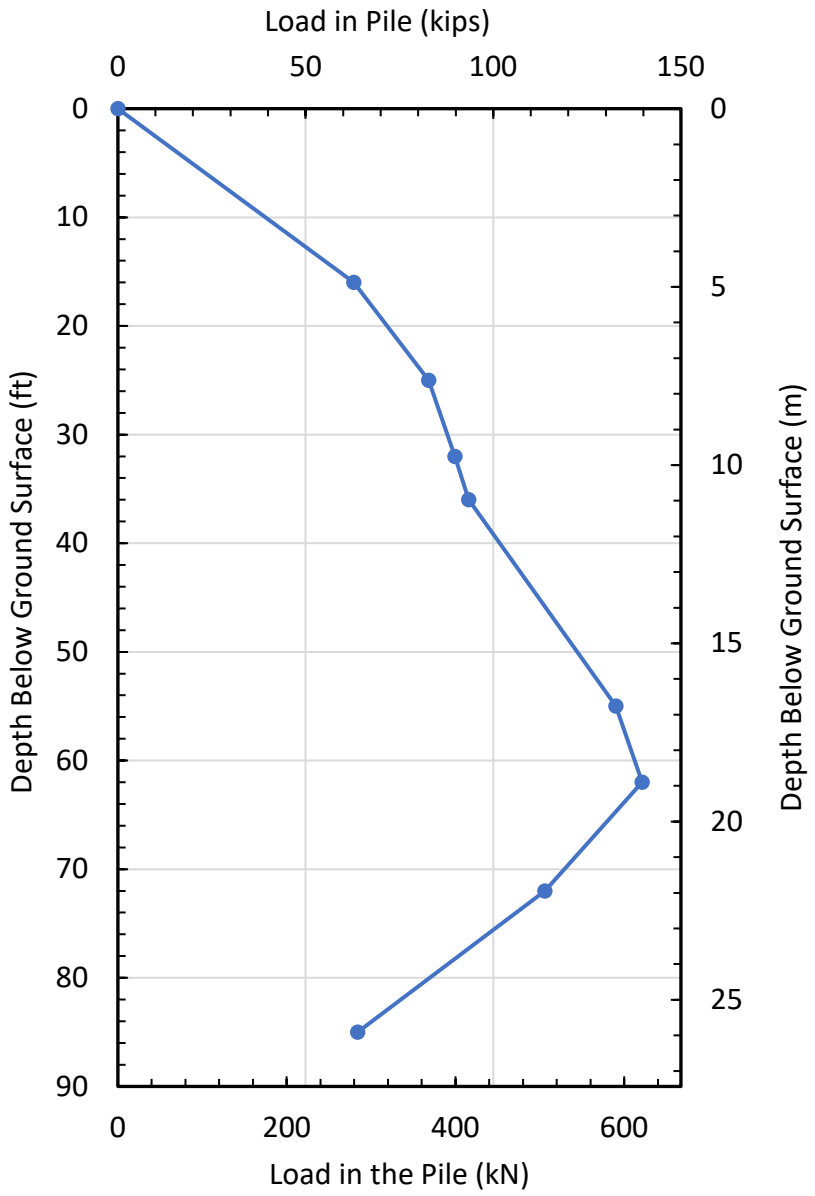

Figure 5.2-5 Change in load in pile vs depth after blast liquefaction for H pile.

The purpose of this study is not only to determine if there is negative skin friction in the liquefied layers after pore pressures dissipate, but to also determine the magnitude of that friction. This has been done by comparing the load transfer or incremental side resistance before and after blasting at consistent depth intervals along the pile. Figure 5.2-8 shows plots of the load transfer before blasting (from CAPWAP EOID) and after blasting (from Figure 5.2-6) at consistent depth intervals along the H pile. The post-blast side resistance is typically similar to

the pre-blast side resistance in the clay layers in the top 30 feet of the profile as well as in the sand layers below 50 feet where liquefaction did not occur. In contrast, the post-blast side friction was typically less than pre-blast side resistance in the zones where liquefaction or elevated pore pressures were measured.

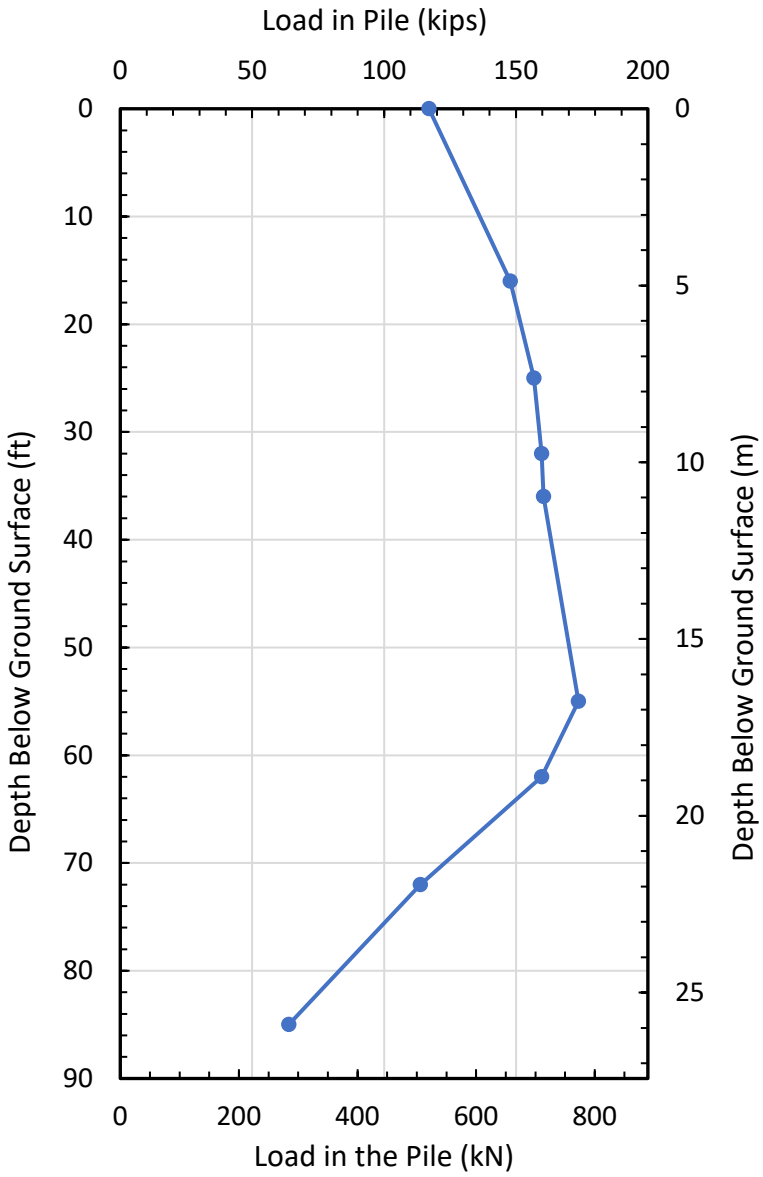

Figure 5.2-6 Load measured in the H-Pile after blasting including the load induced from the pre-blast static loading.

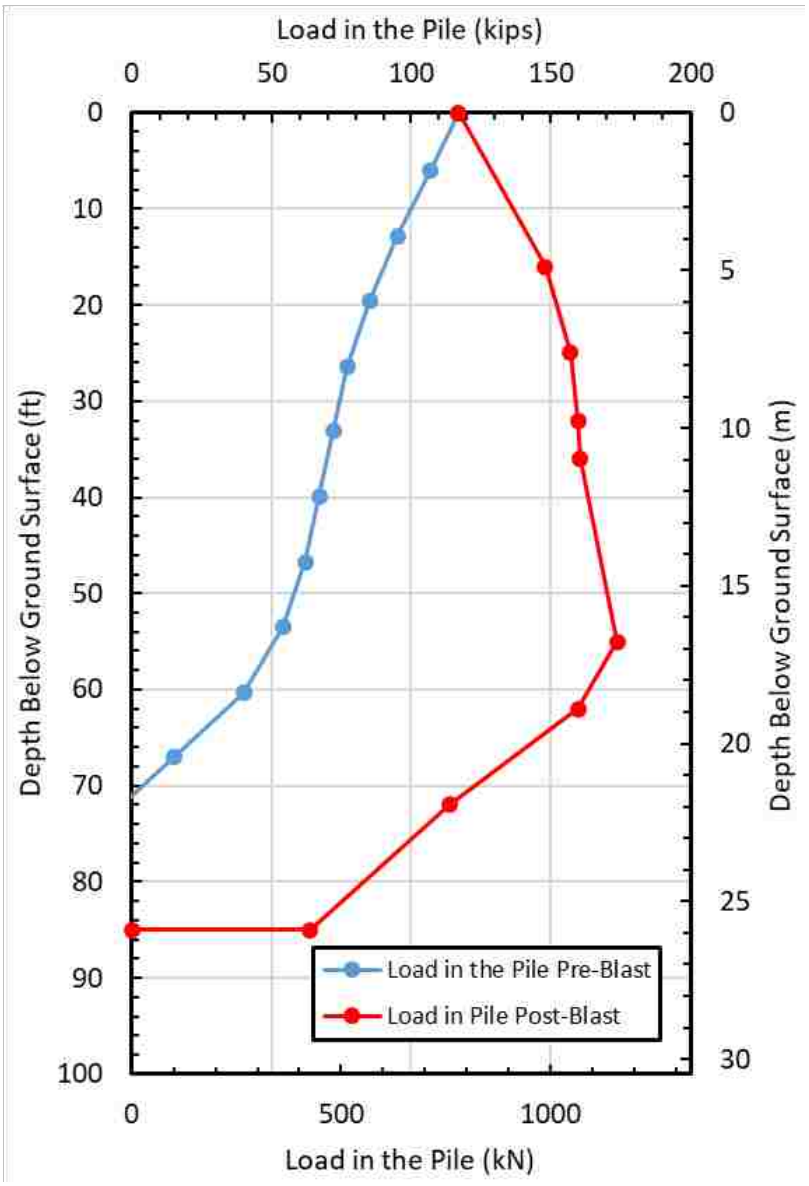

Figure 5.2-7 Load versus depth in the H pile immediately before blast and after blast induced liquefaction and reconsolidation.

The percentage of the side resistance after liquefaction relative to the side resistance before blasting was calculated by dividing the side resistance in a post-blast depth increment by the corresponding pre-blast side resistance in that same depth increment. The pre-blast side resistance was assumed to be what the results from the CAPWAP EOID test indicate. The average of side resistance or negative skin friction in the liquefied zone was found to be 49% of

the positive skin friction prior to blasting, which is very close to that measured in other field tests (Rollins and Strand 2006, Rollins and Hollenbaugh, 2015). The same comparison was made in the non-liquefied layers along the pile as well. The percentage of the pre-blast side resistance compared to the post-blast side resistance in the layers above the liquefied zone was 115% and below the liquefied zone it was 93%. This result suggests that the post-blast negative skin friction in non-liquefied layers will be similar to the positive skin friction before blasting. This result is also consistent with findings from other field tests (Rollins and Hollenbaugh, 2015).

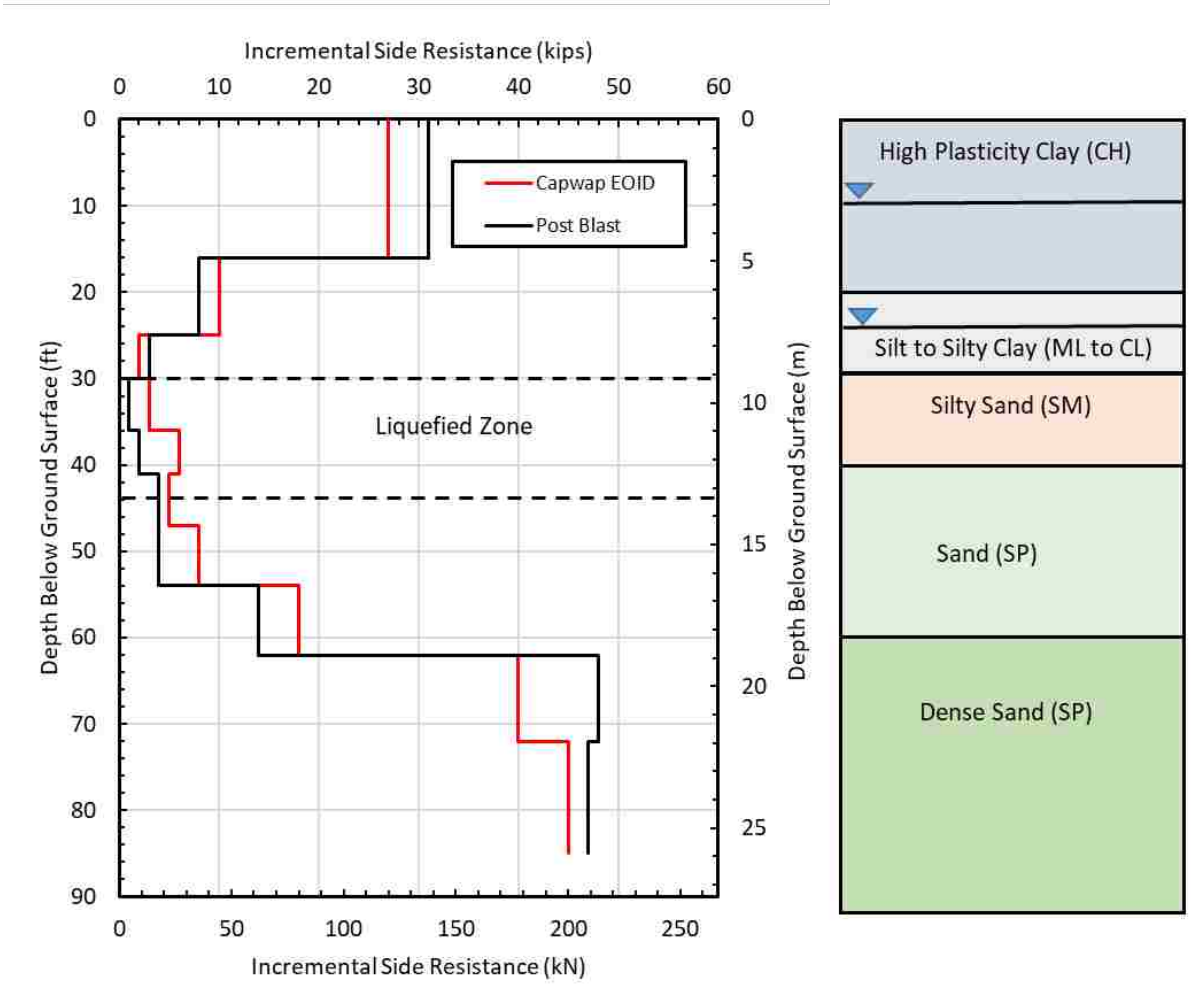

Figure 5.2-8 Comparison of incremental side resistance before and after blast induced liquefaction and reconsolidation for the H-Pile

5.2.5 Summary of Response and Neutral Plane Evaluation for H Pile

Figure 5.2-9 provides plots of the excess pore pressure ratio, pile and soil settlement, and load in the pile after blasting vs. depth, as well as an end-bearing resistance vs. toe settlement curve for the H pile. This figure provides an overall picture of the interaction of the pile and the surrounding soil after the blast liquefaction along with the consistency of the results. The end-bearing resistance vs. toe settlement of the pile was created from a similar normalized graph presented in Figure 3.2-11 (O'Neill and Reese 1999). This was done by multiplying the width of the pile base by the settlement ratio on the abscissa in Figure 3.2-11 and by multiplying the ultimate end bearing by the normalized end-bearing resistance on the ordinate in Figure 3.2-11. This made it possible to see if the estimated end-bearing resistance mobilized by the pile during blasting would produce a settlement that was similar to what was observed during blasting.

As shown in Figure 5.2-9 the majority of the settlement of the soil took place within the liquefied zone from 30 to 46 feet but some settlement occurred below this zone. As noted previously, the settlement of the pile and the soil are equal to 0.28 inches at a depth of 52 feet below the ground which defines the neutral plane based on settlement. In addition, the load in the pile reaches a maximum value at a depth of 55 feet which defines the neutral plane based on load. Although the agreement in the two depths to the neutral plane is not perfect, it is remarkably good. The small discrepancy could be due to only having load values at the locations of strain gauges. The maximum load could align with the depth where the settlement of the pile and soil were equal; however, because a strain gauge is not located at that exact location it is impossible to tell for sure. The exact location of the neutral plane is most likely in the range of the two presented neutral planes.

Negative skin friction increases the load in the pile from the ground surface to the neutral plane while positive skin friction decreases the load in the pile below this depth. Negative skin friction within the liquefied zone is relatively low but not zero. The end-bearing resistance mobilized at the toe of the pile after reconsolidation of the sand was about 64 kips. Based on the estimated ultimate end-bearing resistance of 99 kips this would produce a settlement of about 0.35 inches based on the end-bearing resistance vs. pile toe settlement as shown in Figure 5.2-9. As noted previously, the actual measured pile toe settlement was 0.28 inches. This is a discrepancy of only 0.07 inch which is well within one standard deviation of what was calculated from the O'Neill and Reese (1999) curve. If the 30-kip toe capacity calculated by the CAPWAP analysis for EOID is used, the pile settlement of two inches would have been required to mobilize a 64-kip load, which is well outside of one standard deviation. This result confirms that the toe capacity is close to the predicted 99 kips.

One final point to note is that the neutral plane is located somewhat below the liquefied zone. This is acceptable and expected when the pile does not settle significantly. If the pile had settled more, then the neutral plane could have moved upward into the liquefied zone. However, cohesionless soils subjected to a blast or an earthquake do not have to fully liquefy to produce settlement. Therefore, if the pile doesn't settle much as it develops the necessary end-bearing resistance, then the neutral plane will be deeper in the soil profile where settlements are smaller than in the liquefied layer.

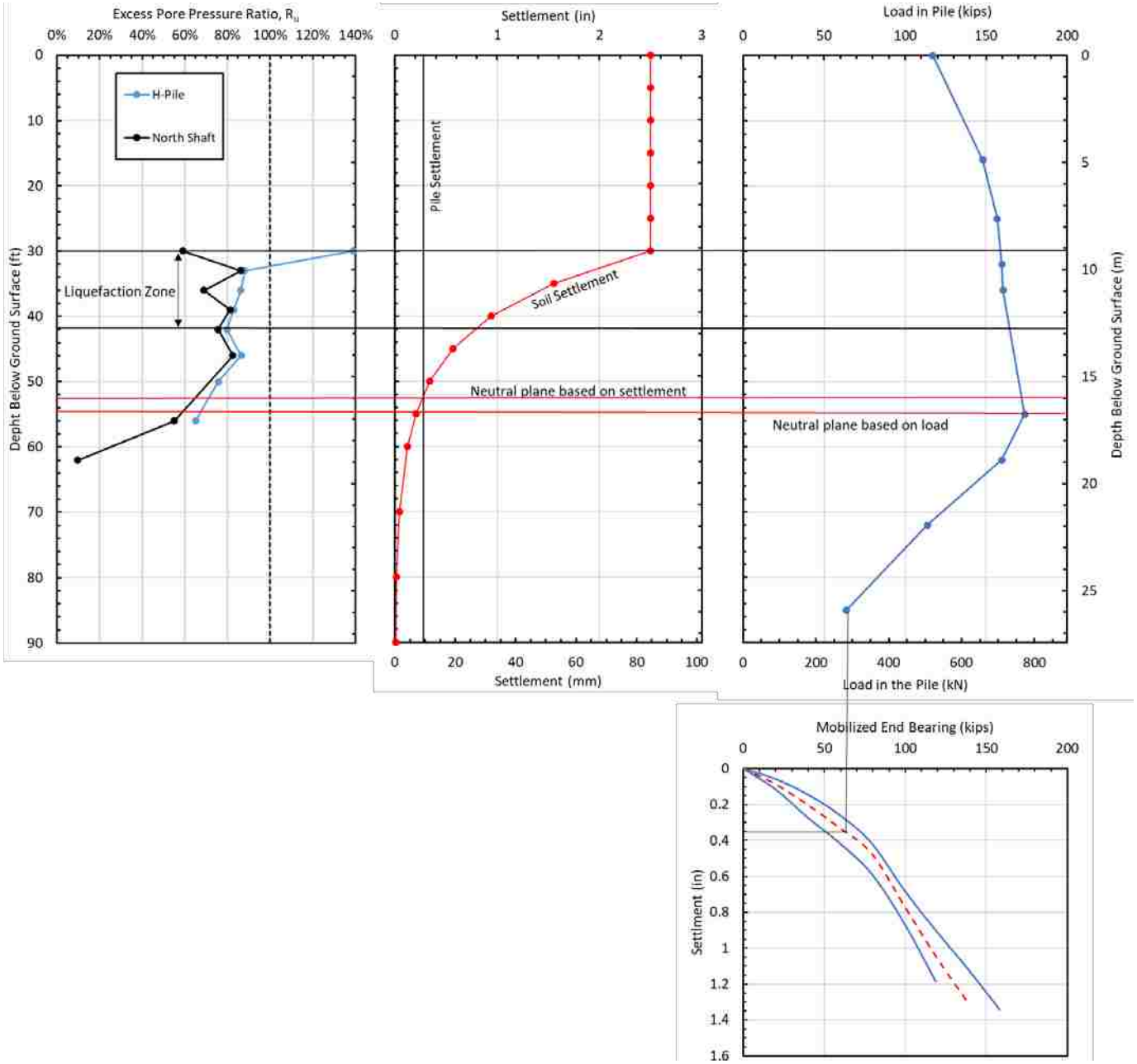

Figure 5.2-9 Pore pressure ratio, settlement, and load in the pile vs. depth along with end-bearing versus settlement curve for H Pile.

5.3 Blast Test Procedures and Test Results for the Closed End Pipe Pile

5.3.1 Blast Test Procedures

Prior to blasting, a dead weight of 118.5 kips was applied to the pipe pile as discussed in Chapter 4. Based on the average CAPWAP capacity of 471 kips, the factor of safety against axial compression failure of the pile prior to liquefaction was about 4. However, if the sand were to liquefy from 30 to 60 feet and the liquefied sand had no skin friction, the axial capacity would drop to 282 kips and factor of safety would be about 2.4.

The blast test for the pipe pile and the adjacent 6-foot diameter drilled shaft involved 13 blast holes spaced nearly uniformly around two rings each centered on the test foundations as shown in Figure 4.7-1. Two of the blast holes at the top of each ring were unavailable for use in the second blast test because explosives were detonated in them during the first blast test. Within each blast hole, six pounds of explosive charges were placed with their centers at 37 and 47 feet below the ground surface, respectively. Gravel stemming was placed to the top of each blast hole to separate the charges and prevent sympathetic detonation as well as to direct the blast pressure to expand radially rather than simply vertically. In addition, three gravel-filled bags were placed atop each blast hole.

The charges in each blast hole were detonated sequentially in a figure eight pattern around the two rings. Within each blast hole the bottom charge was first detonated while the upper charge was detonated after a delay of 176 milliseconds. The charges in the next blast hole were then detonated after a delay of 500 milliseconds. Thus, 156 pounds of explosives (12 pounds in each blast hole) were detonated in a total time of 8.112 seconds. Following blasting,

the dissipation of pore pressure was monitored for approximately 90 minutes. As was the case for the first blast test, there were no physical signs of liquefaction such as sand boils, observed during this second blast test. This could be a result of the 30-foot thick layer of cohesive soil overlying the liquefiable sands at this site that likely restricted the upward flow of water and sand. Owing to the tight time schedule for completing the tests, the pile was then unloaded and the data collection system was disconnected 90 minutes after blasting although excess pore pressure ratios had not yet dissipated to less than 10% of the vertical effective stress at all depths, as discussed subsequently.

5.3.2 Pore Pressure Response Following Blasting

Upon extracting the pore pressure transducers from ground after the first blast, several of them were damaged. Therefore, in the second blast there were only four transducers around the pipe pile and four around the center 6-ft diameter drilled shaft. The transducers were located around a ring approximately 2 meters from the center of each respective deep foundation.

The excess pore pressure ratios were calculated the same way as in the previous blast with the water table at 25 feet. The R_u values were calculated based on the pore water pressures measured by the transducers at depths of 30, 33, 39, 42 and 47 feet below the ground surface. Plots of the peak R_u versus depth around the pipe pile are plotted in Figure 5.3-1 along with the excess pore pressure ratios surrounding the center drilled shaft. The excess pore pressure ratio around the pipe pile was above 0.8 from 30 feet below the ground surface to about 42 feet around the pipe pile and to about 48 feet around the drilled shaft. An excess pore pressure ratio above 0.8 would likely behave as if it were fully liquefied for most practical purposes.

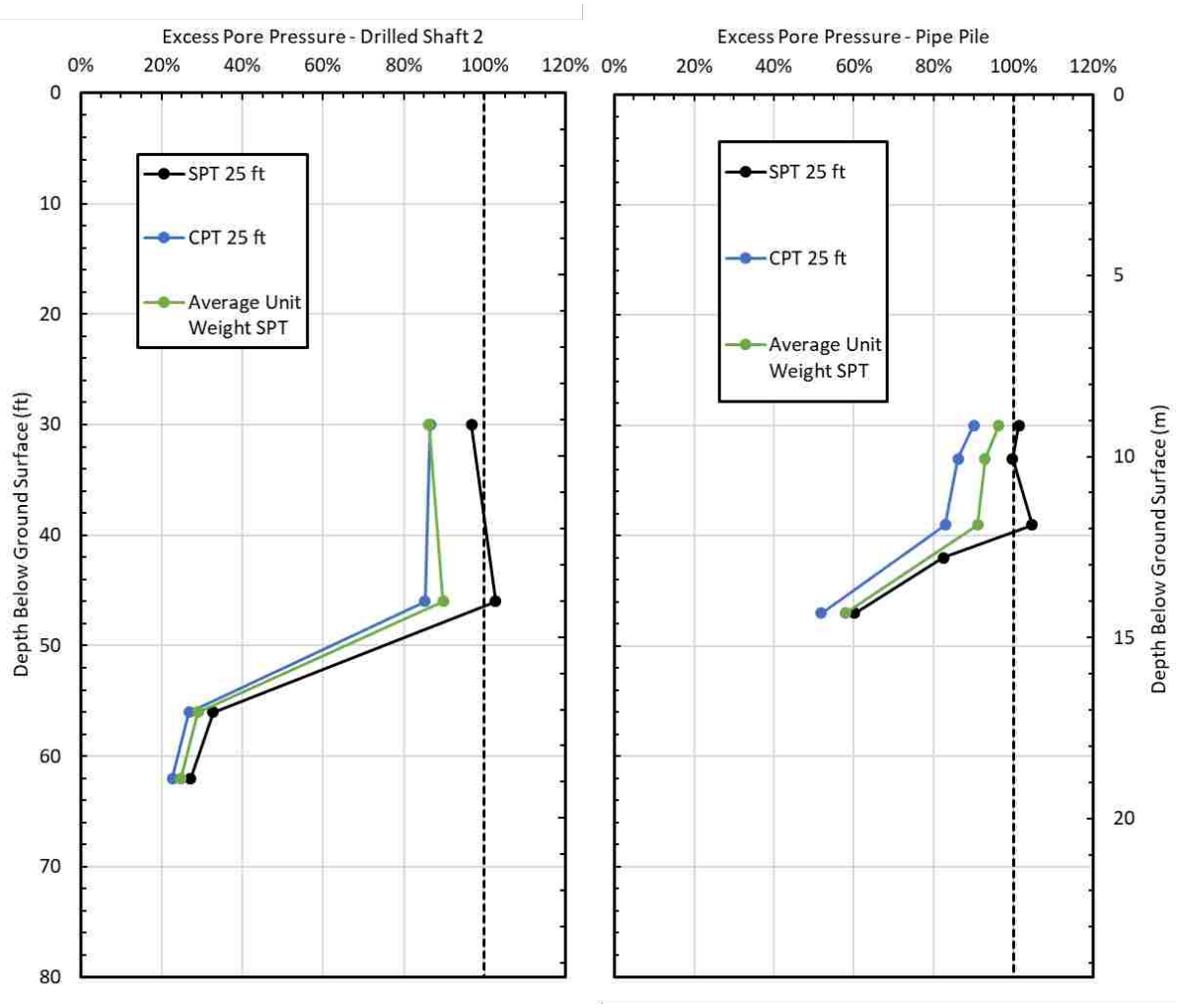

Figure 5.3-1 Excess pore pressure ratio versus depth (a) around the 6-ft diameter drilled shaft and (b) driven pipe pile following the first blast.

Figure 5.3-2 provides plots of the excess pore pressure ratios versus time for each transducer depth. The plots focused on the time immediately after the blast indicate that the top three transducers essentially liquefied while the deeper transducer at 47 feet did not. The pore pressure ratio at a depth of 47 feet dissipated to less than 10% after about 35 minutes; however, the pore pressure ratios at the shallower depths were still between 30 and 50% when the data acquisition system was disconnected 90 minutes after the blast.

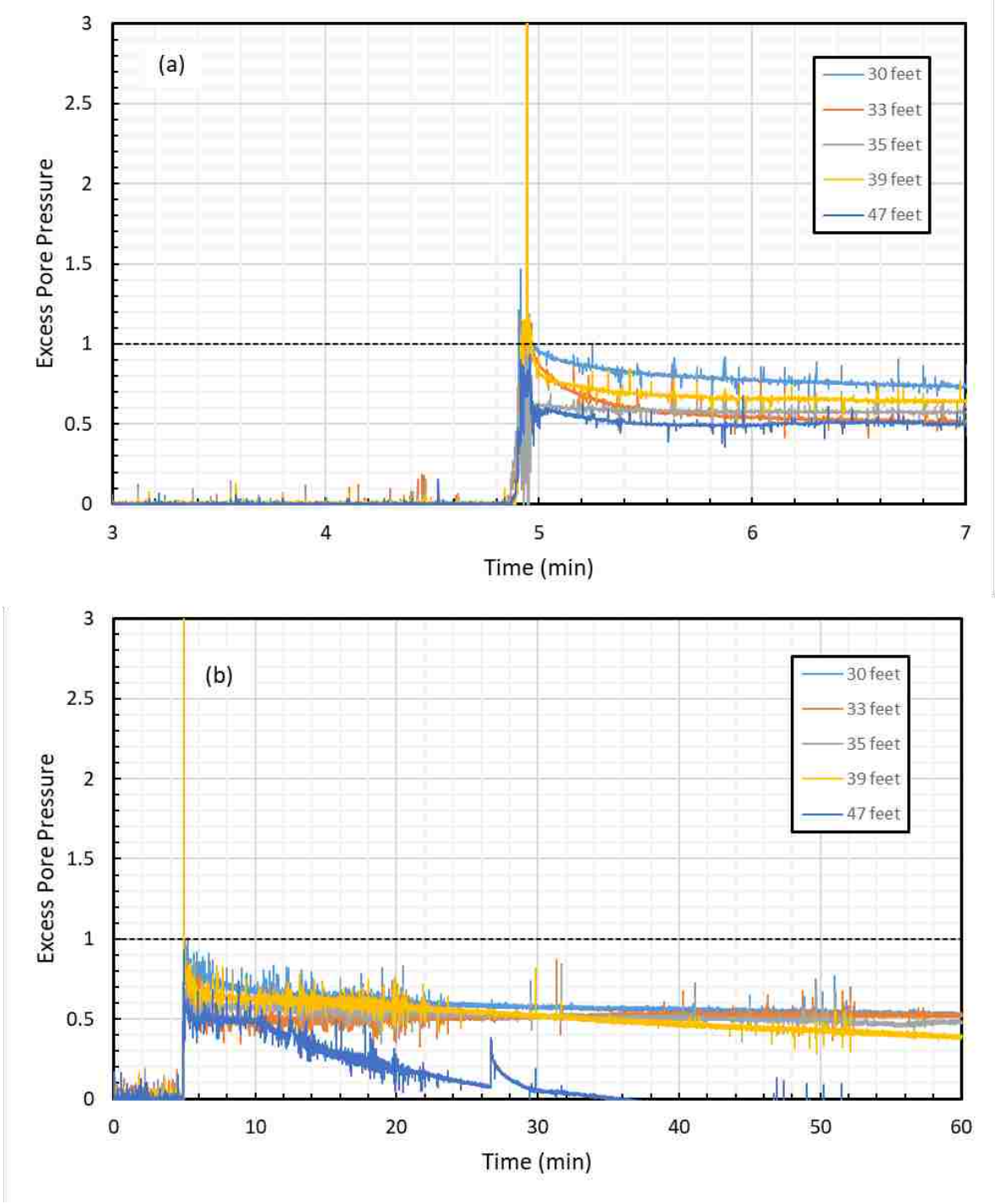

Figure 5.3-2 Excess pore pressure ratios versus time in the soil surrounding the pipe pile for (a) 90 minutes following the blast and (b) within a few minutes immediately following the blast.

5.3.3 Soil and Pile Settlement Following Blasting

The total ground settlement across the site was measured during the second blast in the same way as it was during the first blast. Elevation measurements were made on top of wooden survey stakes spaced at three-foot intervals along a line located about 4 feet north of the center of the pile which extended about half way inward to the drill shaft and about 70 feet outward from the pipe pile. Elevations of the tops of the stakes for this blast were taken 30 minutes and 330 minutes (5.5 hrs.) after the blast and profiles of the measured settlements are plotted in Figure 5.3-4. Although settlement became negligible beyond 60 feet from pipe pile after 30 minutes, settlement was still approximately 0.20 inch at a distance of 70 feet after 330 minutes. About 60% more settlement occurred between the 30 minute and 330 minute readings near the pile as the sand continued to settle as excess pore pressures dissipated. The total settlement of the soil surrounding the pile was about 3.2 inches.

A settlement versus depth profile was also developed using data from the Sondex tube. Once again, this data makes it possible to compare the soil settlement to the settlement of the pile and provides and independent estimation of the location of the neutral plane. The raw settlement versus depth data points collected from the Sondex tube are plotted in Figure 5.3-4. The settlement data for the pipe pile was not as scattered as the data from the H-Pile. Nevertheless, there was still some scatter, and to get a more precise settlement profile a best fit curve and regression equation were generated again as was done in section 5-2. The regression curve was extrapolated to get a better idea of the settlement at deeper depths.

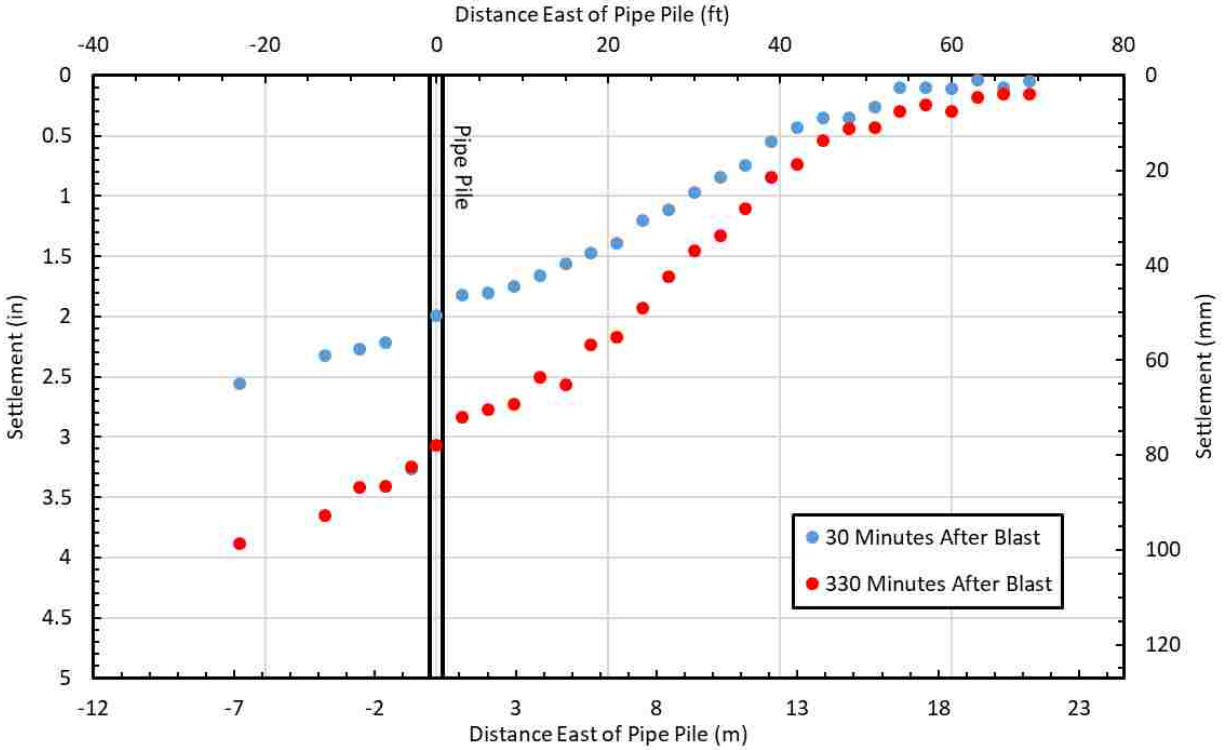

Figure 5.3-3 Liquefaction induced ground surface settlement versus horizontal distance along a line adjacent to the pipe pile and a companion drilled shaft following blasting.

The settlement in the clay layer was again assumed to be equal to the total settlement of the soil profile, which was determined by approximating an average in the center of the available data, which was 2.8 inches. This settlement is slightly lower, but similar to that measured with the survey stakes with the automatic level. The discrepancy could be due to the Sondex tube being located somewhat further from the pile than the survey stake.

The total settlement of the pile was about 0.32 inches. This was measured by attaching a survey rod to the pile cap before blasting, and then taking measurements before and after the blast with an auto level located about 100 feet from the pile. Settlement from pile deformation was once again negligible. Therefore, the neutral plane can be assumed to be at a depth of about 60 feet where the pile and soil settlements are equal as shown in Figure 5.3-4 .

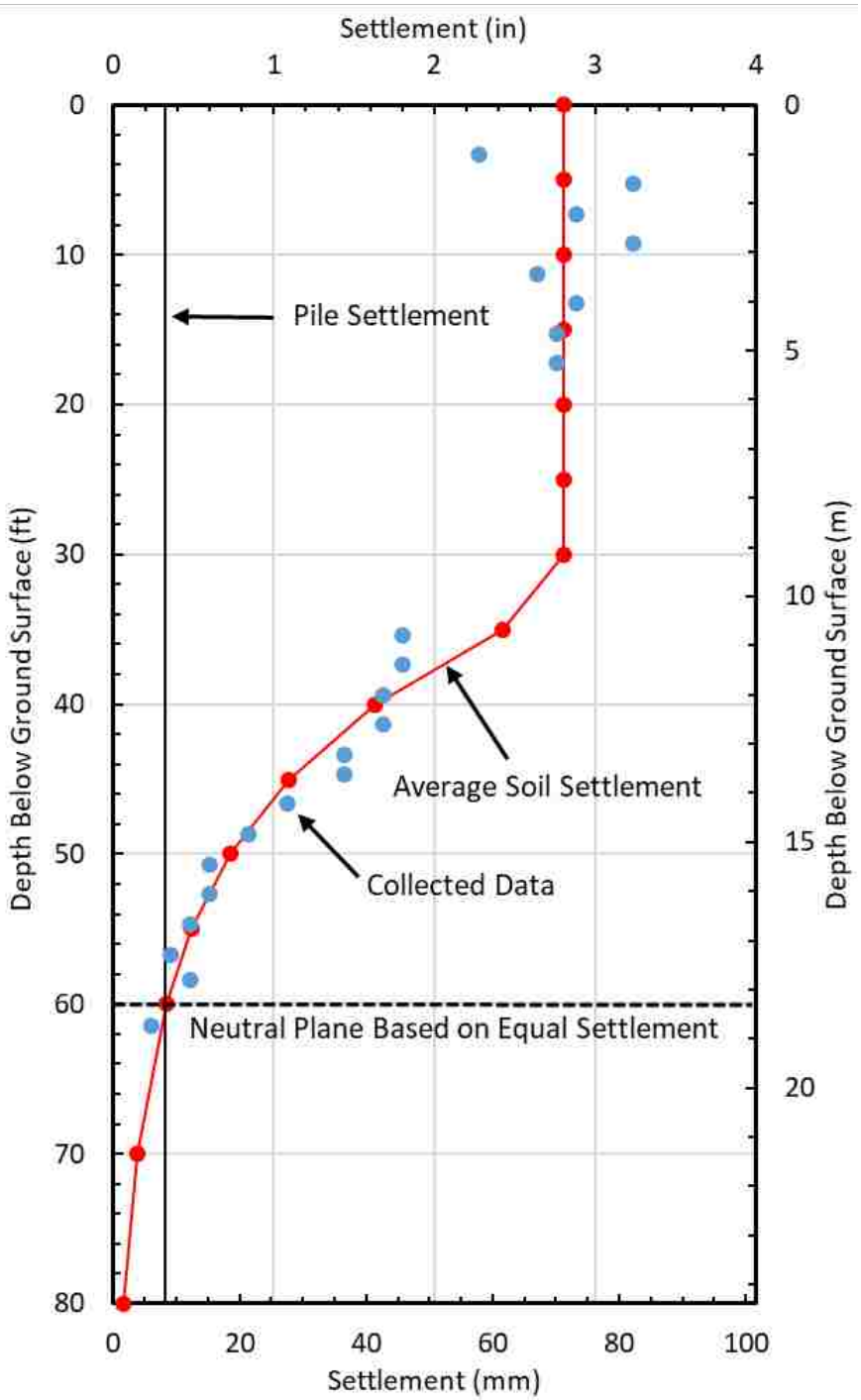

Figure 5.3-4 Settlement of the pipe pile and the surrounding soil following the test blast

The total volumetric strain developed in the soil as it reconsolidated following blast liquefaction was again calculated by taking the total settlement of the liquefied layer (2 inches) and then dividing it by the thickness of the layer of liquefied soil (18 ft). This strain was also

compared to expected strains from earthquakes based on SPT $(N_1)_{60}$ values determined by Tokimatsu and Seed (1987). The volumetric strain generated by the blast was determined to be 0.9%. The expected strain based on the average blowcount over the 18 feet of liquefied soil was about 2%. This is still not as much strain as would be expected by an earthquake, but if the Cetin et al. (2009) depth weighting factor is used, then the expected volumetric strain would be 0.7% which is very close but somewhat lower than the strain measured using blast liquefaction.

5.3.4 Load in the Pile Following Blasting

The pipe pile was loaded one day, and then the blasting for the pipe pile took place the following day. Because of this all instrumentation was disconnected and stored to prevent theft, then reconnected the next day. Thus, the load was zeroed the next day after the blanks had already been added. So, the data recorded during blasting was the load felt in the pile minus the load felt in the pile after adding the blanks. The load felt in the pile during blasting was calculated using strain gauges the exact same way as the static load in the pipe pile was calculated in section 4.6, by using an average of the modulus of steel and a calculated modulus of elasticity of the concrete, weighted by the cross-sectional area of each. The results are shown in Figure 5.3-5.

The load in the pile clearly increases with depth from the ground surface to a depth of 60 ft indicating that the soil is settling relative to the pile and inducing negative skin friction or dragload on the pile. Below this depth the load in the pile decreases indicating that load in being transferred from the pile to the surrounding soil by positive skin friction.

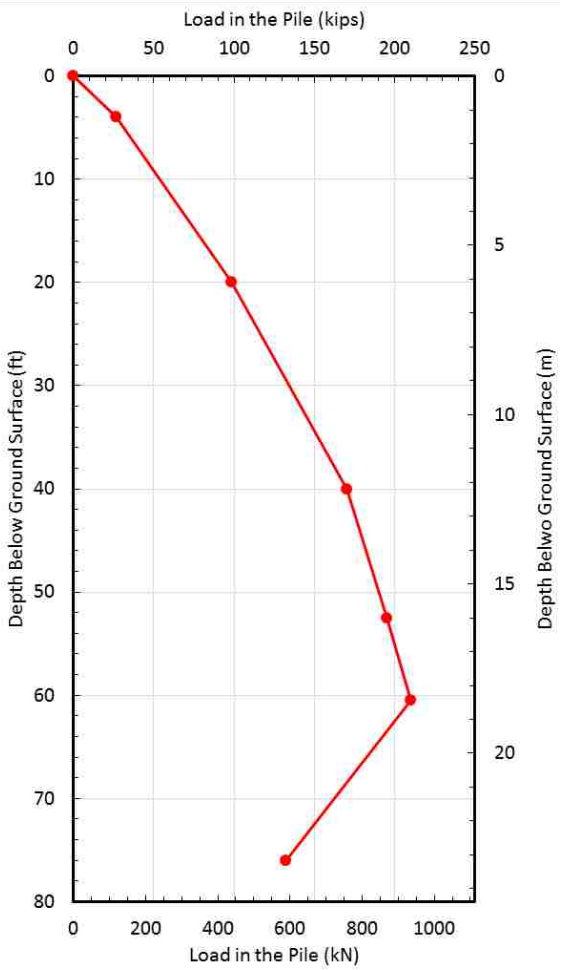

Figure 5.3-5 Change in load in the pipe pile versus depth after blasting.

To obtain the load in the pile versus depth after blasting, it was necessary to add the load in the pile versus depth after placement of the static load to the change in load versus depth curve presented in Figure 5.3-5. This was done by taking the load in the pile versus depth curve based on the End of Adding Blanks curve shown in Figure 4.7-3 and adding it to the curve in Figure 5.3-5. This is a similar process explained in greater detail in section 5-2. The results are presented in Figure 5.3-6. Negative skin friction increases the load in the pile from 118.5 kips at the ground surface to a maximum value of 215 kips at a depth of 61 feet. Below this depth, the load in the pile decreases indicating that the neutral plane is at 61 feet.

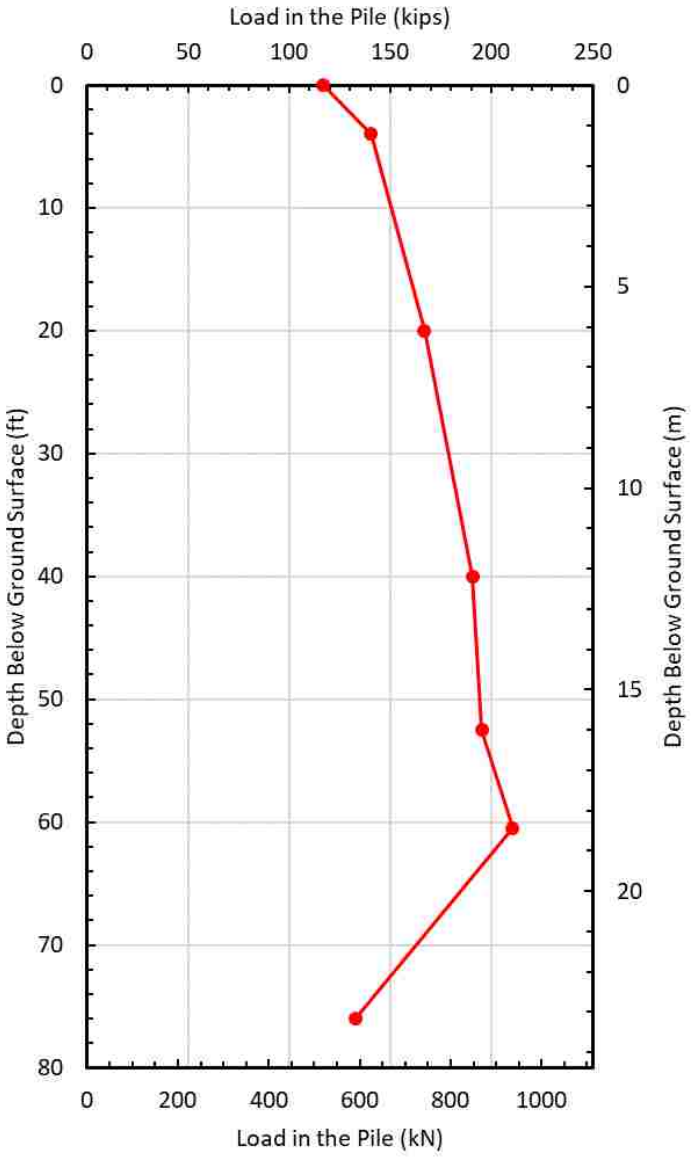

Figure 5.3-6 Load measured in the pipe pile after blasting with the load in the pile from the static load added.

Figure 5.3-7 shows the load versus depth in the pipe pile before and after blasting. They are good reflection of each other which means that the load measured from the strain gauges is a good representation of the loads during blasting, except in the liquefied zone where the curve is steeper, meaning the pile sheds less load in this zone and is only a fraction of what it was before.

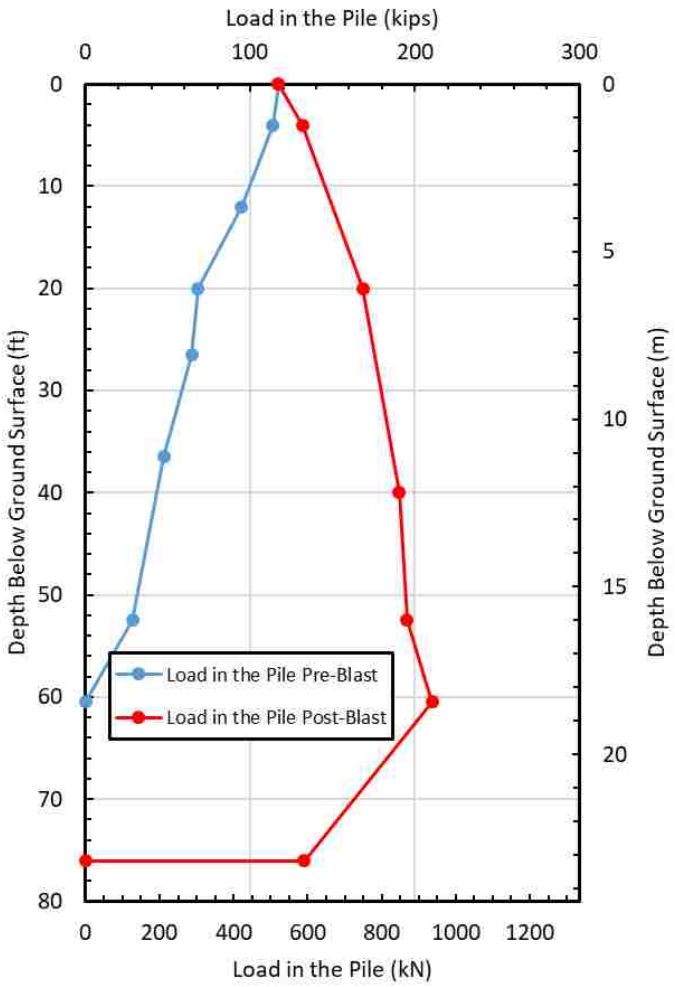

Figure 5.3-7 Load versus depth in the pipe pile immediately before blast and after blast induced liquefaction and reconsolidation.

The comparison of incremental loads in the pipe pile in the liquefied zone from 30 feet to about 45 feet was done the same way in the pipe pile as it was in the H-pile. The incremental load comparisons are shown in Figure 5.3-8. The ratio of skin friction after blasting compared to the skin friction before blasting was 48%. The same comparison was made in the non-liquefied layers of the pile as well. The ratio of the pre-blast loads compared to the post-blast loads in the layers above the liquefied zone was 1.53 and below the liquefied zone it was 0.62.

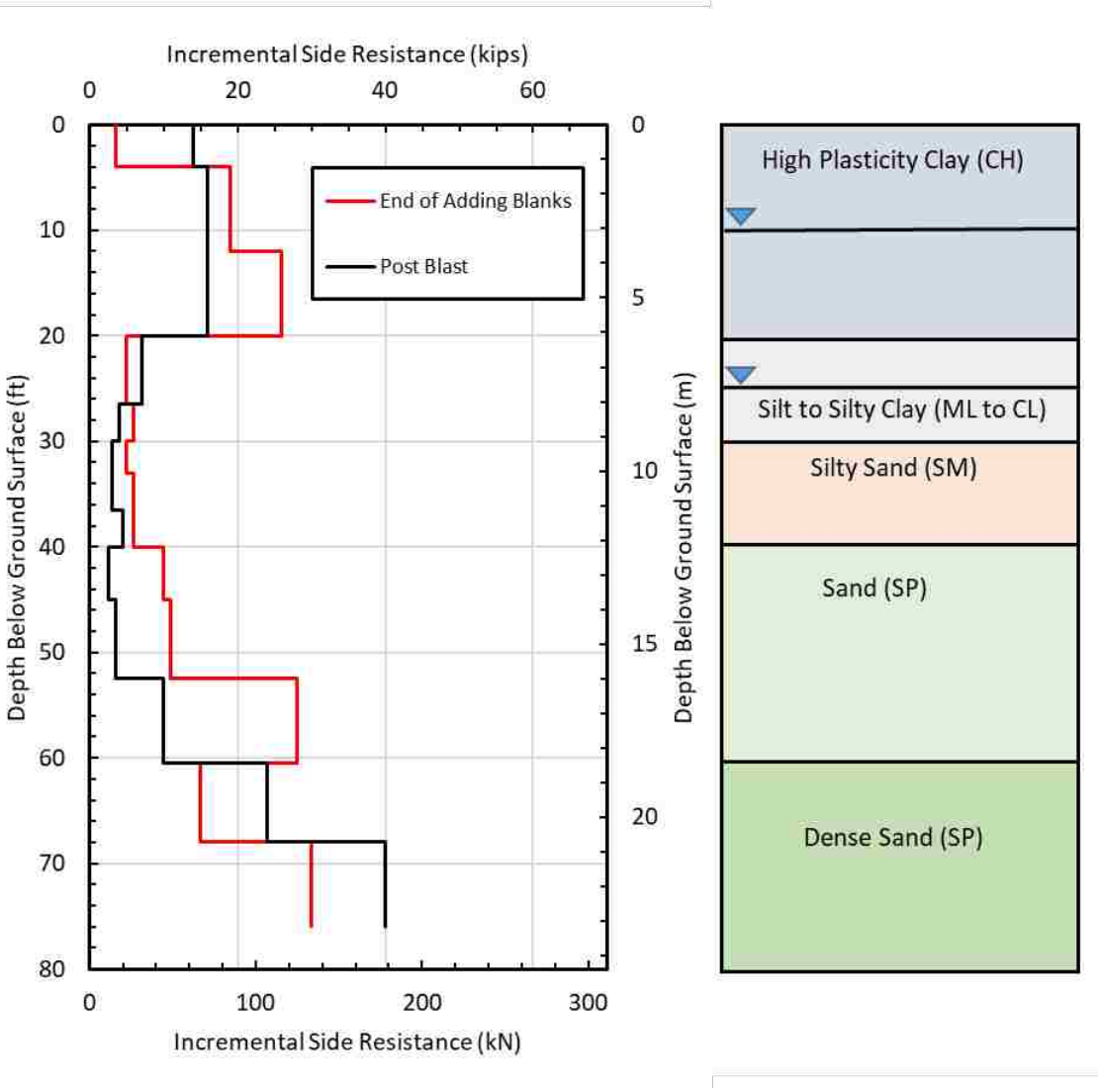

Figure 5.3-8 Comparison of incremental side resistance before and after blast induced liquefaction and reconsolidation for the pipe pile.

5.3.5 Summary of Response and Neutral Plane Evaluation for H Pile

Figure 5.3-9 provides plots of the excess pore pressure ratio, pile and soil settlement, and load in the pile after blasting vs. depth, as well as an end-bearing resistance vs. toe settlement curve for the pipe pile. This figure provides an overall picture of the interaction of the pile and the surrounding soil after the blast liquefaction along with the consistency of the results. The end-bearing resistance vs. toe settlement of the pile was created from a similar normalized graph

presented in Figure 3.2-11 (O'Neill and Reese 1999). This was done by multiplying the width of the pile base by the settlement ratio on the abscissa in Figure 3.2-11 and by multiplying the ultimate end bearing by the normalized end-bearing resistance on the ordinate in Figure 3.2-11. This made it possible to see if the estimated end-bearing resistance mobilized by the pile during blasting would produce a settlement that was similar to what was observed during blasting.

As shown in Figure 5.3-9, the majority of the settlement of the soil took place within the liquefied zone from 30 to 48 feet but some settlement occurred below this zone. As noted previously, the settlement of the pile and the soil are equal to 0.32 inches at a depth of 60 feet below the ground which defines the neutral plane based on settlement. In addition, the load in the pile reaches a maximum value at a depth of 61 feet which defines the neutral plane based on load. Although the agreement in the two depths to the neutral plane is not perfect, it is remarkably good. The small discrepancy is likely due to only having load values at the locations of strain gauges. The exact location of the neutral plane is most likely in the range of the two presented neutral planes.

Negative skin friction increases the load in the pile from the ground surface to the neutral plane while positive skin friction decreases the load in the pile below this depth. Negative skin friction within the liquefied zone is relatively low but not zero. The end-bearing resistance mobilized at the toe of the pile after reconsolidation of the sand was about 132 kips. Based on the estimated ultimate end-bearing resistance of 282 kips this would produce a settlement of about 0.32 inches based on the end-bearing resistance vs. pile toe settlement as shown in Figure 5.3-9. As noted previously, the actual measured pile toe settlement was 0.32 inches. Thus, the end-bearing resistance developed as a result of negative skin friction is consistent with the settlement of the pile.

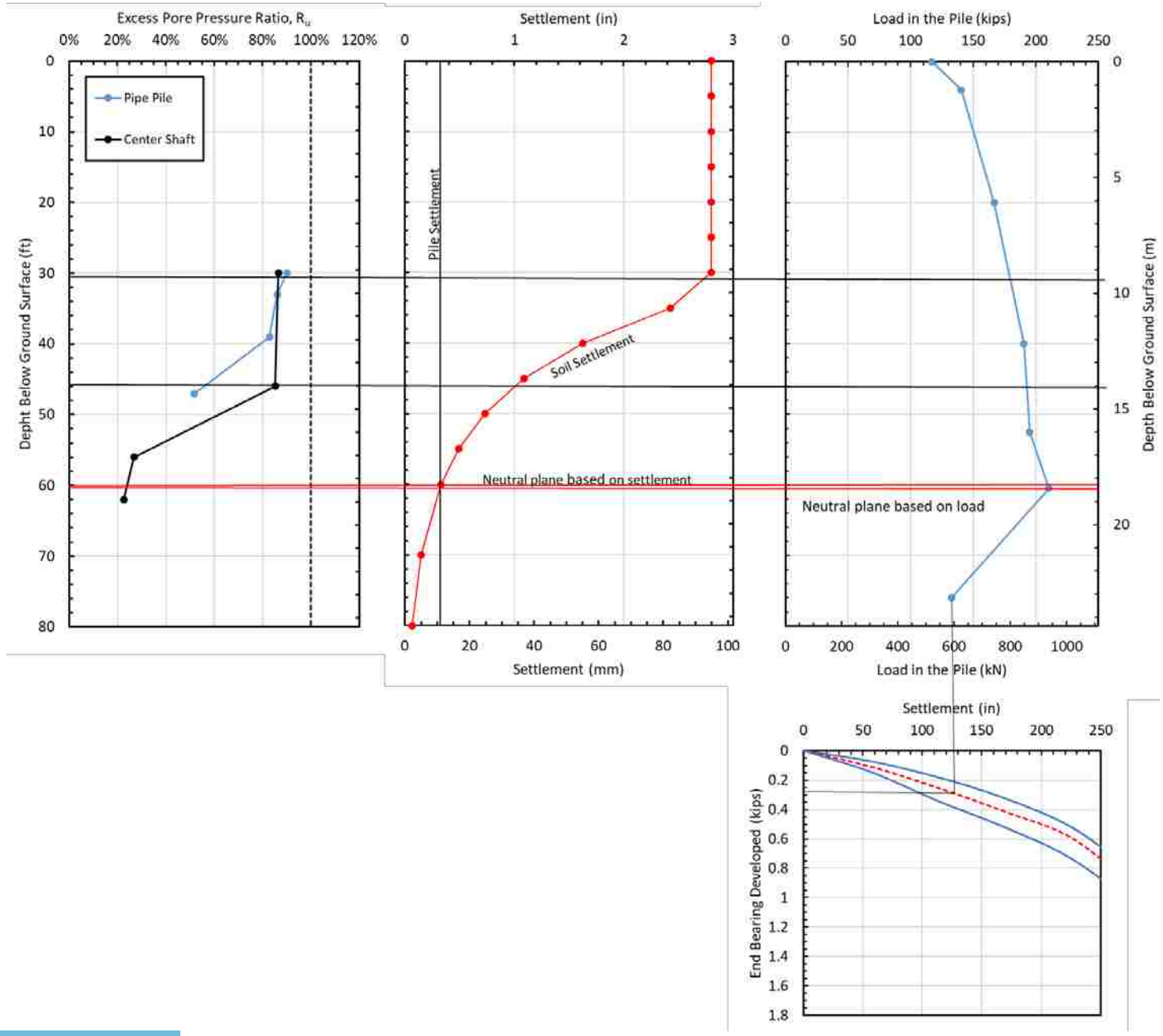

Figure 5.3-9 Pore pressure ratio, settlement, and load in the pile vs. depth along with end-bearing vs. settlement curve for pipe pile.

5.4 Blast Test Procedures and Test Results for the Pre-Cast Concrete Square Pile

5.4.1 Blast Test Procedures

Prior to blasting, a dead weight of 118.5 kips was applied to the pipe pile as discussed in Chapter 4. Based on the average CAPWAP capacity of 557 kips, the factor of safety against axial compression failure of the pile prior to liquefaction was about 4.7. However, if the sand were to liquefy from 30 to 60 feet and the liquefied sand had no skin friction, the axial capacity would drop to 250 kips and factor of safety would be about 2.1.

The blast test for the concrete square pile and the adjacent 4-foot diameter drilled shaft involved 13 blast holes spaced nearly uniformly around two rings each centered on the test foundations as shown in Figure 4.7-1. Two of the blast holes at the top of each ring were unavailable for use in the third blast test because explosives were detonated in them during the second blast test. Within each blast hole, seven pounds of explosive charges were placed with their centers at 37 and 47 feet below the ground surface, respectively. Gravel stemming was placed to the top of each blast hole to separate the charges and prevent sympathetic detonation as well as to direct the blast pressure to expand radially rather than simply vertically. In addition, three gravel-filled bags were placed atop each blast hole.

The charges in each blast hole were detonated sequentially in a figure eight pattern around the two rings. Within each blast hole the bottom charge was first detonated while the upper charge was detonated after a delay of 176 milliseconds. The charges in the next blast hole were then detonated after a delay of 500 milliseconds. Thus, 182 pounds of explosives (14 pounds in each blast hole) were detonated in a total time of 8.112 seconds. The blast charges

were detonated close to dark. For this reason, the instrumentation was disconnected about 105 minutes after blasting.

5.4.2 Pore Pressure Response Following Blasting

While extracting the pore pressure transducers from ground to move them from around the pipe pile and 6-ft diameter drilled shaft a number of the transducers were damaged or became inoperable. Therefore, in the third blast test there were only three transducers available for placement around the concrete pile and two transducers around the third drilled shaft. The transducers were located approximately 2 meters from the center of each respective deep foundation. Transducers around the pre-stressed concrete pile were installed at depths of 31, 33.5 and 46.5 feet below the ground surface.

The excess pore pressure ratios were calculated based on the measured pore water pressure from transducers at depths of 31, 33.5, and 46.5 feet. Plots of R_u versus depth around both the concrete pile and the third drilled shaft are shown in Figure 5.4-1. This allows us to see how much of the soil had effectively liquefied. The R_u was above 0.8 from 31 feet to about 46.5 feet below the ground surface around the concrete square pile. Ru was only above 0.8 at a depth of 35 feet around the third drilled shaft. Because there were more explosives used than in the first two blasts, and the total settlement of the soil in the second blast was more than in the first two blasts, and the lack of data below 46.5 feet, it is expected that the soil effectively liquefied from 30 feet to about 50 feet.

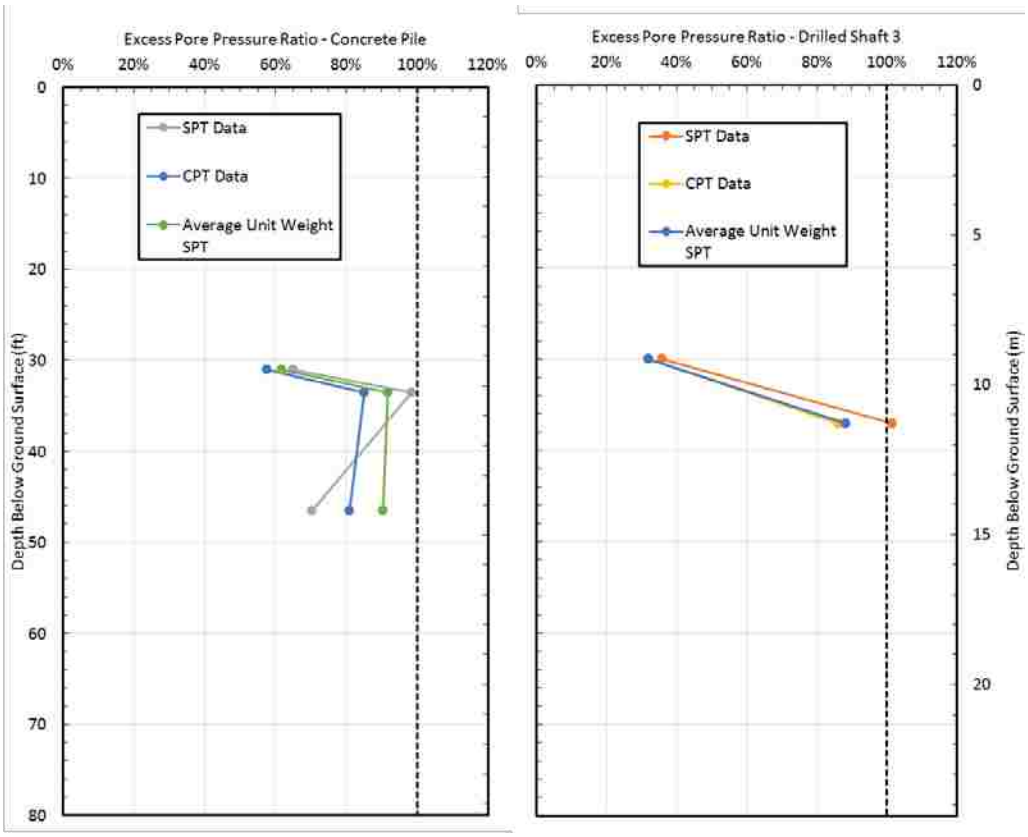

Figure 5.4-1 Excess pore pressure ratio versus depth (a) around the 4-ft diameter drilled shaft and (b) driven concrete pile following the first blast.

Plots of R_u versus time are shown in Figure 5.4-2. The pore pressures closer to the clay layer once again took longer to dissipate than the pore pressures deeper into the sand layers. The pore pressure ratios at 31 and 33.5 feet managed to dissipate to less than 50% after 90 minutes, but the pore pressure ratio at 46 feet dissipated to less than 10% about 40 minutes after the blast.

In contrast to the previous blast tests, there was some surface evidence of liquefaction during the blast test around the concrete pile. After the blast, water was observed flowing upward near the interface between the pile and the surrounding soil. Perhaps the higher explosive charge weights created a small gap at the interface between the pile and soil which provided an escape route for the water in the liquefied zone. Nevertheless, no sand ejecta was observed in the water.

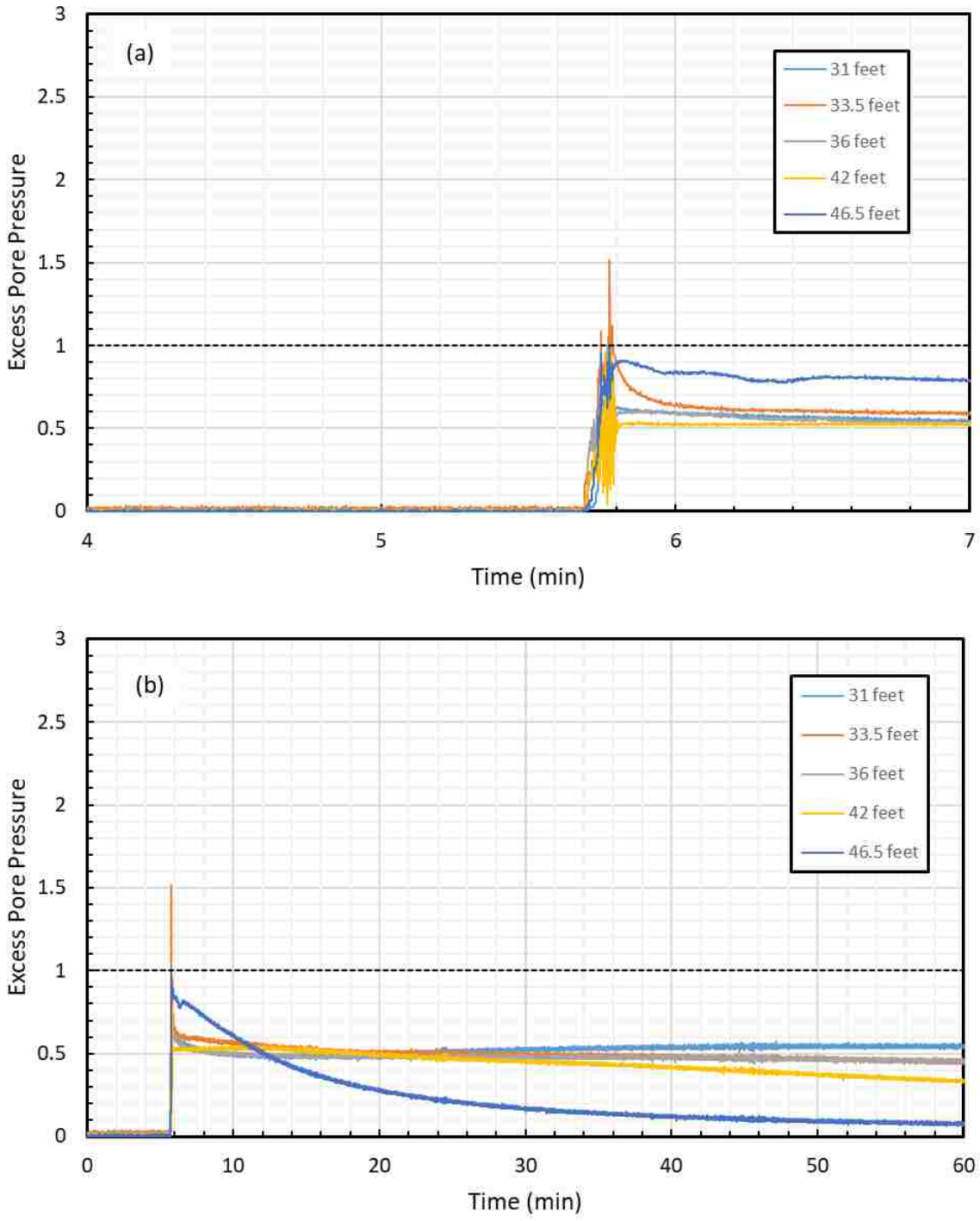

Figure 5.4-2 Excess pore pressure versus time in the soil surrounding the concrete square pile for 105 minutes following the blast, and focused on the time directly following the blast.

5.4.3 Soil and Pile Settlement Following Blasting

The total ground settlement across the site was measured during the third blast in the same way as it was during the previous blasts. Elevation measurements were made on top of wooden survey stakes spaced at 3-foot intervals along a line located about 4 feet north of the center of the pile which extended about 70 feet outward from the concrete pile. Settlement was also measured at selected points in the direction of the drilled shaft. Elevations on the tops of the stakes for this blast were taken 20 minutes, 80 minutes (1.33 hours), and 750 minutes (12.5 hours) after the blast and profiles of the measured settlements are plotted in Figure 5.4-3. The settlement profiles clearly show the settlement increases as pore pressure continue to dissipate with time. Although settlement became negligible beyond 60 feet from pipe pile after 20 minutes, settlement was still approximately 0.20 inch at a distance of 70 feet after 750 minutes. About 33% more settlement occurred between the 20 minute and the 80 minute readings, while about 90% more settlement occurred between the 20 minute reading and the 750 minute reading. The total settlement of the soil surrounding the pile was about 3.4 inches 12.5 hours after blasting when pore pressure ratios had likely returned to zero.

The settlement data collected from the Sondex tube for the third blast was scattered, but once again had a clear pattern. Therefore, a best fit curve was created, and an exponential equation was derived just as was done in the precious two sections. A settlement versus depth profile is available in Figure 5.4-4. For the profile below the available data, the regression curve was extrapolated. The settlement in the clay layer was assumed to be 3.4 inches based on the settlement measured from the wooden stakes. The total pile settlement was 0.28 inches. This was measured by fixing a survey rod to one of the weights on top of the pile cap,

and taking a measurement before and after the blast. The depth where the soil and pile settlement were equal was about 70 feet.

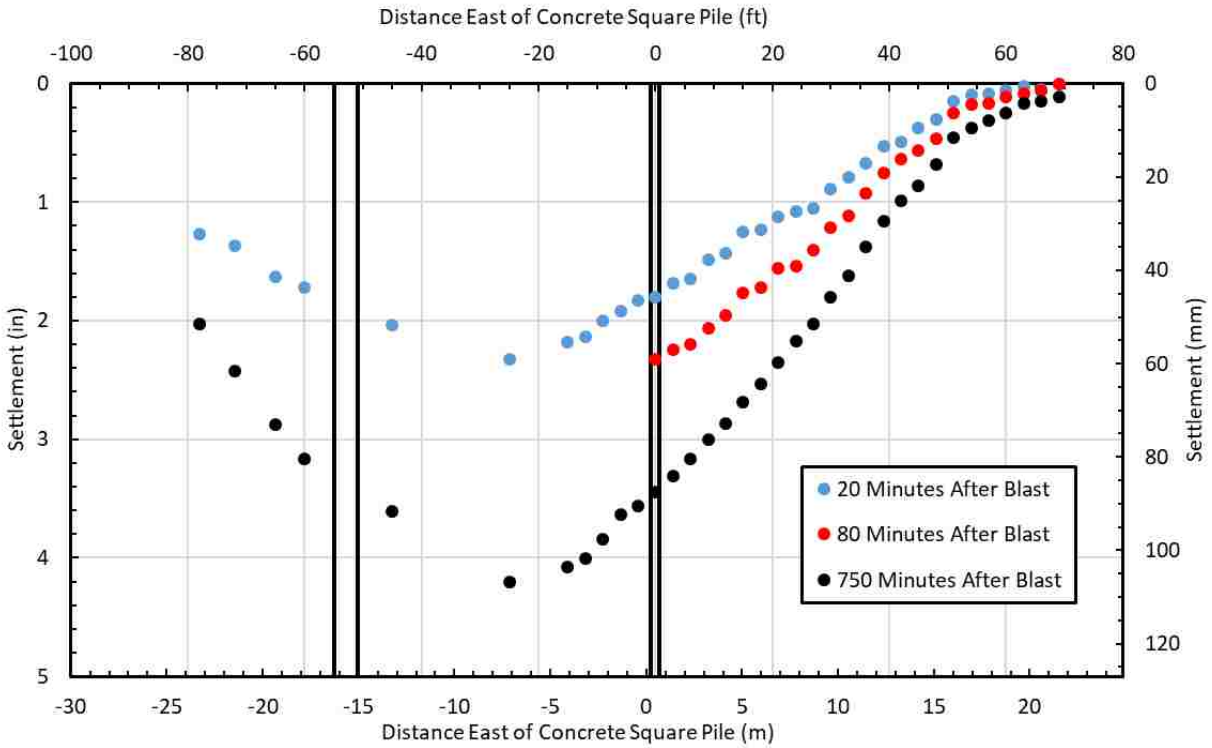

Figure 5.4-3 Liquefaction induced ground surface settlement versus horizontal distance along a line adjacent to the concrete pile and a companion drilled shaft following blasting

Prior to blasting an orange line was drawn on the pile and soil at the ground surface to measure the differential settlement. Figure 5.4-5 shows this line post blast after the soil had a chance to settle, however it is not a picture of the pile after all settlement has occurred. Knowing that the pile is 18 inches wide the total settlement based on how much the soil displaced can be measured. This is done by measuring the gap and comparing it to the known length of 18 inches. Following this procedure, the settlement was about 2.5 inches.

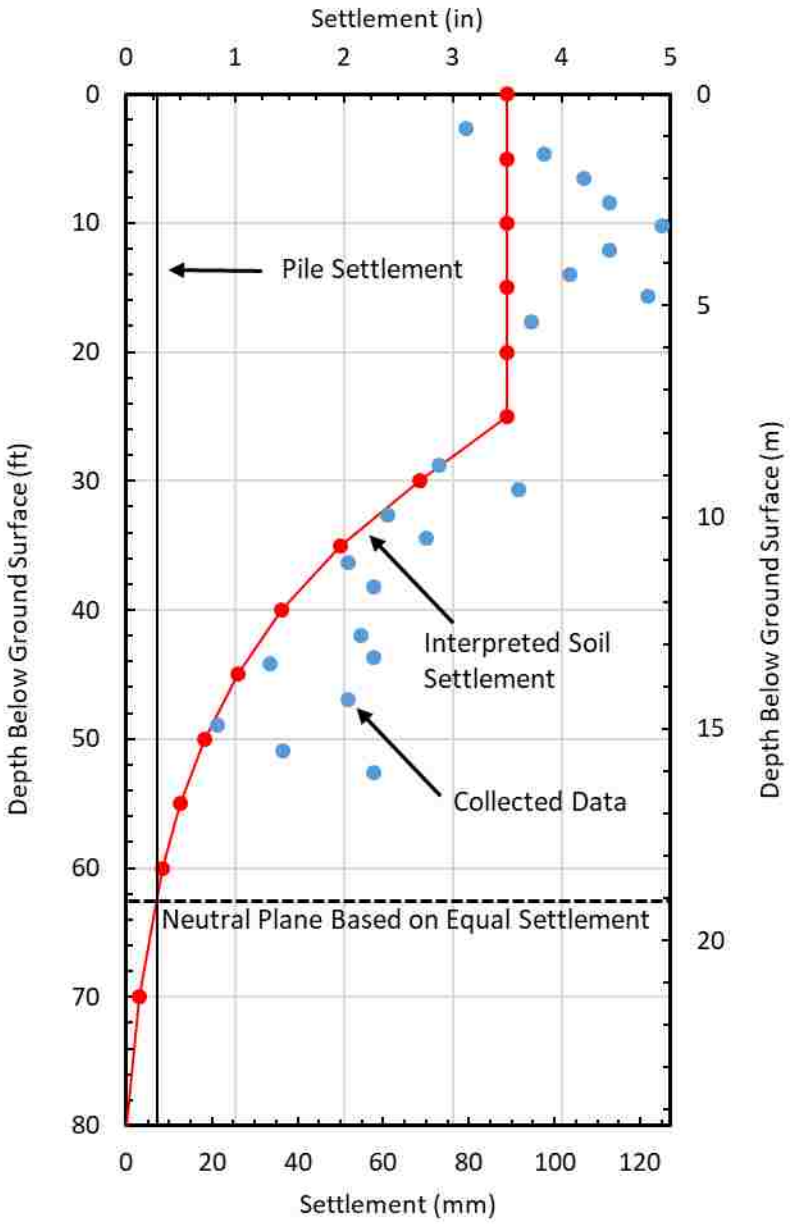

Figure 5.4-4 Settlement of the concrete pile and the soil surrounding it after the test blast

The total volumetric strain developed in the soil as it reconsolidated following blast liquefaction was again calculated by taking the total settlement of the liquefied layer (2 inches) and then dividing it by the thickness of the layer of liquefied soil (20 ft). The volumetric strain generated by the blast was determined to be 0.9%. This strain was also compared to expected strains from earthquakes based on SPT $(N_1)_{60}$ values determined by Tokimatsu and Seed (1987).

The expected strain based on the average blowcount over the 20 feet of liquefied soil was about 2%. This is still not as much strain as would be expected by an earthquake, but if the Cetin et al. (2009) depth weighting factor is used, then the expected volumetric strain would be 0.65% which is very close but somewhat lower than the strain measured using blast liquefaction.

Figure 5.4-5 Photo showing offset between the pre-stressed concrete pile and the surrounding soil after blast test. The painted pile section was initially flush with the ground surface prior to the blast.

5.4.4 Load in the Pile Following Blasting

The load in the concrete square pile was calculated by using equation 4-1. The modulus of elasticity of the concrete square pile was calculated using equation 4.2, and the strain was read directly from the gauges. The compressive strength of the concrete used to construct the pile was 9,930 psi. The strain gauges were zeroed out before the blast, even though the pile was loaded and blasted in the same day. This is due to the unrealistic data readings that were recorded during the static loading of the pile. The unrealistic readings may have been due to the particularly

heavy rain that was occurred prior to the static loading. The weather did dry up as the day wore on and the strain readings in the afternoon seemed more realistic. It was our hope that the dry weather and zeroing out the strain gauge readings would give more reliable results. The measured change in load in the pile versus depth after the blast is shown in Figure 5.4-6. Once again this is the change load in the pile after blasting without accounting for the load in the pile produced by static loading.

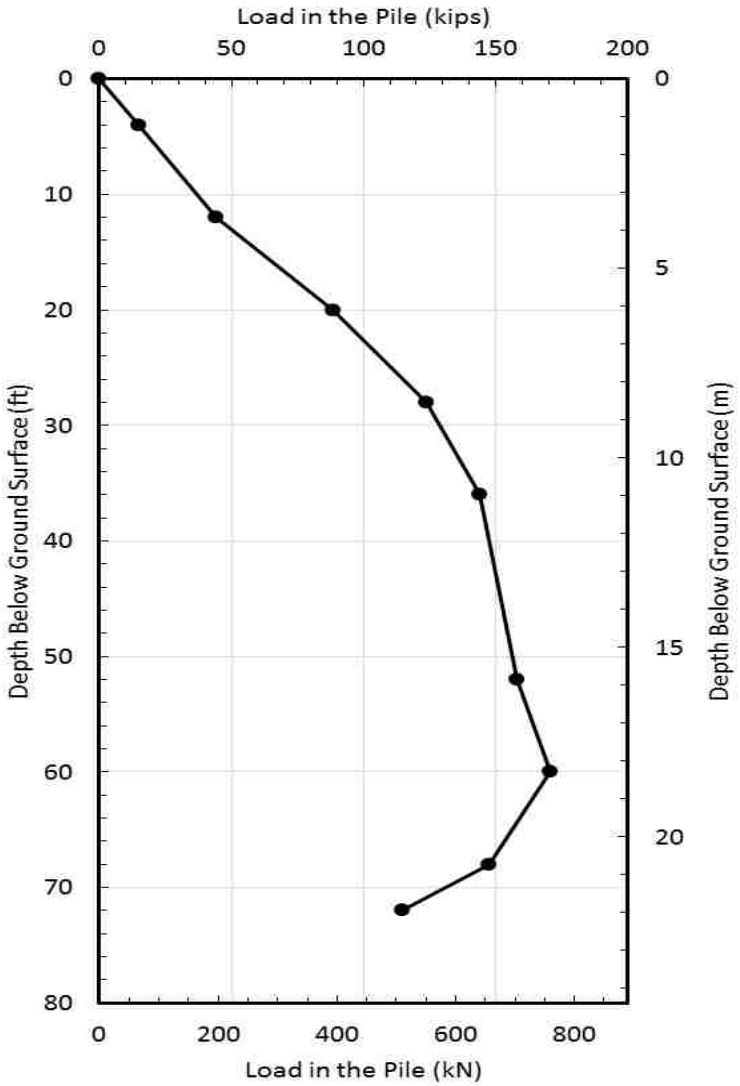

Figure 5.4-6 Change in load in the concrete pile versus depth after blasting.

To obtain the load in the pile versus depth after blasting, it was necessary to add the load in the pile versus depth after placement of the static load to the change in load versus depth curve presented in Figure 5.4-6. This was done by taking the load in the pile versus depth curve based on the CAPWAP EOID curve shown in Figure 4.5-3 and adding it to the curve in Figure 5.4-6. This is the same process explained in greater detail in section 5-2. The resulting load versus depth curve is shown in Figure 5.4-7. Negative skin friction increased the pile in the pile from 118 kips to about 170 kips, which means that the pile only gained 52 kips over 70 feet of depth. This could be due to water and loose sand being ejected at the interface with the concrete pile such that the friction around the pile was lessened due to the presence of this loose material along the pile. This is consistent with the observation of water flowing upward near the pile interface after the test blast. It is also consistent with the fact that there was no reduction in skin friction in the upper clay layers during the first two blasts when no evidence of liquefaction was observed at the ground surface.

The maximum load in the concrete square pile at this point occurred at a depth of about 60 feet. However, if the downdrag in the layers above the liquefied zone was not as vertical, then the maximum would have been greater and the neutral plane determined from the maximum load could have been deeper. However, the neutral plane of the concrete pile measured from the max load in the concrete square pile is be believed to be 60 feet, which is about 5 feet shallower than what was indicated by the settlement neutral plane.

Figure 5.4-8 compares the load in the pile versus depth immediately before the blast to the load after blast induced liquefaction and reconsolidation. This is done to see if the load in the pile after blasting was a reflection, except in the liquefied zone, of the load in the pile before blasting. In this case it is not a good reflection. This may be due to water and sand being forced

to the surface from the lower layers causing a decrease in skin friction along the shaft in the clay layers. If that were the case, then the load felt in the pile would increase, and thus would become a better match to the load in the pile prior to blasting.

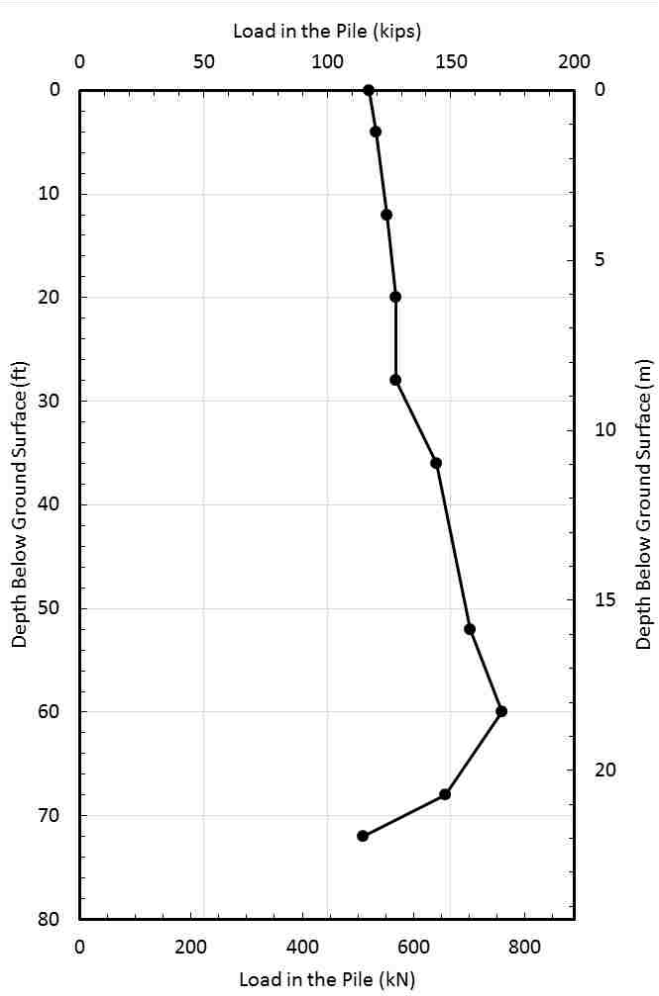

Figure 5.4-7 Load versus depth in the concrete pile immediately before blast and after blast induced liquefaction and reconsolidation.

The incremental side resistance comparisons are shown in Figure 5.4-9. The side resistance after the blast were smaller than the side resistance before the blast in the liquefied zone. However, the side resistance was also significantly smaller in the upper 30-foot-thick clay layer as well. The side resistance in the layers below the liquefied zone after the blast are comparable to the side resistance before the blast. On average, the side resistance in the liquefied

zone was about 47% of the e percent of the side resistance prior to blasting. The same comparison was made in the non-liquefied layers of the pile as well. The ratio of the pre-blast resistance compared to the post-blast resistance in the clay layers above the liquefied zone was 0.21 while in layers below the liquefied zone it was 2. The lower ratio above the liquefied zone once again could be due to the pile losing friction in the upper layers. The higher ratio below may be due to mobilizing more load because of lack of skin friction above the liquefied layer, especially considering that the largest difference in load is right at the pile tip, but it is so high that it is unreasonable were that not the case.

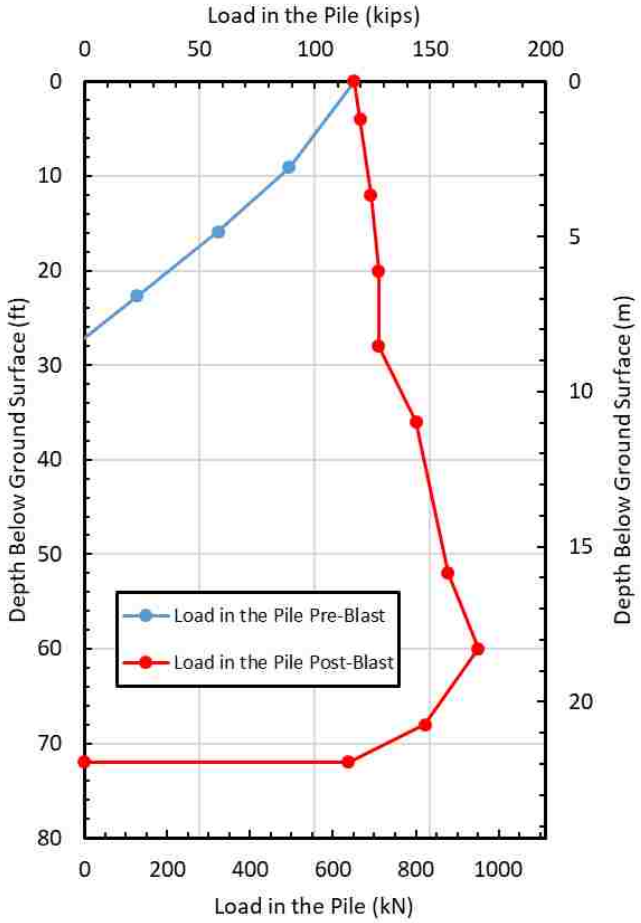

Figure 5.4-8 Comparison of the pre-blast load in the concrete pile versus depth curve after static loading with the post-blast curve after liquefaction and reconsolidation.

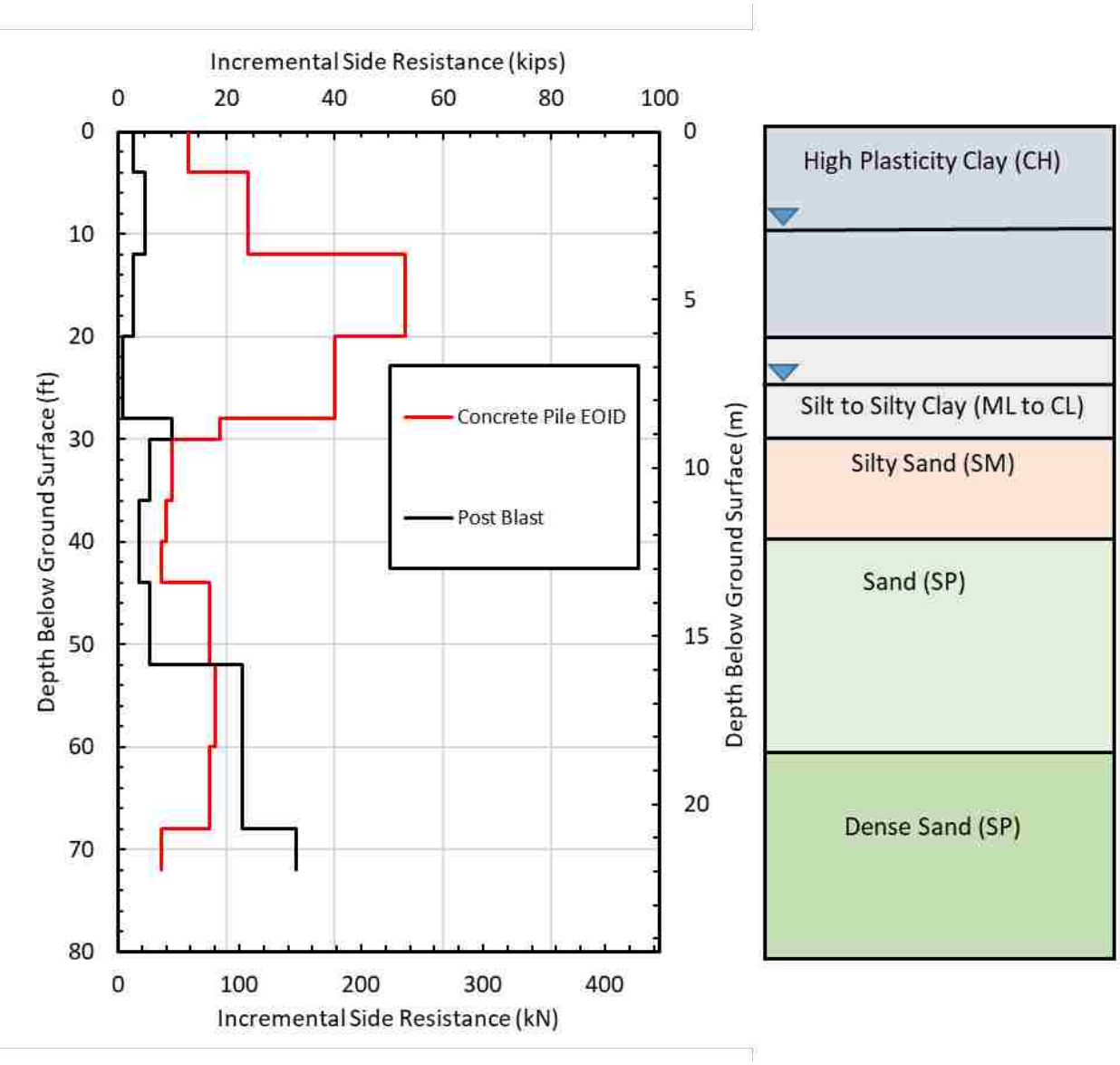

Figure 5.4-9 Incremental side resistance in the Concrete Pile

5.4.5 Summary of Response and Neutral Plane Evaluation for H Pile

Figure 5.4-10 provides plots of the excess pore pressure ratio, pile and soil settlement, and load in the pile after blasting vs. depth, as well as an end-bearing resistance vs. toe settlement curve for the pipe pile. This figure provides an overall picture of the interaction of the pile and the surrounding soil after the blast liquefaction along with the consistency of the results. The end-bearing resistance vs. toe settlement of the pile was created from a similar normalized

graph presented in Figure 3.2-11 (O'Neill and Reese 1999). This was done by multiplying the width of the pile base by the settlement ratio on the abscissa in Figure 3.2-11 and by multiplying the ultimate end bearing from the CAPWAP EOID analysis by the normalized end-bearing resistance on the ordinate in Figure 3.2-11. This makes it possible to determine if the estimated end-bearing resistance mobilized by the pile during blasting would produce a settlement that was similar to what was observed during blasting.

The soil liquefied from about 30 feet to 50 feet and for the third time the location of the neutral plane is outside of the liquefied zone. The neutral planes do not line up; and are about 10 feet apart. This may be due to the load in the concrete pile not being able to fully develop before the data acquisition system was disconnected. Another contributor to the discrepancy would have been not having enough strain gauges, and thus not being able to know the load at the location of the settlement neutral plane would have made it impossible to determine if the max load was at the same location or not. Either way, it is reasonable to say based on the results of the max load and the settlement, the neutral plane is likely between 60 and 65 feet and due to the concrete pile not being able to fully mobilize its load after blasting, it is likely closer to the 60 foot depth.

The estimated end bearing resistance from the post blast analysis was about 114 kips, which according to the O'Neill and Reese (1999) Q-z curve, would mean the pile should have settled about 0.32 inches based on an ultimate end-bearing resistance of 250 kips. The actual recorded pile settlement was 0.28 inches. Thus, we can determine that the load determined in the blast is reasonable.

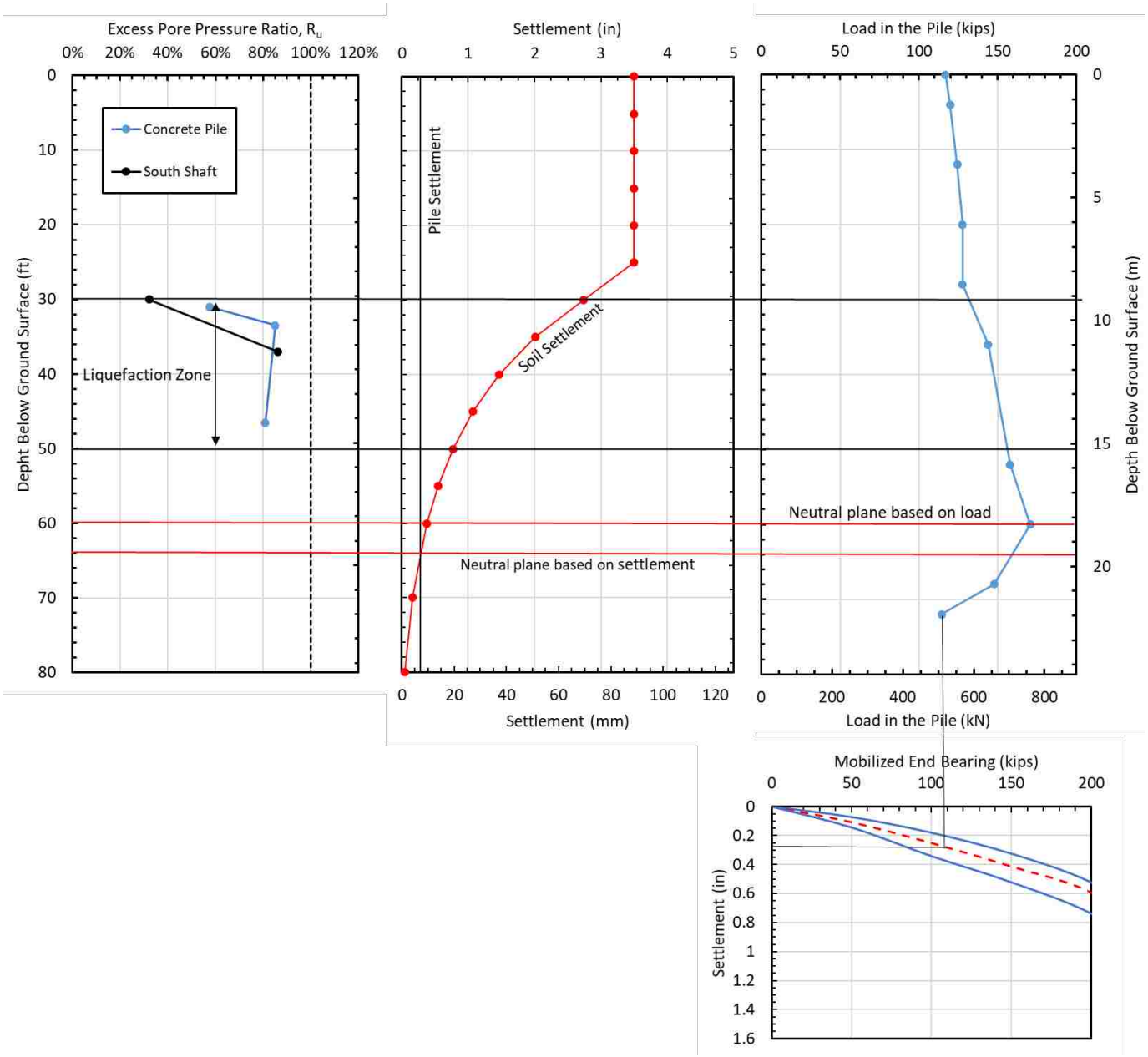

Figure 5.4-10 Pore pressure ratio, settlement, and load in the pile vs. depth along with end-bearing vs. settlement curve for concrete pile

5.5 Comparison of the Three Blasts

Figure 5.5-1 provides a comparison of the load in the pile versus depth for all three test piles after blast induced liquefaction and reconsolidation. All three piles show negative skin friction developing to a depth of between 55 and 61 feet. The load versus depth curve for the concrete square pile is more vertical than the other two piles and does not reach as high of a maximum load as the other two piles. Because the concrete pile has the largest shaft capacity, it might be expected to have the highest negative friction and to create the greatest downdrag forces. This reduced resistance could potentially be caused by several factors. First, the data acquisition system had to be disconnect the data acquisition system before the excess pore pressures had completely dissipated, although this was the case in previous blast. This would mean that the skin friction may have increased as settlement continued and the maximum load would not have been completely developed because the soil didn't finish settling. Another possibility may be water and sand ejecta moving upward along the interface of the pile. As the pore pressures dissipated, water escaped along the shaft thus potentially reducing the skin friction at the interface. However, it is difficult to determine the exact mechanism because it has not happened before on other blast tests and this experiment wasn't set up to measure this phenomenon, but there was a small water flow observed leaving the ground around the pile after blasting.

A comparison of the interpreted soil settlements surrounding each pile post blast is presented in Figure 5.5-2. The settlement of the soil surrounding the H-pile and the pipe pile were calculated by finding a regression curve that fit the data, however, the data from the concrete pile was calculated using a regression curve that only fit part of the data and was adjusted based on what was interpreted to be correct. The concrete pile had the most weight per

charge for the blast, but only one pound per hole more than the pipe pile. This would lead to believe that the soil surrounding the concrete pile would have a similar settlement to the soil surrounding the pipe pile. Toward the toes of the piles, however, the soil is much denser and leads to similar settlement in all three piles. Based on these observations, the interpreted settlement profile from the concrete pile can be considered accurate.

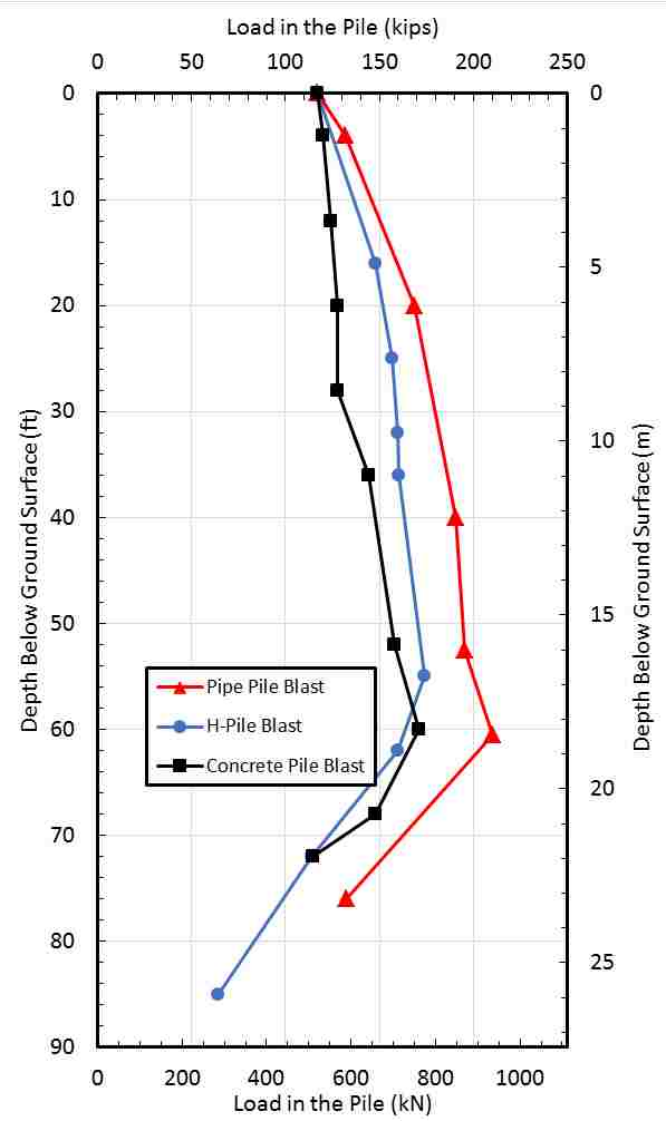

Figure 5.5-1 Comparison of the loads in the pile following blast induce liquefaction and reconsolidation for all three test piles

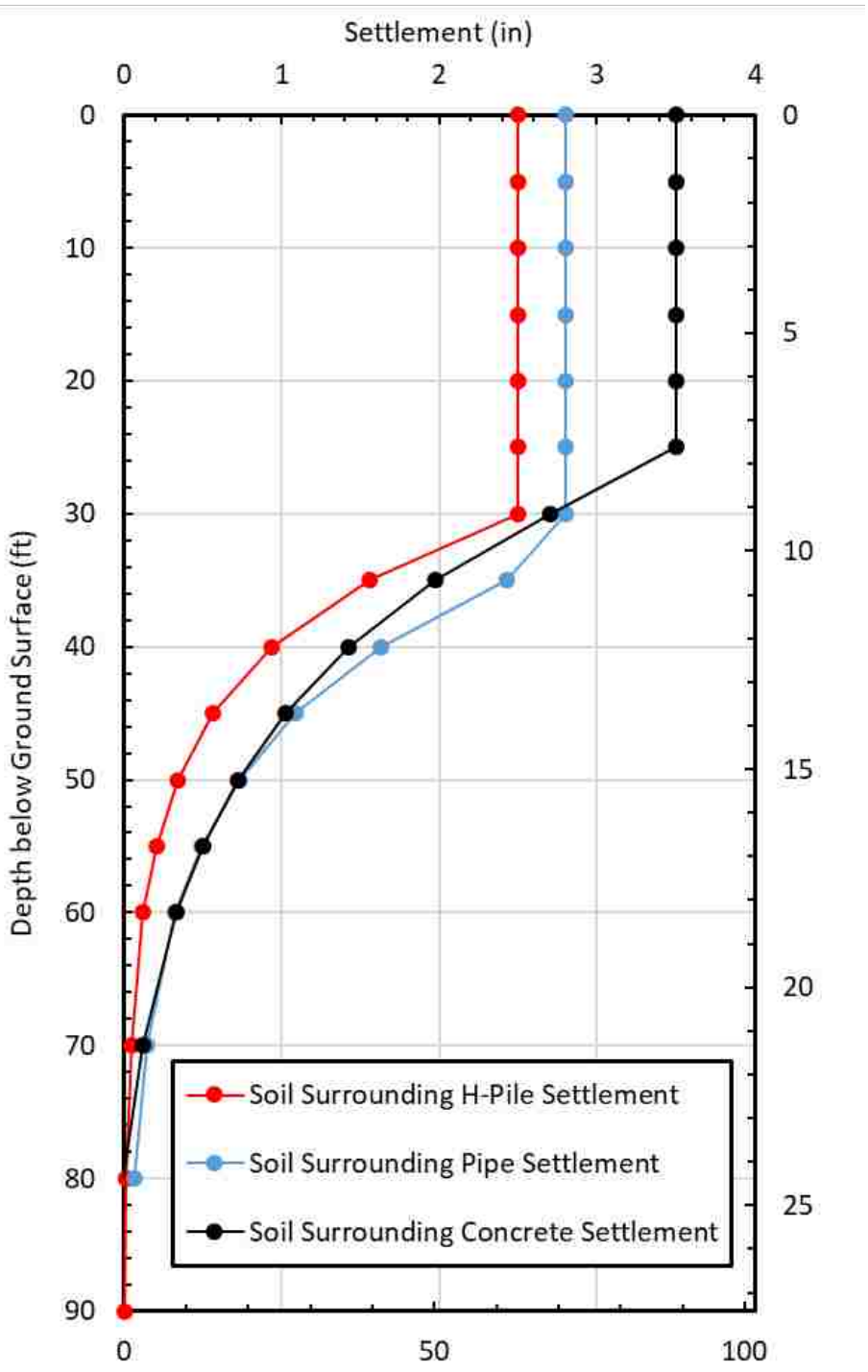

Figure 5.5-2 Comparison of the interpreted settlement profiles of the soil surrounding each profile.

5.5.1 Vibration Attenuation from the Blast Liquefaction Tests

Peak particle velocity produced by blasting has been correlated to damage to buildings and disturbance to humans. To provide a record of the ground motions produced by the blasting, peak particle velocity was measured as a function of distance for each blast test using two Instantel Minimate seismographs as shown in Figure 5.5-3. The seismographs were located at distances ranging from 30 to 168 ft from the closest blast hole. The measured peak particle velocities (PPVs) ranged from 0.24 to 0.025 meters per second. Measured peak particle velocity was plotted as a function of the scaled distance as shown in Figure 5.5-4 and a best-fit equation was developed based on the data. PPV in meters per second was given by the equation

$$\mathrm{PPV} = 1.67(\mathrm{SRSD})^{-1.425} \qquad 5\text{-}2$$

Where,

$$\mathrm{SRSD} = \frac{\mathrm{D}}{\mathrm{W}^{0.5}} \qquad 5\text{-}3$$

and D is the distance from the blast charge in meters and W is the charge weight in kg. The data points and the best-fit curve equation for this study predicts somewhat higher PPVs than that observed in the blast liquefaction tests conducted at Treasure Island in San Francisco Bay (Ashford et al. 2004). The charge weights in this study were significantly higher that used at Treasure Island which may partially explain the difference.

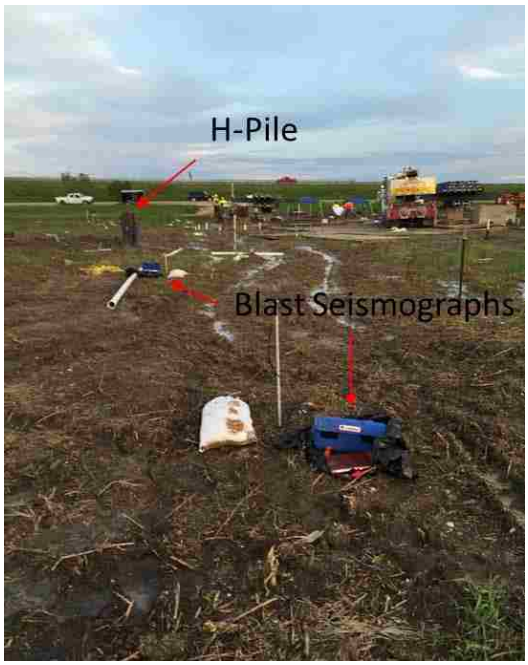

Figure 5.5-3 Photograph of two Instantel Minimate blast seismographs in place prior to blast liquefaction test around the concrete pile.

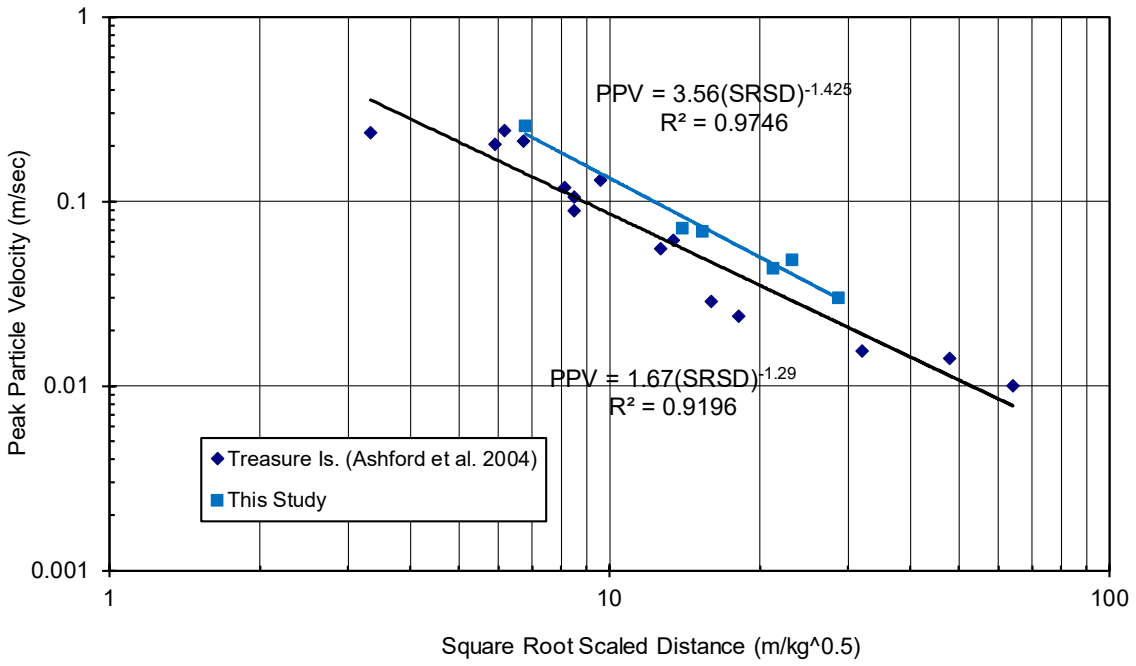

Figure 5.5-4 Peak particle velocity versus distance data and best-fit line for this study in comparison with data points and best fit line from Treasure Island blast tests (Ashford et al. 2004).

5.6 Comparison with Alternative Methods

The Fellinius and Siegel (2008) method of analyzing the location of the neutral plane depends on locating a neutral plane prior to liquefaction. The static neutral plane is formed by pore pressures dissipating around the pile and the surrounding soil settling as a result. In this experiment, there was no downdrag observed prior to liquefaction. Pore pressures remained constant after initial driving and no settlement of the soil was observed prior to blast induced liquefaction. However, the test in this experiment were performed within a two-month time period, it may be that the static neutral plane needs more time to form.

The ASHTO (2012) method of analyzing dragloads treats the skin friction in the liquefied zone as zero, and the location of the neutral plane is only based on pile settlement. The magnitude of the skin friction outside of the liquefied zones in this method is about the same as pre-blast liquefaction skin friction. However, because there is no dragload in the liquefied zone, the maximum load in the pile is under-predicted and less end bearing in mobilized. This would lead to an under-prediction of the pile settlement.

Boulanger and Brandenberg (2004) found that the neutral plane location changed with time, and Wang and Brandenberg (2013) found that the neutral plane is not where settlement of soil and pile are equal, but rather where their relative velocities are equal. In addition, they assume that skin friction in the liquefied layer is zero. This experiment was not designed to measure relative velocity of either the soil or the pile during the experiment. However, it is possible that the location of the neutral plane changes with time. When the pore pressures dissipate and the negative skin friction develops in the liquefied zone, this would create more downward force around the pile causing it to settle even more than it did when skin friction was zero in the liquefied zone and therefore would cause the neutral plane to change as the pile settled more.

6 SUMMARY AND CONCLUSIONS

Blast induced liquefaction tests were performed on an H pile, a pipe pile, and a pre-stressed concrete pile. Prior to blasting, a static load of 118.5 kips was applied to each test pile. The soil profile at the test site generally consisted of 30 feet of clay underlain by medium density sand and silty sand. Blasting produced a liquefied zone between 15 and 20 feet thick immediately below the clay layer. Liquefaction induced ground settlements ranged from 2.5 to 3.5 inches, but pile settlements were only 0.28 to 0.35 inches. Load in the pile was measured by strain gauges following blast induced liquefaction and compared with load in the pile prior to blasting interpreted from CAPWAP analyses, Bi-directional load testing, and static load tests.

Based on the results of the field tests, the following conclusions have been drawn:

1. The magnitude of the skin friction in the liquefied zone was typically 40 to 50% of the skin friction in that zone prior to liquefaction. The measured percentages of skin resistance in the liquefied zone were, 49% for the H-Pile, 38% for the pipe pile and 47% for the concrete square pile. These results are generally consistent with previous full-scale blast liquefaction test results on a driven steel pile (Rollins and Strand, 2006) and auger-cast piles (Rollins and Hollenbaugh, 2015).

2. Post-blast skin friction in the non-liquefied clay layers above the liquefied zone was typically about the same as that before liquefaction. Similarly, post-blast skin friction in the deeper non-liquefied sand layers was reasonably similar to that before blasting. However, for the pre-stressed concrete pile a significant reduction in the skin friction was observed in the clay layer

following liquefaction. This reduction in skin friction may have been caused by water and sand escaping along the interface with the shaft causing a reduction in skin friction.

3. Following blast induced liquefaction and reconsolidation of the liquefied layer, negative skin friction typically developed on the test piles from the ground surface to a depth of 52 to 65 feet. Below this develop, positive skin developed to the bottom of each test pile where end-bearing resistance provided the force necessary to achieve static equilibrium.

4. In all cases, the neutral plane was located below the liquefied layer, but in layers where excess pore pressure ratios had been high enough to produce a small amount of settlement (≈0.25 to 0.50 inches). Because the neutral plane was located below the liquefied layer pile settlements were relatively low in all cases.

5. The location of the neutral plane can be defined as the depth where negative skin friction changes to positive skin friction and the load in the pile is maximum. It is also defined as the depth where the settlement of the pile is equal to the settlement of the soil. Generally, the locations of the neutral plane obtained from maximum load and from equal settlement were consistent with one another. Discrepancies can likely be attributed to the spacing of the strain gauges or uncertainty in the soil settlement measurements. For the H-pile, the neutral plane from settlement was at a depth of 52 feet and the neutral plane from the maximum load was at a depth of about 55 feet. For the pipe pile, the neutral plane from settlement was at 60 feet and the neutral plane based on the maximum load was at a depth of 61 feet. The concrete pile had a neutral plane from settlement of 65 feet, and a neutral plane from the maximum load at a depth of 65 feet.

6. Calculating the settlement of the pile during liquefaction using the neutral plane method and the Q-z curve for end-bearing mobilized proposed by O'Neill & Reese (1999) proved to be very

accurate. All of the measured settlements were much less than one standard deviation of the predicted settlement. For the H pile predicted settlement to mobilize end-bearing was 0.35 inches while the pile actually settled about 0.28 inches. For the pipe pile, settlement predicted to develop end-bearing was 0.32 inches and the pile actually settled 0.32 inches. Lastly, for the concrete square pile, settlement predicted to mobilize end-bearing was 0.32 inches while measured settlement was about 0.28 inches.

REFERENCES

AASHTO, L. (2012). LRFD bridge design specifications. Washington, DC: American Association of State Highway and Transportation Officials.

Andrus, R.D. and Stokoe, K.H., II (2000). "Liquefaction resistance of soils from shear-wave velocity." *J. Geotech. and Geoenvir. Engrg.,* ASCE 126(11), 1015-1025.

Ashford, S.A., Rollins, K.M., and Lane, J.D. (2004) "Blast-induced liquefaction for full-scale foundation testing." *J. Geotech. and Geoenvir. Engrg*., ASCE, Vol. 130, No. 8, 798-806.

Bey, S. M. (2014). "Cost-benefit analyses for load resistance factor design (LRFD) of drilled shafts in Arkansas." Thesis, ProQuest, Ann Arbor.

Boulanger, R.W and Brandenberg, S.J. (2004) "Neutral plane solution for liquefaction-induced downdrag on vertical piles." *Proceedings, ASCE Geo-Trans conference,* ASCE, Reston, VA, 470-479.

Boulanger, R. W., and Idriss, I. M. (2012). "Probabilistic Standard Penetration Test–Based Liquefaction–Triggering Procedure." J. *Geotech. Geoenviron. Eng. Journal of Geotechnical and Geoenvironmental Engineering*, 138(10), 1185–1195.

Boulanger, R. W., and Idriss, I. M. (2015). "CPT-Based Liquefaction Triggering Procedure." J. Geotech. Geoenviron. *Eng. Journal of Geotechnical and Geoenvironmental Engineering*, 142(2), 04015065.

Briaud, J.-L. and Tucker, L. (1997)." Design and Construction Guidelines for Downdrag on Uncoated and Bitumen-Coated Piles." NCHRP Report 393, Transportation Research Board, National Academy Press, Washington, D.C.

Briaud, J.L., et al. (1986). "Development of an improved pile desing procedure for single piles in clays and sands." *Research Report 4981-1 to the Mississippi State Highway Department,* Civil Engineering, Texas A&M University, College Station, Tex.

Bustamante, M., and Gianeselli, L. (1982). "Pile bearing capacity predictions by means of static penetrometer CPT." *Procs., 2nd European symposium on penetration testing*, Amsterdam, Netherlands, 493-500.

Cetin, K. O., Bilge, H. T., Wu, J., Kammerer, A. M., and Seed, R. B. (2009). "Probabilistic Model for the Assessment of Cyclically Induced Reconsolidation (Volumetric) Settlements." J. Geotech. Geoenviron. Eng. Journal of Geotechnical and Geoenvironmental Engineering, 135(3), 387–398.

Eslami, A., and Fellenius, B.H. (1997). "Pile capacity by direct CPT and CPTu methods applied to 102 case histories." Canadian Geotech. J, NRC Canada, 34(6), 886-904.

Fellenius, B.H. (1996). "Basics of Foundation Design, BiTech Publishers Ltd., Richmond, BC, Canada, 134 p.

Fellenius, B.H. (2001). "From Strain Measurements to Load in an Instrumented Pile" *Geotechnical News Magazine,* 19(1), 35-38.

Fellenius, B. H. (2006). "Results from long-term measurement in piles of drag load and downdrag." Canadian Geotechnical Journal Can. Geotech. J., 43(4), 409–430.

Fellenius, B. H., and Siegel, T. C. (2008). "Pile Drag Load and Downdrag in a Liquefaction Event." J. Geotech. Geoenviron. Eng. Journal of Geotechnical and Geoenvironmental Engineering, 134(9), 1412–1416.

Goble, G.G., Likins, G.E. and Rausche, F. (1975). "Bearing capacity of piles from dynamic measurements." Final Report, Dept. of Civil Engienering, Case Western Reserve University, Cleveland, Ohio

Hannigan, P. J., Goble, G. G., Likins, G. E., and Rausche, F. (2006). Design and Construction of Driven Pile Foundations. Federal Highway Administration, National Highway Institute, Washington, DC.

Hollenbaugh, J. E. (2014). "Full-scale testing of blast-induced liquefaction downdrag on auger-cast piles in sand." MS Thesis, Department of Civil and Environmental Engineering, Brigham Young University, Provo, UT.

Idriss, I. M., and Boulanger, R. W. (2010). "SPT-based liquefaction triggering procedures." Report UCD/CGM-10/02, Department of Civil and Environmental Engineering, University of California, Davis, CA, 259 pp.

Ishihara, K. (1990). "Liquefaction and flow failure during earthquakes." Géotechnique, ICE, London, England, 43(3), 351–451.

Ishihara, K., and Yoshimine, M. (1992). "Evaluation of settlements in sand deposits following liquefaction during earthquakes." *Soils and Foundations*, 32(1), 173–188.

Kulhawy, F.H. and Mayne, P.W. (1990). "Manual on estimating soil properties for foundation design." Research Report EERI EL-6800, Electric Power Research Institute, Palo Alto, California.

Lam, S. Y., Ng, C. W., Leung, C. F., and Chan, S. H. (2009). "Centrifuge and numerical modeling of axial load effects on piles in consolidating ground." Canadian Geotechnical Journal Can. Geotech. J., 46(1), 10–24.

Mayne, P.W., Peuchen, J. and Bouwmeester, D. 2010. Soil unit weight estimation from CPT. Proc. 2nd Intl. Symp. on Cone Penetration Testing, Huntington Beach, CA.

O'Neil, M.W. and Reese, L.C. *Drilled Shafts: Construction Procedures and Design Methods*. Publication No. -IF-99-025, US Federal Highway Administration, 1999; 535p

Race, M. L., and Coffman, R. A. (2013). "Effect of Uncertainty in Site Characterization on the Prediction of Liquefaction Potential for Bridge Embankments in the Mississippi Embayment." Geo-Congress 2013.

Race, M. (2015). "Amount of Uncertainty in the Methods Utilized to Design Drilled Shaft Foundations." dissertation, ProQuest, Ann Arbor, MI.

Robertson, P. K., and Cabal, K. L. (2015). Guide to Cone Penetration Testing for Geotechnical Engineering. Gregg Drilling and Testing, Signal Hill, CA.

Robertson, P. K (2010). Soil behavior type from the CPT: an update. Gregg Drilling and Testing, Signal Hill, CA.

Robertson, P. K., and Wride, C. (F. (1998). "Evaluating cyclic liquefaction potential using the cone penetration test." *Canadian Geotechnical Journal Can. Geotech. J.*, 35(3), 442–459.

Robertson, P.K., Wride, C.E., List, B.R., Atukorala, U., Biggar, K.W., Byrne, P.M., Campanella, R.G., Cathro, D.C., Chan, D.H., Czajewski, K., Finn, W.D.L., Gu, W.H., Hammamji, Y., Hofmann, B.A., Howi, J.A., Hughes, J. Imrie, A.S., Kinrad, J.M., Küpper, A., Law, T., Lord, E.R.F., Monahan, P.A., Morgenstern, N.R., Phillips, R., Piché, R., Plewes, H.D., Scott, D., Sego, D.C., Sobkowicz, J., Stewart, R.A., Watts, B.D., Woeller, D.J., Youd, T.L., and Zavodni, Z., (2000). "The Canadian Liquefaction Experiment: an overview." *Can. Geotech. J*, NRC Canada, 37(3), 499-504

Rollins, K.M., Lane, J.D., Dibb, E., Ashford, S.A., Mullins, A.G. (2005). "Pore pressure measurement in blast-induced liquefaction experiments." *Transportation Research Record 1936*, "Soil Mechanics 2005", Transportation Research Board, National Academy Press, Washington DC, p. 210-220.

Rollins, K.M. and Anderson, J.K.S. (2004). "Performance of vertical geocomposite drains based on full-scale testing at Massey Tunnel, Vancouver, B.C." Final Report, NCHRP-IDEA

Project 94, Transportation Research Board, National Academy Press, Washington, D.C., 107 p.

Rollins, K.M. and Strand, S.R. (2006). "Downdrag Forces due to Liquefaction Surrounding a Pile." Proc. 8th National Conference on Earthquake Engineering, Earthquake Engineering Research Institute, 10 p.

Stringer, M.E., Madabhushi, S.P.G. (2013). "Re-mobilization of pile shaft friction after an earthquake." *Canadian Geotechnical Journal*, 50(9), 979-988.

Stringer, M.E. and Madabhushi, S.P.G. (2010) "Measuring shaft friction during earthquakes." Physical Modelling in Geotechnics - Proceedings of the 7th International Conference on Physical Modelling in Geotechnics 2010, ICPMG 2010, 2. pp. 1433-1438.

Tokimatsu, K., and Seed, H.B. (1987). "Evaluation of settlements in sands due to earthquake shaking," *Journal of Geotechnical and Environmental Engineering*, 103(8), 861-878.

Vanikar, S. (1986). "Manual on Design and Construction of Driven Pile Foundations." U.S. Department of Transportation Federal Highway Administration, FHWA-DP-66-1 (Revision 1), 57 pgs.

Wang, R., and Brandenberg, S. J. (2013). "Beam on Nonlinear Winkler Foundation and Modified Neutral Plane Solution for Calculating Downdrag Settlement." J. Geotech. Geoenviron. Eng. Journal of Geotechnical and Geoenvironmental Engineering, 139(9), 1433–1442.

Wang, R. (2016). "Single Piles in Liquefiable Ground." Springer Theses.

Youd, T. L., and Idriss, I. M. (2001). "Liquefaction Resistance of Soils: Summary Report from the 1996 NCEER and 1998 NCEER/NSF Workshops on Evaluation of Liquefaction Resistance of Soils." J. Geotech. Geoenviron. Eng. Journal of Geotechnical and Geoenvironmental Engineering, 127(4), 297–313.

Zhang, G., Robertson, P. K., and Brachman R. W.I. (2002). "Estimating liquefaction-induced ground settlements from CPT for level ground." *Canadian. Geotech. J.*, NRC Canada, 39(5), 1168–1180